

NASA Technical Memorandum 4270

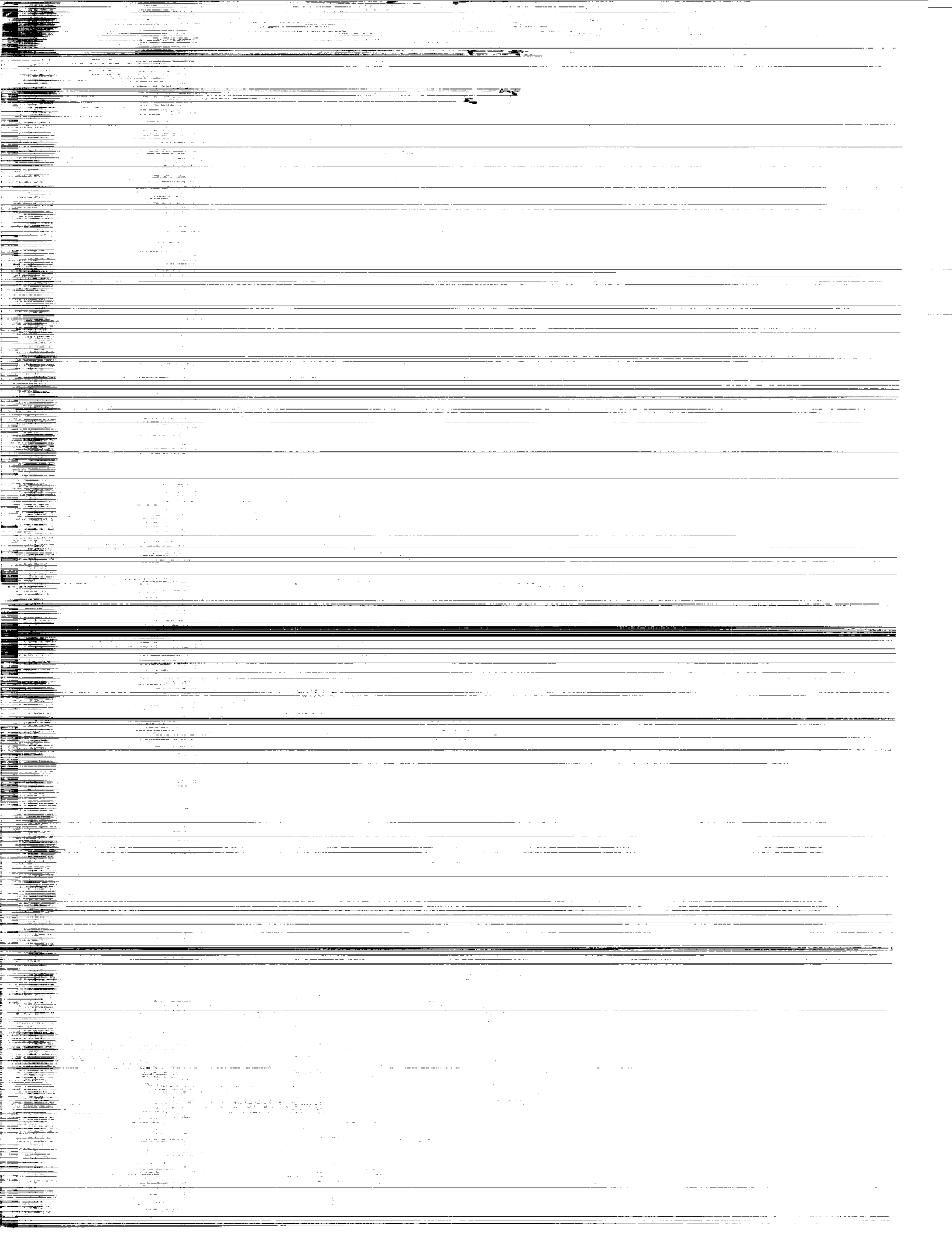
Radiation Health Research, 1986-1990

MARCH 1991

(NASA-TM-4270) RADIATION HEALTH RESEARCH,
1986 - 1990 (NASA) 114 p CSCL 06R

N71-21704

Unclas
H1/52 0001906



NASA Technical Memorandum 4270

Radiation Health Research, 1986–1990

Radiation Health Program,
Life Sciences Division
NASA Office of Space Science and Applications
Washington, D.C.



National Aeronautics and
Space Administration
Office of Management
Scientific and Technical
Information Division

1991

INTRODUCTION

The present volume is a collection of recent abstracts of radiation research sponsored by NASA. Its purpose is to make available a concise summary for use by active investigators, prospective investigators, interested administrators, and the community at large. The period covered from 1986 to 1990 is somewhat arbitrary. Hopefully, this collection goes back far enough to yield an adequate perspective of the research effort and yet does not detain the reader at milestones that already have been achieved.

The research sponsored by NASA and reported here is evidence of a very large return to the taxpayer for a very minimal investment. Much of this research was made possible by the existence of an infrastructure developed by other Federal agencies and with marginal resources riding on other programmatic support. In many cases, this infrastructure no longer exists or is no longer available, and NASA will have to depend much more on its own resources to conduct research critical for our mission. That the research reported in this book was possible at all is in no small measure due to the imagination and farsightedness of a few individuals. Foremost among these was the late Stuart Nachtwey, who stimulated this research effort with the same grace under pressure with which he battled to the end against his final illness. Stu's courage and determination serve as an example to all of us who were privileged to witness them. The work described in this book is our testimonial.

In 1990 the Radiation Health Program became an independent program of the Life Sciences Division in the Office of Space Science and Applications at NASA. This change implements the recommendations of several advisory committees and the policy decisions to expand the radiation research program in recognition of the critical importance of radiation protection to the Space Exploration Initiative. The purpose of the Radiation Health Program is to establish the scientific basis for the radiation protection of humans engaged in the exploration of space, with particular emphasis on lunar and planetary space exploration. It supports scientific research into the fundamental mechanisms of radiation effects on living systems and the interaction of radiation with cells, tissues and organs, as well as the development of instruments and processes dealing with the measurement of radiation and its effects. In pursuit of the Radiation Health Program, the Life Sciences Division supports researchers at universities, NASA centers and national laboratories, establishes interagency agreements for cooperative use and development of facilities, and operates a space-based research program centered on the Life Sciences Satellite (LifeSat).

It is expected that collections similar to the present one will be published at more frequent intervals in the future, reflecting the increasing pace of research sponsored by the Radiation Health Program. The present publication was made possible by the efforts of many people. The principal investigators took time off from their busy schedules to proofread the reprinted abstracts. T. C. Yang and D. Morrison, of the NASA Johnson Space Center, helped prepare the bulk of this volume. M. Jablin, G. Ferraro, R. Teeter, K. Stokes, R. Maggio, and C. Brooks of the Lockheed Engineering and Sciences Co., Washington D.C., and Janice Wallace, Elizabeth L. Hess, April C. Roy, and F. Ronald Dutcher of George Washington University, Washington, D.C., were responsible for proofreading, cross-referencing, and completing the document. Their work is gratefully acknowledged.

Walter Schimmerling
Manager, Radiation Health Program

TABLE OF CONTENTS

	<u>Page</u>
1. PHYSICS	1
1.1. ATOMIC PHYSICS	
Journals	2
Reports/Meetings	4
1.2. NUCLEAR SCIENCE	
Reports/Meetings	5
1.2.1. THEORY	
Journals	5
Reports/Meetings	7
1.2.2. EXPERIMENTAL	
Journals	12
Reports/Meetings	14
1.3. SPACE RADIATION	
1.3.1. COSMIC RAY AND ASTROPHYSICS	
Journals	16
1.3.2. ENVIRONMENTS AND ENVIRONMENTAL MODELS	
Journals	17
Reports/Meetings	18
1.3.3. SOLAR ACTIVITY AND PREDICTION	
Reports/Meetings	18
1.3.4. EXPERIMENTS	
Reports/Meetings	19
1.4. RADIATION TRANSPORT AND SHIELDING	
Reports/Meetings	20
1.4.1. THEORY AND MODEL DEVELOPMENT	
Journals	22
Reports/Meetings	24
1.4.2. EXPERIMENTAL STUDIES	
Journals	30
Reports/Meetings	31
1.5. INSTRUMENTATION	
Journals	34
2. BIOLOGY	35
2.1. MOLECULAR BIOLOGY	
Journals	36

TABLE OF CONTENTS

	<u>Page</u>
2.2. CELLULAR RADIATION BIOLOGY	
Journals	38
2.2.1. TRANSFORMATION, MUTATION	
Journals	39
2.2.2. LETHALITY, SURVIVAL	
Journals	42
Reports/Meetings	45
2.2.3. DNA DAMAGE AND REPAIR	
Journals	46
Reports/Meetings	48
2.3. TISSUE, ORGANS AND ORGANISMS	
Journals	49
Reports/Meetings	50
2.3.1. IN VIVO/IN VITRO SYSTEMS	
Journals	50
Reports/Meetings	51
2.3.2. CARCINOGENESIS AND LIFE SHORTENING	
Journals	52
2.3.3. CATARACTOGENESIS	
Journals	53
Reports/Meetings	55
2.3.4. OTHER EFFECTS	
Journals	61
Reports/Meetings	62
2.4. RADIOPROTECTANTS	
Reports/Meetings	65
2.5. PLANTS	
Journals	66
3. RISK ASSESSMENT	67
3.1. RADIATION HEALTH AND EPIDEMIOLOGY	
Journals	68
Reports/Meetings	69
3.2. SPACE FLIGHT RADIATION HEALTH PHYSICS	
Journals	72
Reports/Meetings	78

TABLE OF CONTENTS

	<u>Page</u>
3.3. INTER- AND INTRASPECIES EXTRAPOLATION	
Journals	84
Reports/Meetings	87
3.4. RADIATION LIMITS AND STANDARDS	
Journals	88
Reports/Meetings	89
4. MICROGRAVITY	91
4.1. MICROGRAVITY	
Journals	92
Reports/Meetings	94
KEYWORD INDEX	99
AUTHOR INDEX	107

1
2
3
4
5
6
7
8
9
10
11
12
13
14
15
16
17
18
19
20
21
22
23
24
25
26
27
28
29
30
31
32
33
34
35
36
37
38
39
40
41
42
43
44
45
46
47
48
49
50
51
52
53
54
55
56
57
58
59
60
61
62
63
64
65
66
67
68
69
70
71
72
73
74
75
76
77
78
79
80
81
82
83
84
85
86
87
88
89
90
91
92
93
94
95
96
97
98
99
100

1
2
3
4
5
6
7
8
9
10
11
12
13
14
15
16
17
18
19
20
21
22
23
24
25
26
27
28
29
30
31
32
33
34
35
36
37
38
39
40
41
42
43
44
45
46
47
48
49
50
51
52
53
54
55
56
57
58
59
60
61
62
63
64
65
66
67
68
69
70
71
72
73
74
75
76
77
78
79
80
81
82
83
84
85
86
87
88
89
90
91
92
93
94
95
96
97
98
99
100

1. PHYSICS

1.1. ATOMIC PHYSICS

JOURNALS

Khan, F., Khandelwal, G. S., and Wilson, J. W. (1988) Differential oscillator strengths and dipole polarizabilities for transitions of the helium sequence. *Physical Review A* 38: 6159-6164.

Oscillator strengths, Dipole polarizabilities, Radial integrals

The dipole radial integral for an initial discrete $1s$ state and a final continuum state has been calculated under the screened hydrogenic model. In this model, single-electron hydrogenic wave functions are employed and the initial and the final states are treated by two different effective-charge parameters. Numerical values of differential oscillator strengths for transitions from $1s^2\ ^1S$ to the continuum for the helium sequence ions are obtained. Also calculated are the dipole polarizabilities, which are found to be in excellent agreement with the results of other authors.

Khan, F., Khandelwal, G. S., and Wilson, J. W. (1988) Static multipole polarisabilities and second-order Stark shift in francium. *Journal of Physics B* 21: 731-737.

Stark effect, Multipole polarizability

The multipole polarisability of the ground state of francium is calculated by utilizing both the variational technique of Davison and the quantum defect theory underlying the Bates-Damgaard method. This approach is also shown to yield reasonable results for other alkali atoms. Second-order Stark shift for the ground state of francium is presented as a function of field strength for possible future experimental comparison.

Khan, F., Khandelwal, G. S., and Wilson, J. W. (1988) $1s^2\ ^1S-1s\ np\ ^1P$ transitions of the helium isoelectronic sequence members up to $Z = 30$. *The Astrophysical Journal* 329: 493-497.

Radial integrals, Oscillator strengths, Effective charge

Radial integrals have been calculated under the one-electron hydrogenic model. Two different values of the effective charge parameter, one for the initial state and the other for the final state, are retained in these formulae. The model is able to reasonably reproduce the existing dipole oscillator strength values with little effort. The dipole oscillator strength values are given for many ions for the first time.

Khan, F., Khandelwal, G. S., and Wilson, J. W. (1990) Moments of dipole oscillator-strength distribution for the helium sequence. *Journal of Physics B: At Mol Opt Phys* 23: 2717-2726.

Oscillator strengths, Helium

The moments $S(\mu)$ for $-6 \leq \mu \leq 2$ and $L(\mu)$ for $\mu=0, 1$, and 2 are calculated for the helium sequence for atomic numbers Z up to 30 under a screened hydrogenic model. In this model, one describes the atom by single-particle hydrogenic wavefunctions and treats the initial and the final state as characterized by two different effective charge parameters Z_i and Z_f , respectively. An asymptotic expansion is made of the differential oscillator strength of the screened hydrogenic model. Assuming the value 287.6 for the coefficient of the term $\Sigma^{-7/2}$ for helium atom as given by

Salpeter and Zaidi, the parameter Z_f is determined for the helium sequence. This approach has resulted in values which are in reasonable agreement with the various moment values of other authors.

Khandelwal, G. S., Khan, F., and Wilson, J. W. (1989) Asymptotic expressions for dipole oscillator strength for transitions of He sequence. *The Astrophysical Journal* 336: 504-506.

Oscillator strengths, Radial integrals, Excitations

The radial integral for $1s^2\ ^1S-1s\ np\ ^1P$ transitions of the He isoelectronic sequence is asymptotically expanded to order n^{-7} to facilitate calculations of the dipole oscillator strength for large n . The threshold differential oscillator strength values are obtained for ions up to $Z=30$ within the screened hydrogenic model.

Khandelwal, G. S., Pritchard, W. M., Grubb, G., and Khan, F. (1989) Screened hydrogenic radial integrals. *Physical Review A* 39: 3960-3963.

Hydrogenic, Radial integrals, Electronic transitions

The screened hydrogenic radial integral both for discrete-discrete and discrete-continuum transitions is expressed in forms suitable for obtaining closed-form expressions for specific transitions. Two effective charge parameters Z_i and Z_f , respectively, for the initial state and for the final state are retained in these formulas. As examples, explicit expressions for a few transitions are derived and a method for obtaining a series for a discrete-discrete radial integral, suitable for large final-state principal quantum numbers, is indicated.

Olsgaard, D. A., Khan, F., and Khandelwal, G. S. (1988) Asymptotic screened hydrogenic radial integrals. *Journal of the Optical Society of America B* 5: 2437-2438.

Radial integrals, Hydrogen transitions

The screened hydrogenic radial dipole integral for discrete-discrete transitions from initial state $n'l'$ to final state nl is asymptotically expanded to the lowest order such that the final quantum number $n \rightarrow \infty$. The analytical expression obtained is in terms of confluent hypergeometric functions, and explicit expressions for a few of the specific transitions are derived from them as examples.

Rustgi, M. L., Pandey, L. N., Wilson, J. W., Long, S. A. T., and Zhu, G. (1988) Distribution of energy in polymers due to incident electrons and protons. *Radiation Effects* 105: 303-311.

Polymers, Protons, Coulomb scattering, Electrons, Electronic excitation, Ionization

The recoil spectrum of nuclei in polymers for incident protons below 10 MeV in energy is calculated by using the Rutherford cross-section with screening corrections. Employing the work of McKinley and Fesbach on the Coulomb scattering of relativistic electrons by nuclei, the recoil spectrum of the nuclei is also calculated for electron energies varying from threshold to 10 MeV. The partitioning of energy between electronic excitation and ionization and nuclear recoil is then studied to search for possible difference in polymer radiation response as a function of radiation energy and type.

1.1. ATOMIC PHYSICS

REPORTS/MEETINGS

Khan, F., Khandelwal, G. S., and Wilson, J. W. (1987) $1s^2\ ^1S - 1s\ np\ ^1P$ transitions of helium isoelectronic sequence members up to $z = 30$. Abstract presented at the Annual Meeting of the Virginia Academy of Sciences, Norfolk, VA, May 20-22, 1987. *Virginia Journal of Science* 38: 70.

Effective charge, Oscillator strengths

Radial integrals have been calculated under the one-electron hydrogenic model. Two different values of the effective charge parameter, one for the initial state and the other for the final state, are retained in these formulae. The model is able to reasonably reproduce the existing dipole oscillator strength values with little effort. The squares of the radial integral values are given for many ions for the first time.

Wilson, J. W., Khandelwal, G. S., and Fogarty, N. T. (1988) X-ray Production in Low Energy Proton Stopping. NASA Technical Memorandum 100619.

X-ray production, Protons, Alloy, Electronic devices

The X-ray yields of stopping protons in an iron-nickel-cobalt alloy are calculated for use in predicting radiation damage in encased electronic devices.

Xu, Y. J., Khandelwal, G. S., Wilson, J. W. (1986) The maximum momentum transfer in proton-hydrogen collisions. *Physics Letters A* 115(1,2): 37.

Hydrogen, Momentum transfer, K-shell electrons, Gas

The upper limit of momentum transfer by a proton to K-shell electrons is calculated in a restricted three-body classical model. The model shows that the infinite upper limit used in practice, is generally good except for low energy protons passing through an extremely rarefied gas.

Xu, Y. J., Khandelwal, G. S., and Wilson, J. W. (1989) Charge Exchange Transition Probability for Collisions Between Unlike Ions and Atoms Within the Adiabatic Approximation. NASA Technical Memorandum 101559.

Charge exchange, Adiabatic approximation

A simple formula for the transition probability for electron exchange between unlike ions and atoms is established within the adiabatic approximation by employing the Linear Combination of Atomic Orbitals (LCAO) method. The formula also involves an adiabatic parameter, introduced by Massey, and thus the difficulties arising from the internal energy defect and the adiabatic approximation are avoided. Specific reaction $\text{Li}^{3+} + \text{H}^+$ and $\text{Be}^{4+} + \text{H} \rightleftharpoons \text{Be}^{3+} + \text{H}^+$ are considered as examples. The calculated capture cross section results of the present work are compared with the experimental data and with the calculation of other authors over the velocity range of 10^7 cm/sec to 10^8 cm/sec.

1.2. NUCLEAR SCIENCE

REPORTS/MEETINGS

Meador, W. E. and Townsend, L. W. (1988) Local Time Displacement as a Symmetry of Nature in Flat Space-Time. NASA Technical Memorandum 100610.

Relativity

Local time displacement is shown to be a true symmetry of Minkowskian physics, thereby demonstrating the empirical equivalence of different choices of the clock synchronization parameter in generalized Lorentz transformations.

1.2.1. THEORY

JOURNALS

Badavi, F. F., Townsend, L. W., Wilson, J. W., and Norbury, J. W. (1987) An algorithm for a semiempirical nuclear fragmentation model. *Computer Physics Communications* 47: 281-294.

Heavy ion fragmentation, Cross sections, Fragmentation model

Interactive program NUCFRAG presents an algorithm for an abrasion/ablation model of heavy ion fragmentation which includes a second order correction for the surface energy term and addition of photonuclear dissociation to provide reasonable representation of the present elemental fragmentation cross sections. Using the Weizsacker-Williams method of virtual quanta, the photodissociation fragmentation cross sections are calculated and added to the nuclear fragmentation cross sections generated by an abrasion/ablation model of heavy ion collision. The photodissociation cross sections are calculated for one nucleon removal only (either a proton or neutron). The nuclear interaction fragmentation cross sections are not calculated for target fragments and peripheral collisions with $\Delta A < 0.5$. On C.D.C. - Cyber/750 at NASA Langley Research Center, compilation takes about 20-30 seconds, while execution about 60-90 seconds.

Cucinotta, F. A., Khandelwal, G. S., Townsend, L. W., and Wilson, J. W. (1989) Correlations in an α - α scattering and semi-classical optical models. *Physics Letters B* 223: 127-132.

Alpha-alpha correlation, Optical models, Coupled-channel equations

We show the equivalence of semi-classical solutions to optical model coupled-channel equations derived from Watson's form of the nucleus-nucleus multiple-scattering series to the Glauber multiple-scattering series. A second-order solution to the semi-classical coupled-channel elastic amplitude is shown to be nearly equivalent to a second-order optical-phase-shift approximation to the Glauber amplitude if the densities of all nuclear excited states are approximated by the ground-state density. Using the Jastrow method to model the two-body density we find an average excited-state density to be of negligible importance in the double-scattering region of α - α scattering.

Gross, F., Maung, K. M., Tion, J. A., Townsend, L. W., and Wallace, S. J. (1989) Pseudoscalar π -N coupling and relativistic proton-nucleus scattering. *Physical Review C* 40: R10-R12.

Protons, Elastic scattering, Two-body relativistic equation

Relativistic p - ^{40}Ca elastic scattering observables are calculated using relativistic NN amplitudes obtained from the solution of a two-body relativistic equation. Results at 200 MeV are presented for three sets of NN amplitudes, two with pure pseudovector coupling for the pion and one with a 25% admixture of pseudoscalar coupling. Differences between the predictions of these three models provide a measure of the uncertainty in constructing Dirac optical potentials from NN amplitudes.

Norbury, J. W., Cucinotta, F. A., Townsend, L. W., and Badavi, F. F. (1988) Parameterized cross sections for Coulomb dissociation in heavy-ion collisions. *Nuclear Instruments and Methods in Physics Research* B31: 535-537.

Coulomb dissociation, Heavy-ion collisions

Simple parameterizations of Coulomb dissociation cross sections for use in heavy-ion transport calculations are presented and compared to available experimental dissociation data. The agreement between calculation and experiment is satisfactory considering the simplicity of the calculations.

Norbury, J. W. (1990) Electric quadrupole excitations in relativistic nucleus-nucleus collisions. *Physical Review C* 42: 711-714.

Electric quadrupole excitations, Heavy-ion collisions

Calculations are presented for electric quadrupole excitations in relativistic nucleus-nucleus collisions. The theoretical results are compared to an extensive data set and it is found that electric quadrupole effects provide substantial corrections to cross sections, especially for heavier nuclei.

Townsend, L. W. and Wilson, J. W. (1988) Comment on "trends of total reaction cross sections for heavy ion collisions in the intermediate energy range." *Physical Review C* 37: 892-893.

Heavy-ion collisions, Total reaction cross sections

The energy-dependent, semiempirical, surface transparency factor of Kox, *et al.*, is accurately represented by a simple analytical expression. Total reaction cross sections obtained using this parametrization agree with Kox's predictions to within four percent.

Townsend, L. W. and Wilson, J. W. (1989) Nuclear cross sections for estimating secondary radiations produced in spacecraft. Presented at the Conference on High Energy Radiation Background in Space (CHERBS 87), Sanibel Island, FL, November 3-5, 1987. AIP Conference Proceedings No. 186, Eds. A. C. Rester, Jr. and J. I. Trombka (American Institute of Physics, New York, 1989), pp. 177-180.

Cross sections, Transport calculations, Electromagnetic dissociation

Methods for estimating nuclear absorption (reaction) and breakup (fragmentation) cross sections for space radiation transport calculations are presented, and comparisons with experimental data are

made. For the fragmentation problem, the importance of electromagnetic dissociation is discussed and calculational methods described.

Wilson, J. W., Townsend, L. W., and Badavi, F. F. (1987) A semiempirical nuclear fragmentation model. *Nuclear Instruments and Methods in Physics Research B18*: 225-231.

Abrasion/Ablation, Heavy ion fragmentation

An abrasion/ablation model of heavy ion fragmentation is derived which includes a second order correction for the surface energy term and provides a reasonable representation of the present elemental fragmentation cross sections. The full development of the model must await the resolution of disagreement among different experiments and an expansion of the experimental data base to a broader set of projectile-target combinations.

Wilson, J. W. and Townsend, L. W. (1989) Nucleon interaction data bases for background estimates. Presented at the Conference on High Energy Radiation Background in Space (CHERBS 87), Sanibel Island, FL, November 3-5, 1987. AIP Conference Proceedings No. 186, eds. A. C. Rester, Jr. and J. I. Trombka (American Institute of Physics, New York, 1989), pp. 192-202.

Nucleon cross sections, Transport codes

Nucleon interaction data bases available in the open literature are examined for potential use in a recently developed nucleon transport code. Particular attention is given to secondary particle penetration and the multiple charged ion products. A brief description of the transport algorithm is given.

1.2.1. THEORY

REPORTS/MEETINGS

Badavi, F. F., Norbury, J. W., Wilson, J. W., and Townsend, L. W. (1988) Accuracy of Analytic Energy Level Formulas Applied to Hadronic Spectroscopy of Heavy Mesons. NASA Technical Memorandum 4042.

Potential models, Mesons, Quarks, Energy levels

In this work, linear and harmonic potential models are used in the nonrelativistic Schrödinger equation to obtain particle mass spectra for mesons as bound states of quarks. The main emphasis is on the linear potential where exact solutions of the S -state ($l=0$) eigenvalues and eigenfunctions and the asymptotic solution for the higher order partial waves ($l>0$) are obtained. A study of the accuracy of two analytical energy level formulas (Cornwall and Sheehy and Von Baeyer) as applied to heavy mesons is also included. Cornwall's formula is found to be particularly accurate and useful as a predictor of heavy quarkonium states. Exact solution for all partial waves of eigenvalues and eigenfunctions for a harmonic potential is also obtained and compared with the calculated discrete spectra of the linear potential. Detailed derivations of the eigenvalues and eigenfunctions of the linear and harmonic potentials are presented in appendixes.

Buck, W. W., Wilson, J. W., Townsend, L. W., and Norbury, J. W. (1987) Possible Complementary Cosmic-Ray Systems: Nuclei and Antinuclei. NASA Technical Paper 2741.

Galactic cosmic rays, Antinuclei, Microlesions

Arguments are presented for the possible existence of antinuclei of charge $|Z| > 2$ and, particularly, galactic cosmic antinuclei. Theoretical antinucleus-nucleus optical model cross sections are calculated and presented for the first time. A brief review of the nucleon-antinucleon interaction is also presented and its connection with the antinucleus-nucleus interaction is made. The predicted cross sections are smooth and show no structure. Finally, the findings are tied together with the formation of microlesions in living tissue.

Cucinotta, F. A., Khandelwal, G. S., Maung, K. M., Townsend, L. W., and Wilson, J. W. (1988) Eikonal Solutions to Optical Model-Coupled Channel Equations. NASA Technical Paper 2830.

Eikonal optical model, Total cross sections, Reaction cross sections

Methods of solution are presented for the eikonal form of the nucleus-nucleus coupled-channel scattering amplitudes. Analytic solutions are obtained for the second-order optical potential for elastic scattering. A numerical comparison is made between the first- and second-order optical model solutions for elastic and inelastic scattering of ^1H and ^4He on ^{12}C . The effects of bound-state excitations on total and reaction cross sections are also estimated.

Cucinotta, F. A., Khandelwal, G. S., Townsend, L. W., and Wilson, J. W. (1988) Correlations and density of excited states in particle scattering. Abstract presented at the Spring Meeting of the American Physical Society, Baltimore, MD, April 18-21, 1988. *Bulletin of the American Physical Society* 33: 1101.

Correlations, Excited states, Coupled-channel equations, Total cross sections

The effects of short-range correlations and deviations of an average ^4He excited state density from the ground state density in medium energy α -nucleus scattering are estimated using semi-classical solutions to optical model coupled-channel equations derived from Watson's form of the nucleus-nucleus multiple scattering series. Calculations are compared to experimental measurements of elastic angular distributions and total and reaction cross sections and Glauber model calculations.

Cucinotta, F. A., Khandelwal, G. S., Maung, K. M., Townsend, L. W., Wilson, J. W., and Norbury, J. W. (1987) Eikonal solutions to optical model coupled channel equations for 1 GeV p - ^{12}C and 1 GeV/nucleon ^4He - ^{12}C scattering. Abstract presented at the Fall 1987 Division of Nuclear Physics Meeting, New Brunswick, NJ, October 15-17, 1988. *Bulletin of the American Physical Society*, 32: 1567-1568.

Coupled-channel equations, Optical models, Eikonal approximation, Total cross sections

Coupled channel Schrodinger equations derived under high energy, optical model considerations are solved in the eikonal approximation. A similarity transformation allows us to sum an infinite series, equivalent to the infinite order multiple scattering series in the eikonal limit, for each scattering amplitude of our channel space. We investigate corrections to the coherent approximation for the elastic channel and obtain non-perturbative, analytic solutions for inelastic channels. Applications are made to 1 GeV p - ^{12}C scattering and 1 GeV/A ^4He - ^{12}C scattering.

Cucinotta, F. A., Norbury, J. W., Khandelwal, G. S., and Townsend, L. W. (1987) Doubly Differential Cross Sections for Galactic Heavy-Ion Fragmentation. NASA Technical Paper 2659.

Heavy ion fragmentation, Differential cross sections, Galactic cosmic rays

An abrasion-ablation T-matrix formulation is applied to the calculation of doubly differential cross sections in projectile fragmentation of 2.1 GeV/nucleon ^{16}O on ^9Be and 86 MeV/nucleon ^{12}C on ^{12}C and ^{108}Ag . An exponential parameterization of the ablation T-matrix is used and the total width of the intermediate states is taken as a parameter. Fitted values of the total width to experimental results are used to predict the lifetime of the ablation stage and indicate a decay time on the order of 10^{-19} s.

Cucinotta, F. A., Norbury, J. W., and Townsend, L. W. (1988) Multiple Nucleon Knockout by Coulomb Dissociation in Relativistic Heavy-Ion Collisions. NASA Technical Memorandum 4070.

Coulomb dissociation, Weizsäcker-Williams method, Nucleon knockout

The Coulomb dissociation contributions to fragmentation cross sections in relativistic heavy-ion collisions, in which more than 1 nucleon is removed, are estimated using the Weizsäcker-Williams method of virtual quanta. Photonuclear cross sections taken from experimental results are folded into target photon-number spectra calculated with the Weizsäcker-Williams method. Calculations for several projectile-target combinations are reported over a wide range of charge numbers and a wide range of incident projectile energies. These results suggest that a multiple nucleon emission process (knockout) by the Coulomb field is of negligible importance in galactic heavy-ion studies for projectiles lighter than ^{56}Fe .

Cucinotta, F. A., Townsend, L. W., Wilson, J. W., and Norbury, J. W. (1990) Coupled channel effects in high-energy alpha particle fragmentation on nuclear targets. Abstract presented at the Fall 1990 Division of Nuclear Physics Meeting, Urbana-Champaign, IL, October 25-27, 1990 (*Bulletin of the American Physical Society*).

Coupled channel, Differential cross sections, Alpha particles

Double differential cross-sections for the two-body dissociation of alpha particles are calculated in the high energy optical model of nuclear multiple scattering. Momentum distributions for forward scattered fragments are often evaluated using a participant-spectator model or the DWBA. Using the high energy optical model, we estimate the importance of coupled channel effects on predictions of inclusive momentum distributions and their role in determining the large momentum components of the two-body overlap functions from small angle data. For elastic fragmentation, interference effects between participant and spectator interactions are shown to be non-negligible for forward scattered fragments.

Khan, F., Khandelwal, G. S., Wilson, J. W., Townsend, L. W., and Norbury, J. W. (1987) Momentum transfer in relativistic heavy ion collisions. Abstract presented at the Annual Meeting of the Virginia Academy of Sciences, Norfolk, VA, May 20-22, 1987. *Virginia Journal of Science* 38: 70.

Relativistic heavy ion, Momentum transfer

Momentum (and Excitation Energy) transfer in Heavy Ion Collisions is investigated assuming an impulsive excitation mechanism. Interaction Representation is used; in the limit of $t_{\text{collision}} \ll t_{\text{nucleonic motion}}$, it is shown that momentum transfer is determined by the "Optical Potential" of the projectile. Assuming constant velocity, momentum transfer is transverse (ΔP_{\perp}). When "constant velocity" assumption is relaxed, it is shown how to obtain momentum transfer (ΔP_{\parallel}) parallel to the beam.

Khan, F., Khandelwal, G. S., Wilson, J. W., Townsend, L. W., and Norbury, J. W. (1988) Excitation-decay contribution to fragment production compared for the reactions [$^{12}\text{C}, ^{11}\text{B} + \text{P}$] and [$^{16}\text{O}, ^{15}\text{N} + \text{P}$] at 1.05 A GeV and 2.1 A GeV on ^{12}C target. Abstract presented at the Spring Meeting of the American Physical Society, Baltimore, MD, April 18-21, 1988 *Bulletin of the American Physical Society* 33: 963.

Fragment production, Inclusive cross section, Impulse approximation

An impulsive excitation formalism is utilized to show the dependence of fragment production cross section on incident energy per nucleon for the reaction ($^{12}\text{C}, ^{11}\text{B} + \text{P}$) on a ^{12}C target. Excitation-decay of projectile fragments was previously shown to be consistent with the inclusive cross section at 2.1 A GeV. Similar analysis are performed for 1.05 A GeV incident energy. These results are compared with the reaction ($^{16}\text{O}, ^{15}\text{N} + \text{P}$) at 1.05 and 2.1 A GeV, respectively, and cross sections predicted for the direct step of the reaction. These will be compared with experimental data from the BEVALAC when they become available.

Khan, F., Khandelwal, G. S., Wilson, J. W., Townsend, L. W., and Norbury, J. W. (1988) Momentum downshifts of projectile fragments in ^{12}C fragmentation at 2.1 A GeV on Be, C, Al, Cu, Ag, and Pb targets. Abstract presented at the 1988 Annual Meeting of the Southeastern Section of the American Physical Society, Raleigh, NC, November 10-12, 1988. *Bulletin of the American Physical Society* 33: 2193.

Projectile fragmentation, Momentum transfer, NUCFRAG

In the Bevalac experiments on ^{12}C fragmentation on various targets at 2.1 A GeV, it was observed that the longitudinal momentum distribution of the projectile fragments showed a mean momentum downshift $\langle P_{11} \rangle$ less than the projectile momentum. We have developed a model of momentum transfer in an impulsive excitation picture between relativistic heavy ions. Guided by the impact parameters from the semi-empirical code NUCFRAG, we have been able to calculate mean momentum downshifts for C, B, Be, Li fragments produced in the collision of ^{12}C on Be, C, Al, Cu, Ag, Pb targets - at 2.1 A GeV. Results will be shown and possible energy dependence will be discussed.

Hong, B. S., Maung, K. M., Wilson, J.W., and Buck, W. W. (1989) Kaon-Nucleus Scattering. NASA Technical Paper 2920.

Kaon, Optical potential, Eikonal approximation, Total cross sections, Absorptive cross sections

The derivations of the Lippmann-Schwinger equation and the Watson multiple-scattering series are given. A simple optical potential is found to be the first term of that series. The number density distribution models of the nucleus, harmonic well and Woods-Saxon are used with our t -matrix taken from the scattering experiments. The parameterized two-body inputs, which are kaon-nucleon total cross sections, elastic slow parameters, and the ratio of the real to the imaginary part of the forward elastic scattering amplitude, are presented. The eikonal approximation was chosen

as our solution method to estimate the total and absorptive cross sections for the kaon-nucleus scattering.

Maung, K. M., Townsend, L. W., and Deutchman, P. A. (1987) Corrections to the impulse approximation of the first-order optical potential. Abstract presented at the Fall Meeting of the Division of Nuclear Physics, New Brunswick, NJ, April 20-23, 1987. *Bulletin of the American Physical Society* 32: 1566.

Optical potential

Corrections to the t_p approximation of the first-order optical potential are discussed. Calculations will be presented for both the Watson and KMT formalisms.

Norbury, J. W., Deutchman, P. A., Townsend, L. W., and Cucinotta, F. A. (1988) A General Formalism for Phase Space Calculations. NASA Technical Paper 2843.

Phase spaces, Heavy-ion collisions

General formulas for calculating the interactions of galactic cosmic rays with target nuclei are presented. Methods for calculating the appropriate normalization volume elements and phase space factors are presented. Particular emphasis is placed on obtaining correct phase space factors for two- and three-body final states. Calculations for both Lorentz-invariant and noninvariant phase spaces are presented.

Norbury, J. W. and Townsend, L. W. (1990) Calculation of Two-Neutron Multiplicity in Photonuclear Reactions. NASA Technical Paper 2968.

Neutrons, Photonuclear reactions, Heavy-ion collisions

The most important particle emission processes for electromagnetic excitations in nucleus-nucleus collisions are the ejection of single neutrons and protons and also pairs of neutrons and protons. Methods are presented for calculating two-neutron emission cross sections in photonuclear reactions. The results are in a form suitable for application to nucleus-nucleus reactions.

Norbury, J. W., Townsend, L. W., and Badavi, F. F. (1988) Computer Program for Parameterization of Nucleus-Nucleus Electromagnetic Dissociation Cross Sections. NASA Technical Memorandum 4038.

Electromagnetic dissociation, Cross sections

A computer subroutine parameterization of electromagnetic dissociation cross sections for nucleus-nucleus collisions is presented that is suitable for implementation in a heavy ion transport code. The only inputs required are the projectile kinetic energy and the projectile and target charge and mass numbers.

Wilson, J. W., Townsend, L.W., Buck, W. W., Chun, S. Y., Hong, B. S., and Lamkin, S. L. (1988) Nucleon-Nucleus Interaction Data Base: Total Nuclear and Absorption Cross Sections. NASA Technical Memorandum 4053.

Neutron total cross sections, Absorptive cross sections, Differential cross sections

Neutron total cross sections are represented for Li to Pu targets at energies above 0.1 MeV and less than 100 MeV using a modified nuclear Ramsauer formalism. The formalism is derived for energies above 100 MeV by fitting theoretical cross sections. Neutron absorption cross sections are represented by analytic expressions of similar form, but shape resonance phenomena of the Ramsauer effect are not present. Elastic differential cross sections are given as a renormalized impulse approximation. These cross section data bases will be useful for nucleon transport applications.

1.2.2. EXPERIMENTAL

JOURNALS

Bastid, N., Alard, J. P., Arnold, J., Augerat, J., Babinet, R., Biagi, F., Brochard, F., Crouau, M., Charmensat, P., Dupieux, P., Fodor, Z., Fraysse, L., Girard, J., Gorodetzky, P., Gosset, J., Laspalles, C., Lemaire, M. C., Le Merdy, A., L'Hote, D., Lucas, B., Marroncle, J., Montarou, G., Parizet, M. J., Poitou, J., Qassoud, D., Racca, C., Rahmani, A., Schimmerling, W., Terrien, Y., and Valette, O. (1990) Exclusive measurements of light fragment production at forward angles in Ne-Pb and Ne-NaF collisions at $E/A = 400$ MeV and 800 MeV. *Nuclear Physics A506*: 637-654.

Light fragments, Diogene, Multiplicities, Production cross sections

Emission of light fragments at small angles is studied in relativistic heavy ion collisions using the Diogene plastic wall for both symmetrical and non-symmetrical target-projectile systems with 400 MeV per nucleon and 800 MeV per nucleon incident neon nuclei. Efficiency of multiplicity measurements in the small angle range for the selection of central or peripheral collisions is confirmed for asymmetric systems. Differential production cross sections of $Z = 1$ fragments show evidence for the existence of two emitting sources. The apparent temperature of each source is obtained from comparison with a thermodynamical model.

Brechtmann, C., Heinrich, W., and Benton, E. V. (1989) Fragmentation cross sections of ^{28}Si at 14.5 GeV/nucleon. *Physical Review C* 39(6): 2222-2226.

^{28}Si , Plastic nuclear track detectors, Charge changing cross sections, Partial cross sections, Electromagnetic dissociation, Fragmentation

We used CR39 plastic nuclear track detectors ($\text{C}_{12}\text{H}_{18}\text{O}_7$) in combination with automatic track measurement techniques to determine total charge changing and partial cross sections for the production of fragments of charge $Z_F=6$ to $Z_F=13$ in collisions of ^{28}Si beam nuclei at 14.5 GeV/nucleon in targets H, C, CR39, ($\text{C}_{18}\text{H}_{38}\text{O}$), Al, Cu, Ag, and Pb. By application of factorization rules, measured partial cross sections are separated into pure nuclear and electromagnetic components. The cross sections for electromagnetic dissociation agree with theoretical models. The results are consistent with a Z^2 dependence of virtual photon spectra.

Dudkin, V. E., Kovalev, E. E., Nefedov, N. A., Antonchik, V. A., Bogdanov, S. D., Ostroumov, V. I., Crawford, H. J., and Benton, E. V. (1990) Multiplicities of secondaries in interactions of 1.8 GeV/nucleon ^{56}Fe nuclei with photoemulsion and the cascade evaporation model. *Nuclear Physics A509*: 783-799.

Multiplicities, ^{56}Fe nuclei, Emulsion, Cascade, Evaporation model, Inelastic interactions

A nuclear photographic emulsion method was used to study the charge-state, ionization, and angular characteristics of secondaries produced in inelastic interactions of ^{56}Fe nuclei at 1.8 GeV/nucleon with H, CNO, and AgBr nuclei. The data obtained are compared with the results of calculations made in terms of the Dubna version of the cascade evaporation model (DCM). The DCM has been shown to satisfactorily describe most of the interaction characteristics for two nuclei in the studied reactions. At the same time, quantitative differences are observed in some cases.

Dupieux, P., Alard, J. P., Augerat, J., Babinet, R., Bastid, N., Brochard, F., Charmensat, P., De Marco, N., Fanet, H., Fodor, Z., Fraysse, L., Girard, J., Gorodetzky, P., Gosset, J., Laspalles, C., Lemaire, M. C., L'Hote, D., Lucas, B., Marroncle, J., Montarou, G., Parizet, M. J., Poitou, J., Qassoud, D., Racca, C., Rahmani, A., Schimmerling, W., and Valette, O. (1988) Proton-proton correlations at small relative momentum in neon-nucleus collisions at $E/A = 400$ and 800 MeV. *Physics Letters B* 200: 17-21.

Proton-proton correlations, Neon, Diogene

Proton-proton small angle correlations have been measured in neon-nucleus collisions, using the 4π detector Diogene, at 400 and 800 MeV per nucleon incident energies. Values of the size of the emitting region are obtained by comparison with the Koonin formula, taking into account the biases of the apparatus. The dependence of the density on target mass and incident energy is also analysed.

Hoffmann, A., Brechtmann, C., Heinrich, W., and Benton, E. V. (1988) Search for projectile fragments with fractional charge in relativistic heavy ion collisions. *Physics Letters B* 200(4): 583-586.

Plastic nuclear track detectors, Fractional charge, Oxygen, Projectile fragments

We measured the charge of about 35,000 projectile fragments with $Z \geq 5e$ produced by 14.5 GeV/nucleon and 200 GeV/nucleon ^{16}O beams in a Pb target using CR39 plastic nuclear track detectors. A minimum track length of 3 mm in the detector without nuclear interaction was required. No evidence for fragments carrying a fractional charge was found.

L'Hote, D., Alard, J. P., Augerat, J., Babinet, R., Brochard, F., Fodor, Z., Fraysse, L., Girard, J., Gorodetzky, P., Gosset, J., Laspalles, C., Lemaire, M. C., Lucas, B., Montarou, G., Parizet, M. J., Poitou, J., Racca, C., Schimmerling, W., Tamain, J. C., Terrien, Y., and Valero, J. (1987) Exclusive measurements of mean pion multiplicities in ^4He -nucleus reactions from 200 to 800 MeV/nucleon. *Physics Letters B* 198: 139-142.

Central collisions, Diogene, Pion production

Mean multiplicities of π^+ and π^- in ^4He collisions with C, Cu, and Pb at 200, 600, and 800 MeV/u, and with C and Pb at 400 MeV/u have been measured using the large solid angle detector Diogene. The dependence of pion multiplicity on projectile incident energy, target mass and proton multiplicity is studied in comparison with intra-nuclear cascade predictions. The discrepancy between experimental results and theory is pointed out and discussed.

Parizet, M. J., Alard, J. P., Rahmani, A., Montarou, G., Augerat, J., Bastid, N., Demaison, P., Dupieux, P., Fraysse, L., Marroncle, J., Raha, S., Babinet, R., Fodor, Z., Gosset, J., L'Hote, D., Poitou, J., Schimmerling, W., Terrien, Y., Valette, O., Lemaire, M. C., Gorodetzky, P., and Racca, C. (1989) Proton production in relativistic heavy ion collisions: Comparison with a thermodynamical model. *International Journal of Modern Physics A* 4: 3689-3703.

Proton production, Diogene, Alpha particles

Experimental results concerning proton production in nuclear collisions, obtained at a Saturne with the Diogene 4- π facility, are compared with the predictions of a thermodynamical model, using collective velocity distributions combined with a statistical thermodynamics in local rest frames. Experimental differential cross sections for alpha + nucleus and neon + nucleus central collisions at incident energies between 200 and 800 MeV per nucleon are well reproduced by the model, for an angular range 30-110 degrees in the laboratory system. Extracted values of the temperatures are compared with those given by other authors.

Wong, M., Schimmerling, W., Phillips, M. H., Ludewigt, B. A., Landis, D. A., Walton, J. T., and Curtis, S. B. (1990) The multiple Coulomb scattering of very heavy charged particles. *Medical Physics* 17(2): 163-171.

Multiple Coulomb scattering, Heavy ions

An experiment was performed at the Lawrence Berkeley Laboratory BEVALAC to measure the multiple Coulomb scattering of 650-MeV/A uranium nuclei in 0.19 radiation lengths of a Cu target. Differential distributions in the projected multiple scattering angle were measured in the vertical and horizontal planes using silicon position-sensitive detectors to determine particle trajectories before and after target scattering. The results were compared with the multiple Coulomb scattering theories of Fermi and Moliere, and with a modification of the Fermi theory, using a Monte Carlo simulation. These theories were in excellent agreement with experiment at the 20 level. The best quantitative agreement is obtained with the Gaussian distribution predicted by the modified Fermi theory.

1.2.2. EXPERIMENTAL

REPORTS/MEETINGS

Khan, F., Khandelwal, G. S., Townsend, L. W., and Wilson, J. W. (1990) Resonant excitation of vibrational levels as the origin of positron peaks. Presented at the 1990 International Conference on Particles and Nuclei (PANIC XII), Cambridge, MA, June 25-29, 1990.

Heavy-ion collisions, Positrons

Resonant excitation of vibrational levels is proposed as a possible mechanism that may explain the observation of anomalous positron peaks from positron bombardment of thorium as well as the famous heavy-ion collision GSI peaks. In the latter case, existence of a "nuclear quasimolecule" formed during the collision of the high-Z nuclei near the Coulomb barrier is assumed. The excitation function for the above process is derived from a model Hamiltonian. The peak in e^+ -Th scattering is reproduced with experimental data on collective (beta, gamma) modes in Th. Systematics of target dependence are explored in some detail. The extension of the above ideas to

the GSI peaks is shown to be compatible with the existence of "nuclear molecules" at these bombarding energies and the resonant excitation of their vibrational levels. Probes other than e^+ are discussed. An interesting consequence of the above explanation may be that not every e^+ and e^- peak from high-Z targets is correlated.

Mitchell, J. W., Guzik, T. G., Wefel, J. P., Crawford, H. J., Engelage, J., Lindstrom, P. J., Schimmerling, W., and Symons, T. J. M. (1987) Projectile fragmentation of ^{16}O at medium energies. Abstract presented at the General Meeting of the Division of Nuclear Physics, New Brunswick, NJ, April 20-23, 1987. *Bulletin of the American Physical Society* 32: 1109.

Projectile fragmentation, Heavy ions, Cross sections

The production of projectile-like fragments has been investigated for ^{16}O beams incident on ~ 1 gm/cm², C, and CH₂ targets with energies of 170, 255, and 360 MeV/n, using a solid-state isotope identification telescope at the Bevalac. The longitudinal and transverse momentum distributions of the principal fragments are measured and are compared to results obtained at other energies and to theoretical models. Partial projectile fragmentation cross sections are determined for both target materials and for hydrogen (by CH₂ - C subtraction). These are compared to data available at higher and lower energies and from other target materials as well as to semi-empirical calculations.

1.3. SPACE RADIATION

1.3.1. COSMIC RAY AND ASTROPHYSICS

JOURNALS

Letaw, J. R., Share, G. H., Kinzer R. L., Silberberg, R., Chupp, E. L., Forrest, D. J., and Rieger, E. (1989) Satellite observation of atmospheric nuclear gamma radiation. *Journal of Geophysical Research* 94: 1211-1221.

Gamma radiation, Gamma NKW, Solar maximum mission, Compton scattering

We present a satellite observation of the spectrum of gamma radiation from the Earth's atmosphere in the energy interval from 300 keV to 8.5 MeV. The data were accumulated by the gamma ray spectrometer on the Solar Maximum Mission over 3.5 years, from 1980 to 1983. The excellent statistical accuracy of the data allows 20 atmospheric line features to be identified. The features are superimposed on a continuum background which is modeled using a power law with index -1.16. Many of these features contain a blend of more than one nuclear line. All of these lines (with the exception of the 511-keV annihilation line) are Doppler broadened. Line energies and intensities are consistent with production by secondary neutrons interacting with atmospheric ^{14}N and ^{16}O . Although we find no evidence for other production mechanisms, we cannot rule out significant contributions from direct excitation or spallation by primary cosmic ray protons. The relative intensities of the observed line features are in fair agreement with theoretical models; however, existing models are limited by the availability of neutron cross sections, especially at high energies. The intensity and spectrum of photons at energies below the 511-keV line, in excess of a power law continuum, can be explained by Compton scattering of the annihilation line photons in traversing an average of about $\sim 21 \text{ g cm}^{-2}$ of atmosphere.

Silberberg, R., Leising, M. D., and Murphy, R. J. (1989) Gamma-ray lines from nucleosynthesis and from cosmic-ray and solar-flare particle interactions. In: *Cosmic Gamma Rays, Neutrinos, and Related Astrophysics*, Eds. M. M. Shapiro and J. P. Wefel. Kluwer Academic Publishers, pp. 289-319.

Solar flare, Gamma-ray lines, Cobalt decay lines, Positrons ionization

Gamma-ray lines provide a versatile probe for sites of nuclear reactions in astrophysical objects. Two sets of nuclear reactions can be explored: (1) build-up reactions of atomic nuclei from lighter constituents (nucleosynthesis), and (2) break-up of heavier nuclei in nuclear spallation reactions, including nuclear excitation reactions. Nucleosynthesis occurs in presupernova stars, in supernova events (e.g., explosive carbon and oxygen burning and silicon burning) and in novae (explosive hydrogen burning). Spallation reactions occur when cosmic rays interact in interstellar clouds, in the galactic gas towards the regions of the galactic center, and with matter near their acceleration sites. Spallation and nuclear excitation are also induced by solar-flare particles. Recent experimental observations include solar lines of several elements observed at the time of the large 27 April 1981 flare and from several other flares, the galactic ^{26}Al line, the e^+ annihilation line from an extended region about the galactic center, and the ^{56}Co decay lines from Supernova 1987A in the Large Magellanic Cloud.

1.3.2. ENVIRONMENTS AND ENVIRONMENTAL MODELS

JOURNALS

Konradi, A., Hardy, A. C., and Atwell, W. (1987) Radiation environment models and the atmospheric cutoff. *Journal of Spacecraft and Rockets* 24: 284-285.

Electrons, Protons, Magnetic field models, AP-8, AE-8, Trapped radiation

Radiation environment models are widely used to predict radiation doses expected on a variety of space flight missions. In these models, omnidirectional electron and proton fluxes are stored in computer codes as functions of particle energies and the parameters B and L , where B is the local magnetic field intensity in Gauss and L is the McIlwain drift shell parameter. While trying to predict radiation doses expected at the space station orbit toward the end of this century, we discovered an artifact of the model that necessitates modifications in the standard method of their use. The following discussion explains this artifact and makes suggestions about how it can be avoided.

The most recent models are the AP-8 for protons and the AE-8 for electrons. Each of these models comes in two variants that incorporate different radiation intensities observed in the atmospheric cutoff region about the 1970 solar maximum (MAX) and about the 1964 solar minimum (MIN). During magnetically quiet periods, magnetic field models, based on the multipole expansion of the internal sources only, represent the Earth's field quite well up to L values of about 4. Experimental evidence indicates that the Earth's magnetic field is changing: the strength of the dipole is decreasing at about 0.09%/year and geomagnetic surface features are drifting westward at a rate of 0.27 deg/year. Thus, to allow a certain amount of temporal extrapolation, the models contain first-order and sometimes second-order time derivatives.

Wilson, J. W., Townsend, L. W., and Farhat, H. (1989) Cosmic-ray neutron albedo dose in low-Earth orbits. *Health Physics* 57: 665-668.

Neutron albedo, Low Earth-orbit, Quality factors

Soon after the discovery of the Van Allen radiations, diffusion of neutrons from the top of the Earth's atmosphere was suggested as a possible source of these trapped radiations (Hess 1959; Hess and Killeen 1961). Previously, atmospheric neutrons had been studied for nearly two decades (Bethe et al. 1940). Their biological significance was generally discounted (ICRP 1966) until Foelsche (1962, 1968) suggested, and it was later confirmed, that the fast neutron and the high-energy neutron components (Foelsche et al. 1974) had been underestimated in previous studies.

Estimates of neutron exposure in low-Earth orbit yield on the order of 0.01 Gyy⁻¹ or about 0.1 Sv_y⁻¹ using the ICRP Publication No. 6 quality factor (ICRP 1964). Recent suggestions that neutron quality factors should be increased (ICRU 1986) raise the importance of neutrons to space exposure estimates, and it now seems prudent to establish a neutron model environment. Extensive studies of atmospheric neutrons by the Langley Research Center (Foelsche et al. 1974; Korff et al. 1979) provide a basis for an Earth albedo neutron environmental model.

1.3.2. ENVIRONMENTS AND ENVIRONMENTAL MODELS

REPORTS/MEETINGS

Wilson, J. W., Khandelwal, G. S., Shinn, J. L., Nealy, J. E., Townsend, L. W., and Cucinotta, F. A. (1990) A simplified model for solar cosmic ray exposure in manned Earth orbital flights. NASA Technical Memorandum 4182.

Low Earth-orbit, Geomagnetic field model, Shuttle

A simple calculational model is derived for use in estimating solar cosmic ray exposure to critical body organs in low Earth orbit at the center of a large spherical shield of fixed thickness. The effects of the Earth's geomagnetic field and the astronauts' self-shielding are evaluated explicitly. The geomagnetic field model is an approximate tilted eccentric dipole with geomagnetic storms represented as an impressed uniform field. The storm field is related to the planetary geomagnetic index K_p . The Shuttle geometry is introduced into the resultant computer code using the Shuttle mass distribution surrounding two locations on the flight deck. The Shuttle is treated as pure aluminum and the astronaut as soft tissue. Short-term average fluence over a single orbit is calculated as a function of the location of the lines of nodes or long-term averages over all lines of nodes for a fixed inclination.

1.3.3. SOLAR ACTIVITY AND PREDICTION

REPORTS/MEETINGS

Nealy, J. E., Simonsen, L. C., Townsend, L. W., and Wilson, J. W. (1990) Deep-space radiation exposure analysis for solar cycle XXI (1975-1986). Presented at the 20th Annual Intersociety Conference on Environmental Systems (ICES), Williamsburg, VA, July 9-12, 1990. SAE Technical Paper Series #901347.

Radiation exposures, Shielding, Dose equivalent, Radiation dosimetry

Ionizing radiation exposures and associated dosimetric quantities are evaluated for the 11-year solar cycle ending in 1986. Solar flare fluences for the 55 largest flares occurring during the cycle are superimposed on the galactic cosmic ray flux. Published summaries of flare data from the Interplanetary Monitoring Platform (IMP)-7 and IMP-8 satellites are used and include flares whose integrated fluences are greater than 10^7 protons/cm² for energies in excess of 10 MeV. A standard cosmic ray environment model for ion flux values at solar minimum and maximum is invoked with an assumed sinusoidal variation between the lower and upper limits. The radiation shielding analysis is carried out for equivalent water-shield thicknesses between 2 and 15 g/cm². Results are expressed in terms of cumulative incurred dose equivalents for deep-space missions lasting between 3 months and 3 years. Since no predominantly large proton flares occurred during this period, this analysis should provide an approximate quantification of doses to be normally expected in the course of a long-duration interplanetary mission. It was found that medium-to-large flare contributions are of greatest importance for the shorter-term missions, while the galactic component dominates for the longer-duration missions. Predicted dose equivalents are presented for various mission durations within any portion of the solar cycle.

Townsend, L. W., Nealy, J. E., and Wilson, J. W. (1988) Preliminary Estimates of Radiation Exposures for Manned Interplanetary Missions from Anomalously Large Solar Flare Events. NASA Technical Memorandum 100620.

Radiation exposures, Solar flare, BRYNTRN, Depth doses, Dose equivalent, SEP, Solar energetic particles

Preliminary estimates of radiation exposures for manned interplanetary missions resulting from anomalously large solar flare events are presented. The calculations use integral particle fluences for the February 1956, November 1960, and August 1972 events as inputs into the Langley Research Center nucleon transport code BRYNTRN. This deterministic code transports primary and secondary nucleons (protons and neutrons) through any number of layers of target material of arbitrary thickness and composition. Contributions from target nucleus fragmentation and recoil are also included. Estimates of 5-cm depth doses and dose equivalents in tissue are presented behind various thicknesses of aluminum, water, and composite aluminum/water shields for each of the three solar flare events.

1.3.4. EXPERIMENTS

REPORTS/MEETINGS

Benton, E. V. and Heinrich, W. (Eds) (1990) *Ionizing radiation exposure of LDEF* (LDEF prerecovery estimates). Department of Physics, University of San Francisco: USF-TR-77.

LDEF, Induced radioactivity, Trapped protons, LET, Neutrons, Secondaries, Spallation products, Recoils

The Long Duration Exposure Facility (LDEF) was launched into orbit by the Space Shuttle *Challenger* mission 41C on April 5, 1984, and was deployed on April 8. The original altitude of the circular orbit was 258.5 nautical miles (479 km) with the orbital inclination being 28.5°. The 21,500 lb NASA Langley Research Center satellite, having dimensions of some 30 x 14 feet, was one of the largest payloads ever deployed by the Space Shuttle. LDEF carried 57 major experiments and remained in orbit five years and nine months (completing 32,422 orbits). It was retrieved by the Shuttle *Columbia* on January 11, 1990. The data and subsequent knowledge that will evolve from the analysis of the LDEF experiments is expected to bear heavily on the design and construction of Space Station Freedom and on other long-term, near-Earth orbital space missions. This publication provides a list of the radiation experiments that flew on LDEF, and describes preliminary results in the following areas: trapped particles and cosmic rays; predictions of LDEF fluxes and dose due to geomagnetically trapped protons and electrons; linear energy transfer spectra; neutrons, secondaries, spallation products and high-LET recoils; induced radioactivity in LDEF; and LDEF radiation exposure as projected from Shuttle missions.

1.4. RADIATION TRANSPORT AND SHIELDING

REPORTS/MEETINGS

Cucinotta, F., Hajnal, F., and Wilson, J. W. (1990) Energy deposition at the bone-tissue interface from nuclear fragments produced by high-energy nucleons. *Health Physics* 59: 819-825

Energy deposition, Bone-tissue interface, Nuclear fragments, High-energy nucleons

The transport of nuclear fragmentation recoils produced by high-energy nucleons in the region of the bone-tissue interface is considered. Results for the differential flux and absorbed dose for recoils produced by 1-GeV protons are presented in a bidirectional transport model. The energy deposition in marrow cavities is seen to be enhanced by recoils produced in bone. Approximate analytic formulae for absorbed dose near the interface region are also presented for a simplified range-energy model.

Townsend, L. W. and Wilson, J. W. (1987) Galactic heavy ion propagation through spacecraft. Invited lecture at the Natural Space Radiation and VLSI Technology Conference, Houston, TX, January 20-21, 1987. NASA CP-10023, pp. II-3-1 to II-3-10.

HZE, Galactic cosmic rays, Spacecraft shielding, Single-event upsets, Material degradation, Radiation dosimetry

As the radiations composing the HZE (high-energy heavy ion) component of galactic cosmic rays traverse a spacecraft, they undergo energy losses, nuclear breakup (fragmentation), and nuclear attenuation processes within the bulk matter comprising the vehicle's structure. As a result of these alterations in energy and composition, the radiation fields within the spacecraft interior may differ appreciably from the external environment. Currently, modern methods of HZE particle interaction and transport are being developed to evaluate the effects of these processes in spacecraft materials. These techniques, presented herein, have direct application to such diverse research topics as (1) single-event phenomena in microelectronic circuitry, (2) solar cell and structural material degradation, and (3) crew radiation dosimetry and shielding requirements. To illustrate the methods, representative calculations of HZE particle transport through nominal spacecraft thicknesses are presented. The results of these calculations show that, for missions beyond the Earth's magnetosphere, shielding thicknesses greater than 10 g/cm² appear to offer only minimal additional protection from galactic cosmic rays. For missions within the magnetosphere, low Z materials appear to be the shield material of choice.

Townsend, L. W., Wilson, J. W., Schimmerling, W., and Wong, M. (1987) Studies of HZE particle interactions and transport for space radiation purposes. Presented at the NASA Space Life Sciences Symposium: Three Decades of Life Science Research in Space, Washington, DC, June 21-26, 1987.

HZE, Space exploration, Radiation shielding, HZE interaction, Transport model

As the era of Space Station, lunar bases, and manned Mars missions approaches, cumulative radiation exposures of career astronauts to biologically significant levels of the high-energy heavy ion (HZE) component of solar and galactic cosmic rays will occur for the first time in the history of manned space flight. Since these HZE particles include nearly all nuclear species, and possess a very broad range of incident energies, considerable attention must be devoted to developing accurate methods of describing their physical interactions and transport through bulk matter in

order to properly assess spacecraft shielding effectiveness, and to evaluate the self-shielding factors of the astronauts' bodies themselves. As these extremely energetic cosmic rays traverse bulk matter, their radiation fields change composition through interactions with any target materials encountered. Aside from continuously losing energy through collisions with atomic orbital electrons, the incident ions collide with target nuclei within the shield and experience nuclear attenuation (absorption) and breakup (fragmentation) reactions. The struck target nuclei also recoil, leaving highly ionized tracks in their wakes. These interactions remove particles from the incident field while concomitantly producing secondary and subsequent generation reaction products. The altered composition of the transported field then results in an internal radiation field within some critical organ of the astronaut's body which differs appreciably from that incident upon the external spacecraft structure. Proper evaluation of the biological damage to this critical organ requires an adequate knowledge of the physical characterizations (energies and composition) of the complex radiation fields incident upon that organ. Studies of the physical transport and interactions of these space radiation fields are presently hampered by a paucity of experimental HZE interaction and transport data. Consequently, an experimental apparatus has been built to study the composition and spectra of heavy ion beams of different types as they pass through various materials of variable thickness. Sufficient measurements will be made to fully specify biologically interesting dosimetric quantities as a function of shield type and depth for each beam type. Because of the large numbers of projectile/target combinations and their nuclear fragmentation products, it is unreasonable to expect that experimental measurements alone will ever provide the necessary interaction and transport data. Therefore, experimentally validated calculational methods are needed to accurately describe them. To this end a NASA-supported collaborative research effort involving theoreticians at Langley Research Center (LaRC) and experimentalists at Lawrence Berkeley Laboratory (LBL) has been established to develop the necessary radiation physics methodologies for properly evaluating future HZE particle shielding and dosimetry requirements for manned space flight. In this presentation current and planned research efforts for the LaRC-LBL collaboration will be described.

Townsend, L. W., Wong, M., Schimmerling, W., and Wilson, J. W. (1987) Development of a nuclear data base for relativistic ion beams. IN: Health Physics of Radiation Generating Machines, Proceedings of the Twentieth Midyear Topical Symposium of the Health Physics Society, Reno, NV, February 8-12, pp. 451-458 (CONF-8602106).

Heavy ion reactions, Model development

The primary limitation on the development of heavy ion beam transport methods is the lack of an accurate nuclear data base. Because of the large number of ion/target combinations, the complexity of the reaction products, and the broad range of energies required, it is unlikely that the data base will ever be compiled from experiments alone. For the last 15 years, relativistic heavy-ion accelerators have been available, but the experimental data base remains inadequate. However, theoretical models of heavy-ion reactions are being derived to provide cross section data for beam transport problems. A concurrent experimental program to provide sufficient experimental data to validate the model is also in progress. Model development and experimental results for model validation will be discussed. The need for additional nuclear fragmentation data is identified.

1.4.1. THEORY AND MODEL DEVELOPMENT

JOURNALS

Wilson, J. W., and Badavi, F. F. (1986) Methods of galactic heavy ion transport. *Radiation Research* 108: 231-237.

Methods, Monte Carlo methods, Heavy ion transport, Boltzmann equation

Two methods of calculating the transition of galactic heavy ions in the Earth's atmosphere are compared with respect to accuracy, generality, and computer efficiency. The most general method is shown to have the highest accuracy and is a simple numerical procedure.

Wilson, J. W., Chun, S. Y., Buck, W. W., and Townsend, L. W. (1988) High energy nucleon data bases. *Health Physics* 55: 817-819.

Data bases, Protons, Monte Carlo, Intranuclear cascade

It is well established that 30% to 50% of the energy absorbed during human exposure to high-energy protons (>400 MeV) is due to secondary radiations produced in nuclear reactions. There are several transport codes for making exposure estimates and two primary data bases which are readily found in the open literature. The first such data base is an intranuclear cascade Monte Carlo derived data set (sometimes the intranuclear cascade code resides within the transport code itself), and the second is an empirical fit to experimental or theoretical cross sections. This note examines the relative differences in results attributable to these data bases.

Wilson, J. W. and Townsend, L.W. (1988) A benchmark for galactic cosmic-ray transport codes. *Radiation Research* 114: 201-206.

Benchmark solution, Galactic cosmic rays, Transport codes, Uncertainties

A nontrivial analytic benchmark solution for galactic cosmic-ray transport is presented for use in transport code validation. Computational accuracy for a previously developed cosmic-ray transport code is established to about 1% by comparison with this exact benchmark. Hence solution accuracy for the transport problem is limited mainly by inaccuracies in the input spectra, input interaction data bases, and the use of a straight-ahead/velocity-conserving approximation.

Wilson, J. W. and Townsend, L. W. (1988) Radiation safety in commercial air traffic: A need for further study. *Health Physics* 55:1001-1003.

ICRU, Exposure, Quality factors

Previous work at Langley Research Center on atmospheric radiation used quality factors, as defined by the International Commission for Radiological Protection (ICRP 1964), which are currently undergoing considerable revision. With the recent recommendation of a new quality factor by the International Commission for Radiological Measure and Units (ICRU 1986), it seems prudent to estimate the resulting changes in the radiation exposure rates in the Earth's atmosphere. As a result of the change in quality factor, it is found that worst case estimates of radiation exposure are now well above the exposure limits of the general population, and a reassessment of radiation impact on commercial aviation is needed if these proposed quality factors are adopted.

Wilson, J. W., Townsend, L. W., and Badavi, F. F. (1987) Galactic HZE propagation through the Earth's atmosphere. *Radiation Research* 109: 173-183.

Earth's atmosphere, HZE, Heavy ion

A comprehensive physical model for galactic heavy ion propagation is presented. The nuclear fragmentation model, is a simplified physical model, but contains the major processes of importance to galactic ions. Comparison is made to measurements of atmospheric ion fluence and the limitations of these comparisons are discussed.

Wilson, J. W., Townsend, L. W., Ganapol, B., Chun, S. Y., and Buck, W. W. (1988) Charged-particle transport in one dimension. *Nuclear Science and Engineering* 99: 285-287.

Transport codes, Boltzmann equation, Numerical solutions

A numerical solution to high-energy charged-particle transport is found by evaluation of the integral equations obtained by inverting the Boltzmann differential operator. An algorithm has been written for either continuous or discrete spectra at the boundary, which allows efficient and accurate evaluation of this rather complicated problem. Present results are compared with analytic solutions based on the perturbation theory.

Wilson, J. W., Townsend, L. W., and Khan, F. (1989) Evaluation of highly ionizing components in high-energy nucleon radiation fields. *Health Physics* 57: 717-724.

Fragment recoil, HZE

The data and models for nuclear fragment recoil distributions produced by high-energy nuclear events in tissue are reviewed. Results for linear energy transfer distributions in soft tissue are derived, and a simple model is developed for use in radiation studies and risk estimates.

Wilson, J. W., Townsend, L. W., Lamkin, S. L., and Ganapol, B. D. (1990) A closed form solution to HZE propagation. *Radiation Research* 122: 223-228.

Analytical solution, Transport codes

An analytical solution for high-energy heavy ion transport assuming straight-ahead and velocity-conserving interactions with constant nuclear cross-reactions is given in terms of a Green's function. The series solution for the Green's function is rapidly convergent for most practical applications. The Green's function technique can be applied with equal success to laboratory beams as well as to galactic cosmic rays allowing laboratory validation of the resultant space shielding code.

1.4.1. THEORY AND MODEL DEVELOPMENT

REPORTS/MEETINGS

Atwell, W., Beever, E. R., Hardy, A. C., and Cash, B. L. (1989) A radiation shielding model of the Space Shuttle for space radiation exposure estimations. Presented at Advances in Nuclear Engineering Computation and Radiation Shielding, American Nuclear Society, Santa Fe, NM, April 9-13, 1989.

Shuttle shielding model, Shuttle, Computerized anatomical man model, Dose equivalent

An analytical shielding model of the Space Shuttle has been developed for use in determining the expected space radiation dose exposures to astronauts and radiation-sensitive payloads and experiments for various Shuttle missions. The shielding model consists of approximately 2000 volume elements (geometrical shapes) that was constructed using engineering drawings, specification sheets, materials lists, and other available data. The Shuttle model is used as an input data file to the Elemental Volume Dose Program (EVDP) to compute the shield distribution about any location (dose point) in the spacecraft. Models of the naturally occurring space radiation and a computerized anatomical man model are used to compute the absorbed dose and/or dose equivalent for any mission scenario. The models and computational techniques are reviewed and discussed. A comparison of the Shuttle mission space radiation exposure calculations with measurements obtained from onboard active and passive dosimeters is discussed.

Ganapol, B. D., Townsend, L. W., and Wilson, J. W. (1989) Benchmark Solutions For the Galactic Heavy Ion Transport Equations: Energy and Spatially Dependent Problems. NASA Technical Paper 2878.

Transport codes, Benchmark solution, Analytical methods, Monoenergetic beams

Nontrivial benchmark solutions are developed for the galactic ion transport (GIT) equations in the straight-ahead approximation. These equations are used to predict potential radiation hazards in the upper atmosphere and in space. Two levels of difficulty are considered: (1) energy independent and (2) spatially independent. The analysis emphasizes analytical methods never before applied to the GIT equations. Most of the representations derived have been numerically implemented and compared with more approximate calculations. Accurate ion fluxes (to 3 to 5 digits) are obtained for nontrivial sources. For monoenergetic beams, both accurate doses and fluxes are found. The benchmarks presented herein are useful in assessing the accuracy of transport algorithms designed to accommodate more complex radiation protection problems. In addition, these solutions can provide fast and accurate assessments of relatively simple shield configurations.

Ganapol, B. D., Wilson, J. W., and Townsend, L. W. (1988) Benchmark solutions for the galactic ion transport equations. Invited lecture presented at the Annual Meeting of the American Nuclear Society, San Diego, CA, June 12-16, 1988. *Transactions of the American Nuclear Society* 56: 276-277.

Galactic cosmic rays transport, Model verification, Benchmark solution

In the upper atmosphere and in space, high-energy heavy ions called galactic cosmic rays originating in deep space or in our sun are the major ionizing particles. Not only is the unscattered radiation of concern, but also the secondary particles generated from direct nuclear or Coulombic fragmentation are responsible for a significant fraction of the absorbed dose. Thus, to ensure the proper shielding of space bases and interplanetary vehicles, reliable dose and flux computational models must be found. For this reason, the National Aeronautics and Space Administration has

initiated an effort to develop multidimensional deterministic methods to analyze proposed shield configurations. This paper discusses the partial verification of proposed ion transport algorithms obtained by comparisons to standard solutions -- benchmarks -- of the governing galactic ion transport (GIT) equations.

Nealy, J. E., Wilson, J. W., and Townsend, L. W. (1988) Solar-Flare Shielding with Regolith at a Lunar-Base Site. NASA Technical Paper 2869.

Solar flare shielding, Regolith, BRYNTRN, Lunar colony

The Langley Baryon Transport computer code BRYNTRN has been used to predict time-integrated radiation-dose levels at the lunar surface caused by high proton flux from solar flares. This study addresses the shielding requirements for candidate lunar habitat configurations necessary to protect crew members from large and unpredictable radiation fluxes. Three solar proton events have been analyzed, and variations in radiation intensity in a shield medium due to the various primary particle energy distributions are predicted. Radiation-dose predictions are made for various slab thicknesses of a lunar soil model. Results are also presented in the form of dose patterns within specific habitat configurations shielded with lunar material.

Nealy, J. E., Wilson, J. W., and Townsend, L. W. (1989) Preliminary analyses of space radiation protection for lunar base surface systems. Presented at the 19th Intersociety Conference on Environmental Systems (ICES), San Diego, CA, July 24-26, 1989. SAE Technical Paper Series #891487.

Galactic cosmic rays, HZE particles, Transport codes, Dose equivalent

Radiation shielding analyses are performed for candidate lunar base habitation modules. The study primarily addresses potential hazards due to contributions from the galactic cosmic rays (heavy ions). The NASA Langley Research Center's high energy nucleon and heavy ion transport codes are used to compute propagation of radiation through conventional and regolith shield materials. Computed values of linear energy transfer are converted to biological dose-equivalent using quality factors established by the International Commission on Radiological Protection. Spectral fluxes of heavy charged particles and corresponding dosimetric quantities are computed for a series of thicknesses in various shield media and are used as an input data base for algorithms pertaining to specific shielded geometries. Dosimetric results are presented as isodose contour maps of shielded configuration interiors. The dose predictions indicate that shielding requirements are substantial, and an abbreviated uncertainty analysis shows that better definition of the space radiation environment as well as improvement in nuclear interaction cross-section data can greatly increase the accuracy of shield requirement predictions.

Shinn, J. L., Wilson, J. W., and Nealy, J. E., and Cucinotta, F. A. (1990) Comparison of Dose Estimates Using the Buildup-Factor Method and a Baryon Transport Code (BRYNTRN) with Monte Carlo Results. NASA Technical Paper 3021.

Monte Carlo, BRYNTRN, Transport codes, Shielding

Results of continuing efforts toward validating the buildup-factor method and the baryon transport code (BRYNTRN), which use the deterministic approach to solving radiation transport problems and are the candidate engineering tools in space radiation shielding analyses, are presented. A simplified theory of proton-buildup factors assuming no neutron coupling has been derived to verify a previously chosen form for parameterizing the dose-conversion factor that includes the secondary-particle buildup effect. Estimates of dose in tissue made by the two deterministic approaches and the Monte Carlo method are compared for cases with various thicknesses of

shields and various types of proton spectra. The results are in reasonable agreement, but there is some overestimation by the buildup-factor method when the effect of neutron production in the shield is significant. Future improvement, including neutron coupling in the buildup-factor theory, is suggested to alleviate this shortcoming. Impressive agreement for individual components of doses, such as those from the secondaries and heavy-particle recoils, is obtained between BRYNTRN and Monte Carlo results.

Silberberg, R., Tsao, C. H., and Letaw, J. R. (1988) Transport of cosmic ray nuclei in various materials. *Transactions of the American Nuclear Society* 56: 275.

ICU, Single event evaluation, HZE, GCR, Shielding

Cosmic-ray heavy ions have become a concern in space radiation effects analyses. Heavy ions rapidly deposit energy and create dense ionization trails as they traverse materials. Collection of the free charge disrupts the operation of microelectronic circuits. This effect, called the single-event upset, can cause a loss of digital data. Passage of high linear energy transfer particles through the eyes has been observed by Apollo astronauts. These heavy ions have great radiobiological effectiveness and are the primary risk factor for leukemia induction on a manned Mars mission.

Models of the transport of heavy cosmic-ray nuclei through materials depend heavily on our understanding of the cosmic-ray environment, nuclear spallation cross sections, and computer transport codes. Our group has initiated and pursued the development of a full capability for modeling these transport processes. A recent review of this ongoing effort is presented in Letaw, Silberberg and Tsao (1988). In this paper, we discuss transport methods and present new results comparing the attenuation of cosmic-rays in various materials.

Simonsen, L. C., Nealy, J. E., Townsend, L. W., and Wilson, J. W. (1990) Space radiation shielding for Martian habitats. Presented at the 20th Annual Intersociety Conference on Environmental Systems (ICES), Williamsburg, VA, July 9-12, 1990. SAE Technical Paper Series #901346.

Shielding, Mars, Transport codes, Regolith

Radiation shielding analyses are performed for a candidate Mars base habitat. The Langley cosmic ray transport code and the Langley nucleon transport code are used to quantify the transport and attenuation of galactic cosmic rays and solar flare protons through both the Martian atmosphere and regolith shielding. Doses at the surface and at various altitudes were calculated in a previous study using both a high-density and a low-density Mars atmosphere model. This study extends the previous low-density results to include the further transport of the ionizing radiation that reaches the surface through additional shielding provided by Martian regolith. A four-compound regolith model, which includes SiO_2 , Fe_2O_3 , MgO , and CaO , was selected based on the chemistry of the Viking I Lander site. The spectral fluxes of heavy charged particles and the corresponding dosimetric quantities are computed for a series of thicknesses in the shield media after traversing the atmosphere. These data are then used as input to algorithms for a specific shield geometry. The results are presented as the maximum dose received in the center of the habitat versus various shield thicknesses for a base at an altitude of 0 km and 8 km.

Townsend, L. W., Ganapol, B. D., and Wilson, J. W. (1989) Benchmark solutions for heavy ion transport code validation. Abstract presented at the 37th Annual Meeting of the Radiation Research Society, Seattle, WA, March 18-23, 1989.

Benchmark, Boltzmann equation, Transport codes

Nontrivial analytic benchmark solutions for heavy ion transport are presented for use in validating deterministic computer code solution algorithms used to predict dosimetric quantities in laboratory beam and space radiation shielding applications. Benchmark solutions to the one-dimensional Boltzmann transport equation are presented for three forms of the equation: (1) spatially independent; (2) energy independent; and (3) coupled spatial and energy dependent. To illustrate the application of these benchmarks to actual radiation transport problems, representative comparisons between the benchmarks and numerical solutions obtained from transport codes developed by the authors for use in galactic cosmic ray shielding studies are made.

Townsend, L. W. and Wilson, J. W. (1988) Nuclear cross sections for hadronic transport. Invited lecture presented at the Annual Meeting of the American Nuclear Society, San Diego, CA, June 12-16, 1988. *Transactions of the American Nuclear Society* 56: 277-279.

Cross sections, Hadronic transport

The need to develop suitable methods for describing the interactions and transport of high-energy hadrons through extended matter is important for a variety of applications, including cosmic ray studies, exposure to space radiation, spacecraft shielding, radiobiological studies, accelerator shield design, and clinical uses in cancer therapy. For most of these applications, the transport equation can neglect target fragmentation and use the straight-ahead approximation. Accurate values for the cross sections are essential to solving transport equations. Unfortunately, experimental data for these cross sections are sparse. Hence, theoretical methods, validated by comparison to experiment, must be used to provide the cross sections.

Townsend, L. W. and Wilson, J. W. (1990) Interaction of space radiation with matter. Presented at the 41st Annual Congress of the International Astronautical Federation, Dresden, Germany, October 6-12, 1990.

Radiation transport, Galactic cosmic rays, Transport codes, Sensitivity-analysis

The physical interactions of high-energy space radiations with bulk matter are described, with particular emphasis on the nuclear and electromagnetic interactions of solar and galactic cosmic rays. Methods of incorporating these interactions into radiation transport models that accurately describe the propagation of the incident cosmic rays and their subsequent-generation reaction products are also explained. Representative results for solar and galactic cosmic ray doses and dose equivalents are presented for various aluminum and water absorber depths. For the first time, the main contributions to human exposure in space from galactic cosmic rays will be presented on a component by component basis, including a breakdown of the dose-equivalent contributions into primary ions, heavy fragments, alpha particles, neutrons, and protons. For the galactic cosmic ray environment outside of the Earth's magnetosphere, over 70 percent of the total dose equivalent results from only seven nuclear species (hydrogen, helium, carbon, oxygen, silicon, magnesium, and iron ions). Of these, the largest single contributor is cosmic ray iron and its secondaries, which account for nearly one-fourth of the unshielded total dose equivalent during solar minimum.

Townsend, L. W., Wilson, J. W., and Nealy, J. E. (1988) Preliminary Estimates of Galactic Cosmic Ray Shielding Requirements for Manned Interplanetary Missions. NASA Technical Memorandum 101516.

Galactic cosmic rays, Shielding, Transport codes, Doses, Dose equivalent, Aluminum, Water, Uncertainties

Estimates of radiation risk to the blood-forming organs from galactic cosmic rays are presented for manned interplanetary missions. The calculations use the Naval Research Laboratory cosmic ray spectrum model as input into the Langley Research Center galactic cosmic ray transport code. This transport code, which transports both heavy ions and nucleons, can be used with any number of layers of target material consisting of up to five different constituents per layer. Calculated galactic cosmic ray doses and dose equivalents behind various thicknesses of aluminum and water shielding are presented for solar maximum and solar minimum periods. Estimates of risk to the blood-forming organs are made using 5-cm depth dose/dose equivalent values for water. These results indicate that at least 5 g/cm² (5 cm) of water or 6.5 g/cm² (2.4 cm) of aluminum shielding is required to reduce the annual exposure below the currently recommended limit of 50 rem. Because of the large uncertainties in fragmentation parameters and the input cosmic ray spectrum, these exposure estimates may be uncertain by as much as 70 percent. Therefore, more detailed analyses with improved inputs could indicate the need for additional shielding.

Townsend, L. W., Wilson, J. W., Shinn, J. L., Nealy, J. E., and Simonsen, L. C. (1990) Radiation protection effectiveness of a proposed magnetic shielding concept for manned Mars missions. Presented at the 20th Annual Intersociety Conference on Environmental Systems (ICES), Williamsburg, VA, July 9-12, 1990. SAE Technical Paper Series #901343.

Magnetic shielding

The effectiveness of a proposed concept for shielding a manned Mars vehicle using a confined magnetic field configuration is evaluated by computing estimated crew radiation exposures resulting from galactic cosmic rays and a large solar event. In this study, the incident radiation spectra are transported through the spacecraft structure/magnetic shield using the deterministic space radiation transport computer codes developed at Langley Research Center. The calculated exposures unequivocally demonstrate that magnetic shielding could provide an effective barrier against solar flare protons, but is virtually transparent to the more energetic galactic cosmic rays. It is then demonstrated that through proper selection of materials and shield configuration, adequate and reliable bulk material shielding can be provided for the same total mass as needed to generate and support the more risky magnetic field configuration.

Wilson, J. W., Lamkin, S. L., Farhat, H., Ganapol, B. D., and Townsend, L. W. (1989) A Hierarchy of Transport Approximations for High Energy Heavy (HZE) Ions. NASA Technical Memorandum 4118.

Transport codes, Cross sections, Analytical solution

The transport of high-energy heavy (HZE) ions through bulk materials is studied with energy dependence of the nuclear cross sections being neglected. A three-term perturbation expansion appears to be adequate for most practical applications for which penetration depths are less than 30 g/cm² of material. The differential energy flux is found for monoenergetic beams and for realistic ion beam spectral distributions. An approximate formalism is given to estimate high-order terms.

Wilson, J. W., Nealy, J. E., Atwell, W., Cucinotta, F. A., Shinn, J. L., and Townsend, L. W. (1990) Improved model for solar cosmic ray exposure in manned Earth orbital flights. NASA Technical Paper 2987.

Shielding, Shuttle

A calculational model is derived for use in estimating solar cosmic ray exposure to a critical body organs in low Earth orbit at the center of a large spherical shield of fixed thickness. The effects of the Earth's geomagnetic field and the astronauts' self-shielding are evaluated explicitly. The geomagnetic field model is an approximate tilted eccentric dipole with geomagnetic storms represented as an impressed uniform field. The storm field is related to the planetary geomagnetic index K_p . The code is applied to the Shuttle geometry using the Shuttle mass distribution surrounding two locations on the flight deck. The Shuttle is treated as pure aluminum and the astronaut as soft tissue. Short-term average fluence over a single orbit is calculated as a function of the location of the lines of nodes or long-term averages over all lines of nodes for a fixed inclination.

Wilson, J. W., Townsend, L. W., and Atwell, W. (1987) Preliminary Estimates of Galactic Cosmic Ray Exposures for Manned Interplanetary Missions. NASA Technical Memorandum 100519.

Heavy ion, Aluminum, Solar periods, HZE

Preliminary estimates of radiation exposures resulting from galactic cosmic rays are presented for interplanetary missions. The calculations use the Naval Research Laboratory cosmic ray spectrum model as input into the Langley Research Center galactic cosmic ray transport code. The heavy ion portion of the transport code can be used with any number of layers of target material, consisting of up to five different constituents per layer. The nucleonic portion of the transport code can be used with any number of layers of target material of arbitrary composition except hydrogen. Calculated galactic cosmic ray particle fluxes, doses, and dose equivalents behind various thicknesses of aluminum shielding are presented for solar maximum and solar minimum periods.

Wilson, J. W., Townsend, L. W., Chun, S. Y., Buck, W. W., Khan, F., and Cucinotta, F. (1988) BRYNTRN: A Baryon Transport Computer Code Computation Procedures and Data Base. NASA Technical Memorandum 4037.

BRYNTRN, Transport codes, Data bases

The present report describes the development of an interactive data base and a numerical solution to the transport of baryons through an arbitrary shield material based on a straight ahead approximation of the Boltzmann equation. The code is most accurate for continuous energy boundary values, but gives reasonable results for discrete spectra at the boundary with even a relatively coarse energy grid (30 points) and large spatial increments (1 cm in H_2O).

Wilson, J. W., Townsend, J. W., Ganapol, B. D., and Lamkin, S. L. (1988) Methods for high energy hadronic beam transport. Invited lecture presented at the Annual Meeting of the American Nuclear Society, San Diego, CA, June 12-16, 1988. Transactions of the American Nuclear Society 56: 271-272.

Transport codes

The equations of transport in one dimension have found numerous applications and reasonably represent many of the properties of hadron transport. This paper discusses several such equations, some of which are used as the basis for new transport codes for baryons of mass number greater

than or equal to one. These codes are now being extended to couple with the meson field and to the negative baryon number fields.

Wilson, J. W., Townsend, L. W., Nealy, J. E., Chun, S. Y., Hong, B. S., Buck, W. W., Lamkin, S. L., Ganapol, B. D., Khan, F., and Cucinotta, F. (1989) BRYNTRN: A Baryon Transport Model. NASA Technical Paper 2887.

BRYNTRN, Boltzmann equation, Transport codes, Shielding

This report describes the development of an interaction data base and a numerical solution to the transport of baryons through an arbitrary shield material based on a straight ahead approximation of the Boltzmann equation. The code is most accurate for continuous-energy boundary values but gives reasonable results for discrete spectra at the boundary using even a relatively coarse energy grid (30 points) and large spatial increments (1 cm in H₂O). The resulting computer code is self-contained, efficient, and easy to use. The code requires only a very small fraction of the computer resources required for Monte Carlo codes.

1.4.2. EXPERIMENTAL STUDIES

JOURNALS

Schimmerling, W., Miller, J., Wong, M., Rapkin, M., Howard, J., Spieler, H. G., and Jarret, B. V. (1989) The fragmentation of 670A MeV Neon-20 as a function of depth in water: 1. Experiment. *Radiation Research* 120: 36-71.

Neon, Neon transport, Fluence spectra, Water

We present the final analysis of an experiment to study the interaction of a beam of 670A MeV neon ions incident on a water column set to different thicknesses. The atomic number Z (and, in some cases, the isotopic mass A) of primary beam particles and of the products of nuclear interactions emerging from the water column close to the central axis of the beam was obtained for nuclei between Be ($Z=4$) and Ne ($Z=10$) using a time-of-flight telescope to measure the velocity and a set of silicon detectors to measure the energy loss of each particle. The fluence of particles of a given charge was obtained and normalized to the incident beam intensity. Corrections were made for accidental coincidences between multiple particles triggering the TOF telescope and for interactions in the detector. The background due to beam particles interacting in beam line elements upstream of the detector was calculated. Sources of experimental artifacts and background in each particle identification experiments designed to characterize heavy ion beams for radiobiological research are summarized, and some of the difficulties inherent in this work are discussed. Complete tables of absolutely normalized fluence spectra as a function of LET ∞ are included for reference purposes.

Townsend, L. W. and Wilson, J. W. (1988) An evaluation of energy-independent heavy ion transport coefficient approximations. *Health Physics* 54: 409-412.

Transport theory, Depth doses, Neon, Bragg curve

Using a one-dimensional transport theory for laboratory heavy ion propagation, evaluations of typical energy-independent transport coefficient approximations are made by comparing theoretical depth-dose predictions to published experimental values for incident 670 MeV/nucleon ²⁰Ne beams

in water. Results are presented for cases where the input nuclear absorption cross sections, or input fragmentation parameters, or both, are fixed.

1.4.2. EXPERIMENTAL STUDIES

REPORTS/MEETINGS

Miller, J., Schimmerling, W., Wong, M., Shavers, M. R., and Rapkin, M. (1989) The transport of a 670 MeV accelerated neon beam in water: I. Experimental. Abstract presented at the 37th Annual Meeting of the Radiation Research Society, Seattle, WA, March 18-23, 1989.

Transport, Neon, Fluence spectra

We present the final analysis of an experiment to study the interaction of a beam of 670 MeV/A neon ions incident on a water column set to different thicknesses. The electrical charge Z (and in some cases the isotopic mass A) of primary beam particles and of the products of nuclear interactions emerging from the water column close to the central axis of the beam was obtained for nuclei between Be ($Z=4$) and Ne ($Z=10$) using a time-of-flight telescope to measure the velocity and a set of silicon detectors to measure the energy loss of each particle. The fluence of particles of a given charge was obtained and normalized to the incident beam intensity. Corrections were made for accidental coincidences between multiple particles triggering the TOF telescope, and for interactions in the detector. The background due to beam particles interacting in beam line elements upstream of the detector was calculated. Sources of experimental artifacts and background in particle identification experiments designed to characterize heavy ion beams for radiobiological research are summarized and some of the difficulties inherent in this work are discussed.

Schimmerling, W. (1988) Physical considerations relevant to HZE-particle transport in matter. Invited paper presented at the 1988 Annual Meeting of the American Nuclear Society, San Diego, CA. *Transactions of the American Nuclear Society* 56: 272-273.

HZE, Accelerator beams, Validations, Dosimetry

Heavy-ion accelerators are being seriously considered for driving inertial confinement fusion reactors, and high-energy heavy nuclei in the cosmic radiation are likely to place significant constraints on satellite power system deployment and space-based power generation. The use of beams of heavy nuclei in an increasing number of current applications, as well as their importance for the development of the state of the art of the future, makes it necessary to develop at the same time a good understanding of their transport through matter.

Recently, transport methods have been developed to determine the radiation field produced by relativistic heavy nuclei incident on layers of absorbers of different composition. These HZE transport methods need to be validated by comparison with experimental data; accordingly, a research program to develop heavy-ion transport predictions for space radiation shielding and dosimetry was established at the Lawrence Berkeley Laboratory several years ago. The properties of HZE particles that are relevant for transport calculations are discussed in this paper and illustrated with results from this program, as well as from the broader spectrum of relativistic heavy-ion research.

Schimmerling, W., Wong, M., Ludewigt, B., Phillips, M., Alpen, E. L., Powers-Risius, P., and DeGuzman, R. J. (1989) Biophysical aspects of heavy ion interactions in matter. Presented at the Conference on High Energy Radiation Background in Space (CHERBS 87), Sanibel Island, FL, November 3-5, 1987. AIP Conference Proceedings No. 186, Eds. A. C. Rester, Jr. and J. I. Trombka (American Institute of Physics, New York, 1989), pp. 369-380.

HZE particles, Fragmentation experiments, Neon, Multiple Coulomb scattering, GCR, Transport methods, Water

The biological effects of high energy, high charge nuclei (HZE particles) occupy a central role in the management of space radiation hazards due to galactic cosmic rays. For the energy range of interest, the mean free path for nuclear interactions of these heavy ions is comparable to the thickness of the material traversed, and a significant fraction of stopping particles will undergo a nuclear reaction with the nuclei of the stopping material. Transport methods for HZE particles are dependent on models of the interaction of man-made systems with the space environment to an even greater extent than methods used for other types of radiation. Hence, there is a major need to validate these transport codes by comparison with experimental data. The basic physical properties of HZE particles will be reviewed and illustrated with the results of nuclear fragmentation experiments performed with the 670-MeV neon ions incident on a water absorber and with measurements of multiple Coulomb scattering of uranium beams in copper. Finally, the extent to which physical measurements yield radiobiological predictions is illustrated for the example of neon.

Shavers, M. R., Schimmerling, W., Curtis, S. B., Miller, M., Wong, M., Wilson, J. W., and Townsend, L. W. (1989) The transport of a 670 MeV accelerated neon beam in water: II. Transport codes and comparison with Experiment I. Abstract presented at the 37th Annual Meeting of the Radiation Research Society, Seattle, WA, March 18-23, 1989.

Transport codes, NKW transport, Fluence spectra, Validations

Detailed model calculations of the transport of 670 MeV neon ions incident on a water absorber have been made and compared with experimental data using the HZESEC code developed at LBL and the LBLBEAM code developed at NASA-Langley. For every thickness of water a model calculation was made of the measured differential fluence spectrum (number of particles of charge Z per cm^2 per LET interval). Theoretical differential fluence spectra were corrected for the fraction of the fluence actually detected, calculated using the PROPAGATE code developed at LBL, and folded with the experimental energy resolution for comparison with experimental spectra. The shape of the model spectra conform quite closely to the shape of the experimental spectra over most of the absorber depth. Near the Bragg peak, small differences in stopping power lead to significant differences between theoretical and experimental spectra. The differential spectra provide a sensitive test of model fragmentation cross sections, stopping power and attenuation lengths.

Wilson, J. W., Schimmerling, W., Wong, M., and Townsend, L. W. (1987) Heavy ion beams in extended materials: Computational methods and experiment. In: Health Physics of Radiation generating Machines, Proceedings of the Twentieth Midyear Topical Symposium of the Health Physics Society, Reno, NV, February 8-12, pp. 442-450 (CONF-8602106).

Heavy ion transport, Shielding, Radiation quality

The transport of heavy ion beams in extended materials is a problem of interest in accelerator and space shielding, radiation therapy, and astrophysical and radiobiological studies. The beam particles change their energy and direction of motion through atomic/molecular collisions and undergo occasional radical transformation in nuclear collision. In health physics applications, a heavy ion beam of initially well defined radiation quality is transformed into a complex mixture of diverse quality components after passing through a modest amount of material. This transformation of radiation quality must be understood to adequately explain the biological response of tissue to heavy ion radiation. A theoretical/experimental program to define an ion beam and its products in extended matter is described.

1.5. INSTRUMENTATION

JOURNALS

Brackenbush, L. W., Braby, L. A., and Anderson, G. A. (1989) Characterising the energy deposition events produced by trapped protons in low Earth orbit. *Radiation Protection Dosimetry* 29: 119-121.

Trapped protons, Low-LET, Tissue-equivalent proportional counter

Humans and equipment in space vehicles in low Earth orbit are exposed to a wide variety of radiations, but the majority of the dose is due to trapped protons, which have energies of the order of 100 MeV and are low LET particles. These high energy particles produce nuclear fragmentation with high LET secondaries that may be responsible for a significant fraction of dose equivalent. In order to understand better the biological effectiveness of this radiation environment, a portable tissue equivalent proportional counter spectrometer has been developed that automatically records the distribution of energy in a small tissue-like site as a function of time. This instrument weighs about 700 g and will be flown on a number of future Space Shuttle flights.

Fanton, J. W., Cordts, R. E., Harris, R. K., Romo, D., and Wood, D. H. (1988) Radioisotope imaging of brain tumors in two rhesus monkeys. *Laboratory Animal Science* 38(2): 214-217.

Radioisotope imaging, Brain tumors, Rhesus monkeys, PET

Nuclear imaging involves the systemic administration of a radionuclide (radioisotope) to a patient after which a picture or image is generated by recording relative quantities of radiation emitted from regions of interest in the patient. The picture is formed from the digital radioactive counts acquired during the procedure. This information can be recorded by a computer so that images and digital information can be recreated for later analysis. By integrating the intensity of regions of the screen images, objective measurement of differences in radioactivity level can be made.

Nuclear brain scans are a sensitive technique for screening brain tumors in both animals and humans and have been described as the most practical of nuclear scan procedures for use in veterinary medicine. In this study, nuclear scans of two rhesus monkeys provided accurate images of intracranial neoplasia.

Ngo, D. M., Wilson, J. W., Buck, W. W., and Fogarty, T. N. (1989) Nuclear-Fragmentation Studies for Microelectronic Applications. NASA Technical Memorandum 4143.

Microelectronic applications, Intranuclear cascade, Single-event upsets

A formalism for target fragment transport is presented with application to energy-loss spectra in thin silicon devices. Predicted results are compared with experiments using the surface-barrier detectors developed by J. P. McNulty. The intranuclear-cascade, nuclear-reaction model does not predict the McNulty experimental data for the highest energy events. A semiempirical nuclear cross section gives an adequate explanation of McNulty's experiments. Application of the formalism to specific electronic devices is discussed.

2. BIOLOGY

2.1. MOLECULAR BIOLOGY

JOURNALS

Lett, J. T. (1989) Double strand breakage in DNA and cellular radiation sensitivity: linear energy transfer and the oxygen effect. In: *Oxygen Radicals in Biology and Medicine*, Eds. M. G. Simic, J. F. Ward and K. S. Taylor. New York: Plenum Press, pp. 419-428.

Double strand breaks, Oxygen effect, Direct and indirect action

Despite more than three decades of extensive research, identification of the chemical changes responsible for the lethal effects of ionizing radiation has yet to be achieved. Indeed, although the general consensus of opinion associates lethal radiation events with damage, and especially double-strand breaks, in DNA, there is still lively debate even about the relative contributions of the direct and indirect effects of sparsely ionizing radiations at the cellular level. Causes for the protraction in this elucidation process usually can be traced to the difficulty in determining chemical change in mammalian cells after radiation doses of radiobiological significance, to the inflexibility of classical positions, and to an increase in the reluctance of governmental agencies to underwrite experiments with other than predictable outcomes. Some recent signs are more encouraging, however, because definitive scientific advances now seem possible, but they are more likely to come from laboratories in Europe where the expression of originality has not been blunted by dogma and warranty. Areas where modern ideas must provoke much-needed advances in the understanding of the chemistry of strand breakage induced in cellular DNA by ionizing radiations are discussed here.

In the early 1960's, perceptive experiments with dilute solutions of deoxyribonucleoproteins demonstrated that the constituent proteins provided the DNA with extensive protection against free radicals formed in the surrounding water by radiation. Limitations to the role played by such radicals in the DNA chemistry underlying cellular radiosensitivity, i.e., some of the effects attributed more usually to the indirect action of ionizing radiation, were implied by such behavior. Concurrent and subsequent findings about the efficiencies of strand breakage in DNA, DNA gels of limited water contents, mammalian cells and so forth, also were consistent with that interpretation. Yet during the last 20 years, the preponderance of chemical studies on radiation-induced change in DNA have been predicated upon the contrary opinion. Justification for that experimental approach often is related to conclusions, which are based upon reaction rates in liquid water, that $\cdot\text{OH}$ radicals diffuse 20-30 Å in cells. Nowadays, challenge to the notion of the pre-eminence of such indirect action in determining cellular radiosensitivity is strengthening as understanding broadens about the role played by the structure and hydration (solvation) of deoxyribonucleoprotein in radiation chemical processes involving cellular DNA.

Lett, J. T., Bergtold, D. S., and Keng, P. C. (1986) Effects of LET_∞ on the fate of DNA damage induced in rabbit sensory cells *in situ*: Fundamental aspects. In: *Mechanisms of DNA Damage and Repair*, eds. M. C. Simic, L. Grossman, and Upton, A. C. New York: Plenum Publishing Co., pp. 139-150.

Cellular radiosensitivity, RBE, Murine lymphoblast, Repair

For half a century, radiobiological theory was dominated by the notion that cellular radiosensitivity to ionizing radiations could be explained solely on the basis of the physics of energy deposition. The process was extended even to explanations for the variation in relative biological effectiveness (RBE) with increased linear energy transfer (LET_∞) associated with densely-ionizing, particulate radiations. In more recent years, examination of the radiation responses of the repair-deficient S/S

variant of the L5178Y murine leukemic lymphoblast has demonstrated that radiobiological theories which do not incorporate metabolic modification of radiochemical damage are untenable.

Todd, P., Hymer, S. S., Delcourt, S. G., and Kunze, M. E. (1989) Overview of techniques of analysis of cell damage. In: *Multilevel Health Effects Research: From Molecules to Man*, Eds. J. F. Park and R. A. Pelroy. Proceedings of the Twenty-Seventh Hanford Life Sciences Symposium on Health and the Environment. Columbus, OH: Battelle Press, pp. 109-117.

Cell damage, Chromosome aberrations, DNA damage, Flow cytometry, Affinity labelling, Recombinant DNA

Most physical and chemical methods for analyzing cell damage have been developed for cells damaged *in vitro*. In many cases, these methods can be transferred, with minor modifications, to the analysis of cell damage *in vivo*. Molecular end points for cell damage include: chemical modifications of DNA, chromosome aberrations, point mutations, gene deletions/translocations, malignant transformation, and reproductive death.

For each of these end points, *in vivo* methods of analysis have been developed, including centrifugation and electrophoresis of unlabeled DNA, use of probes to detect DNA damage, characterization of severe chromosome damage by flow cytometry, somatic mutant cell identification by image analysis and flow cytometry, electrophoresis of cellular proteins, and flow cytometry, image analysis, and electrophoresis for detecting cell population shifts. In most cases, problems of sensitivity, specificity, and analysis of large cell populations had to be solved to apply these methods *in vivo*. Affinity labelling and recombinant DNA technology have played an important role in nearly all cases.

Many of these methods are also useful in cell bioprocessing and biotechnology. Newer techniques, developed mainly for biotechnology applications but with potential for analysis of cell damage, include selective cell retrieval by laser scanning microscopy, single cell manipulation by optical trapping, and cell electroporation and electrofusion.

2.2. CELLULAR RADIATION BIOLOGY

JOURNALS

Lett, J. T. (1987) Cellular radiation biology in consolidation and transition. *British Journal of Cancer* 55: 145-152.

Mouse lymphoblasts, Cellular repair, Synchronous cell cultures, RBE, Heavy ions HZE particles

Cellular radiation biology currently is undergoing changes common to all science in which the understanding in one area is becoming solidified while in another area conclusion of the classical phase is being engendered by the needs of modern thought. Aspects of these changing circumstances are discussed here from the standpoint of the roles played by direct and indirect action in cell death and the position that promulgation of the correct explanations of the radiosensitivities of mammalian cells can be facilitated if use of such classical operational definitions as sublethal and potentially lethal damage is discontinued. The latter consideration will be supported by a summary of the responses of synchronous populations of the L5178Y S/S murine leukaemic lymphoblast to ^{20}Ne , ^{28}Si , ^{40}Ar , ^{56}Fe and ^{93}Nb ions of energies broadly in the region of 500 MeV/u.

Lett, J. T. (1986) Opportunities for electron microscopy in space radiation biology. *Scanning Electron Microscopy* 1: 229-236.

Tissue damage, Electron microscopy, New Zealand white rabbits, Stem cell populations, Cell culture

Densely ionizing, particulate radiations in outer space are likely to cause to mammalian tissues biological damage that is particularly amenable to examination by the techniques of electron microscopy. This situation arises from the fact that once the density of ionization along the particle track exceeds a certain value, small discrete lesions involving many adjacent cells may be caused in organized tissues. Tissue damage produced by ionization densities below the critical value also affords opportunities for electron microscopic evaluation, as is shown by the damage produced in optic and proximate tissues of the New Zealand white rabbit in terrestrial experiments. Late radiation sequelae in nondividing, or terminally differentiating, tissues, and in stem cell populations, are of special importance in these regards.

It is probable that evaluations of the hazards posed to astronauts by galactic particulate radiations during prolonged missions in outer space will not be complete without adequate electron microscopic evaluation of the damage those radiations cause to organized tissues.

Lett, J. T., Cox, A. B., and Bergtold, D. S. (1986) Cellular and tissue responses to heavy ions: Basic considerations. *Radiation and Environmental Biophysics* 25:1-12.

Photoreceptors, Heavy ions, Radiosensitivity, New Zealand white rabbits, Mouse cells, HZE

Responses of the S/S variant of the L5178Y murine leukemic lymphoblast, the photoreceptor cell of the rabbit retina and the lenticular epithelium of the rabbit to heavy ions (^{20}Ne , ^{28}Si , ^{40}Ar and ^{56}Fe) are described and discussed primarily from the standpoint of the need for a comprehensive theory of cellular radiosensitivity from which a general theory of tissue radiosensitivity can be constructed.

The radiation responses of the very radiosensitive, repair-deficient S/S variant during the G₁- and early S phases of the cell cycle were found to be unlike those of normally radioresistant cells in culture: the relative biological effectiveness (RBE) did not increase with the linear energy transfer (LET_∞) of the incident radiation. Such behavior could be anticipated for a cell which is lacking the repair system that operates in other (normal) cells when they are exposed to ionizing radiations in the G₁ phase of the cell cycle. The S/S variant does exhibit a peak of radioresistance to X-photons mid-G₁ + 8 h into the cell cycle, however, and as the LET_∞ was increased, the repair capacity responsible for that radioresistance was reduced progressively.

Sensory cells (photoreceptors) in the retina of the New Zealand white (NZW) rabbit are very radioresistant to ionizing radiations, and several years elapsed after localized exposure (e.g., 5-10 Gy) to heavy ions (²⁰Ne, ⁴⁰Ar) before photoreceptor cells were lost from the retina. During the first few weeks after such irradiations, damage to DNA in the photoreceptor cells was repaired to a point where it could not be demonstrated by reorienting gradient sedimentation under alkaline conditions, a technique that can detect DNA damage produced by <0.1 Gy of X-photons. Restitution of DNA structure was not permanent, however, and months or years later, but *before* loss of photoreceptor cells from the retina could be detected, progressive deterioration of the DNA structure began.

2.2.1. TRANSFORMATION, MUTATION

JOURNALS

Mei, M.-T., Craise, L. M., and Yang, T. C. H. (1986) Induction of proline prototrophs in CHO-K1 cells by heavy ions. *International Journal of Radiation Biology* 50: 213-224.

Chinese hamster ovary cells, CHO-K1, X-rays, Iron ions, Neon ions, Silicon ions, Ethyl-methane sulphonate, 5-azacytidine, RBE, Proline phototroph

Using an established mammalian cell line, Chinese hamster ovary cells (CHO-K1), we have observed the induction of prototrophs by various heavy ions. This cell line requires proline for normal growth in medium with low serum concentration. X-rays, three types of heavy particles (600 MeV/u iron, 670 MeV/u neon, and 320 MeV/u silicon ions), ethyl-methane sulphonate and 5-azacytidine were used to induce revertants which were proline independent. Log-phase cells treated with 5-azacytidine showed a very high reversion frequency. The induction frequency per viable cell appears to be dose dependent for these four types of radiation, and the dose-response curves are approximately linear. Our results also indicate that the effectiveness of high-LET particles in inducing proline prototrophs is much greater than that of low-LET radiation. The RBE value for the induction of prototrophs was calculated for neon, silicon, and iron particles and found to be about 1.3, 1.7 and 4.5, respectively. At equal survival level, the reversion frequency for X-rays and EMS was about the same.

Nelson, G. A., Schubert, W. W., Marshall, T. M., Benton, E. R., and Benton, E. V. (1989) Radiation effects in *Caenorhabditis elegans*: Mutagenesis by high and low LET ionizing radiation. *Mutation Research* 212: 181-192.

C. elegans, Mutations, RBE, Heavy ions

The nematode *C. elegans* was used to measure the effectiveness of high-energy ionized particles in the induction of 3 types of genetic lesions. Recessive lethal mutations in a 40-map unit autosomal region, sterility, and X-chromosome nondisjunction or damage were investigated. Induction rates

were measured as a function of linear energy transfer, LET_{∞} , for 9 ions of atomic number 1-57 accelerated at the BEVALAC accelerator. Linear kinetics were observed for all 3 types of lesions within the dose/fluence ranges tested and varied strongly as a function of particle LET_{∞} . Relative Biological Effectiveness (RBE) values of up to 4.2 were measured and action cross sections were calculated and compared to mutagenic responses in other systems.

Todd, P. (1986) The evolving microlesion concept. *Advances in Space Research* 6: 187-189.

Microlesions, Carcinogenesis, HZE, Harderian gland, Particle tracks

The "microlesion concept," introduced by D. Grahn in the 1970's, was further explored using published quantitative carcinogenesis data. Laboratory experiments performed by T. C. H. Yang and co-workers and by R. J. M. Fry and co-workers using the Fe ion beam of the Lawrence Berkeley Laboratory Bevalac have resulted in quantitative data on *in vitro* and *in vivo* (respectively) carcinogenesis in mouse systems. These data sets were interpreted on the basis of track calculations, and it was found that the action cross section for tumor induction in cultured cells is approximately 0.032 mm^2 and that it is about 1/1000th as great in mouse Harderian gland cells. This great difference in carcinogenic sensitivity is a reflection of the biological differences between these two highly promoted systems, neither of which may be quantitatively applicable to humans in space.

Yang, T. C., Craise, L. M., Mei, M-T., and Tobias, C. A. (1986) Dose protraction studies with low- and high-LET radiations on neoplastic cell transformations *in vitro*. *Advances in Space Research* 6(11): 137-147.

Heavy ions, Low rate effect, C3H10T1/2, Low dose-rate effect, Low-LET, High-LET, Neoplastic cell transformation, Sparing, Argon, Iron,

A major objective of our heavy-ion research is to understand the potential carcinogenic effects of cosmic rays and the mechanisms of radiation-induced cell transformation. During the past several years we have studied the relative biological effectiveness of heavy ions with various atomic numbers and linear energy transfer on neoplastic cell transformation and the repair of transformation lesions induced by heavy ions in mammalian cells. All of these studies, however, were done with a high dose rate. For risk assessment, it is extremely important to have data on the low-dose-rate effect of heavy ions. Recently, with confluent cultures of the C3H10T^{1/2} cell line, we have initiated some studies on the low-dose-rate effect of low- and high-LET radiation on cell transformation. For low-LET photons, there was a decrease in cell killing and cell transformation frequency when cells were irradiated with fractionated doses and at low dose rate. Cultured mammalian cells can repair both subtransformation and potential transformation lesions induced by X rays. The kinetics of potential transformation damage repair is a slow one. No sparing effect, however, was found for high-LET radiation. There was an enhancement of cell transformation for low-dose-rate argon (400 MeV/u; 120 keV/ μm) and iron particles (600 MeV/u; 200 keV/ μm). The molecular mechanism for the enhancement effect are unknown at present.

Yang, T. C., Craise, L. M., and Rhim, J. S. (1990) Neoplastic transformation of human epidermal keratinocytes by low- and high-LET radiations. Poster presented at the 38th Annual Meeting of the Radiation Research Society, New Orleans, LA. April 7-12, 1990.

Human epithelial cells, SV40, RBE

For assessing radiation risk, it is important and necessary to understand the responses of human cells, especially the epithelial cells, to various radiation modalities. Recent advances in culturing

human epithelial cells and in establishing immortal cell lines provide unique opportunities to study the carcinogenic effects of radiation in human epithelial cells. In our laboratories, we have developed techniques and methods that allow quantitative study of neoplastic transformation of human epithelial cells. Human epidermal keratinocytes (HEK-271), immortalized by SV40 adeno-12 hybrid virus, are nonproducer, nontumorigenic, and maintain density inhibition property. After growing in culture for 6 weeks, transformed foci, showing extensive piling-up of cells, were found in irradiated cells, while control cells formed only monolayers. These transformed cells were able to grow in soft agar media, suggesting anchorage-dependent growth, an important property of tumorigenic cells. Our studies with X rays and 470 MeV/u argon ions showed an RBE about 2.3 at 10% survival level. Dose-response curves for neoplastic cell transformation gave RBE about 3.7 and 7.0 at high and low doses correspondingly for 470 MeV/u argon ions.

Yang, T. C., Craise, L. M., and Rhim, J. S. (1990) Quantitative studies on radiogenic transformation of human epithelial cells *in vitro*. Abstract presented at the 81st Annual Scientific Meeting of the American Association for Cancer Research, Washington, DC, May 23-26, 1990.

Human epithelial cells, Nude mouse, Cell transformation, High-LET

Quantitative data are important for risk assessment and for model development. Biophysical models are valuable for understanding the basic processes of carcinogenesis. In our laboratories, we have developed a cell system and methods for a quantitative determination of neoplastic transformation of human epithelial cells. Human epidermal keratinocytes (RHEK-271), immortalized by SV40 adeno-12 hybrid virus, are nonproducer, nontumorigenic, and maintain density inhibition property. Confluent RHEK-271 cells were irradiated and then plated into dishes at proper density. After a 6-week incubation with weekly changes of media, transformed foci, showing extensive piling-up of cells, were formed in the irradiated cells. These transformed foci can be identified and scored easily under a dissecting stereo microscope. Anchorage independent growth test of these transformed cells gave positive results, and the tumorigenic test in athymic nude mouse is underway. We have obtained the dose-response curves for X-rays and heavy ion radiation and found that the transformation frequency per survivor increased curvilinearly with X-ray doses and was higher for a given dose for high-LET radiation. Our experimental results demonstrated that this cell system is very useful for quantitative measurement as well as for mechanistic studies of radiation carcinogenesis.

Yang, T. C., Craise, L. M., and Tobias, C. A. (1988) Initial primary lesion important for radiogenic cell transformation. Abstract presented at the 36th Annual Meeting of the Radiation Research Society, Philadelphia, PA, April 16-21, 1988.

Cultured mammalian cells, Cell transformation, C3H10T1/2, DNA strand breaks

For studying radiation carcinogenesis at the cellular and molecular level, cultured mammalian cells have been found to be useful model systems. Various investigators have shown that ionizing radiation can cause neoplastic cell transformation directly and that the nuclear DNA is the primary target. In general, radiation-induced cell transformation involves multistep processes including initiation, fixation, promotion, and progression into the malignant state. We have collected and analyzed cell transformation data obtained with heavy ions for gaining some understanding of the molecular nature of the initial primary lesion important for the initiation of cell transformation by radiation. Our simple analysis indicates that two specific primary ionizations within 80Å may be sufficient to form a transformation lesion in C3H10T1/2 cells. For verifying this finding, we have carried out further studies with restriction endonucleases, and preliminary results suggest that DNA strand breaks more than two bases apart can induce cell transformation.

Yang, T. C., Craise, L. M., and Tobias, C. A. (1989) Molecular lesions important for neoplastic cell transformation by ionizing radiation. In: *Cell Transformation and Radiation-Induced Cancer*, Eds. K. H. Chadwick, C. Seymour, and B. Barnhart. New York: Adam Hilger Co., pp. 301-308.

Neoplasia, Cell transformation, C3H10T1/2, Double strand breaks, Human mammary epithelial cells, Human keratinocytes

Radiation cell transformation is a multistep process. At present we know very little about the molecular nature of lesions important for radiogenic cell transformation and evolution of initial damages into final malignant growth. A simple analysis of our heavy ion data of C3H10T1/2 cells indicated that DNA double-strand breaks may be important for cell transformation. Further studies with restriction endonucleases showed support for this finding. Recently we have succeeded in inducing morphological transformation of human keratinocytes and growth variants of human mammary epithelial cells with X-rays and heavy ions.

Yang, T. C., Craise, L. M., and Tobias, C. A. (1989) Effects of fractionated doses on mutation and neoplastic cell transformation by heavy ion radiation. Abstract presented at the 37th Annual Radiation Research Society, Seattle, WA, March 18-23, 1989.

Heavy ions, Iron, C3H10T1/2, Transformation, HGPRT mutation, Fractionated doses

In our laboratory we have observed that high-LET heavy ions, e.g., 600 MeV/u iron particles, at a low dose rate can be more effective than those at a high dose rate in inducing neoplastic cell transformation, and that this low-dose-rate enhancement effect is LET-dependent. Recently we have extended these studies to determine whether fractionated doses can give similar enhancement effects for somatic mutation and cell transformation. Confluent C3H10T1/2 cells were irradiated by single or fractionated doses of heavy ions, and the transformation frequency was determined. Experimental results showed no significant difference between cells irradiated by single and multifractions of 600 MeV/u iron particles for survival and cell transformation. For mutation studies, we used confluent Rat-2 cells to determine the induction of 6-TG¹ mutants by heavy ions. Our results indicated that single and fractionated doses of 400 MeV/u argon ions were equally effective in killing cells and inducing HGPRT mutation. So far we have not found any enhancement effects of fractionated doses for mutation and cell transformation.

2.2.2 LETHALITY, SURVIVAL

JOURNALS

Lett, J. T. (1990) Damage to DNA and chromatin structure from ionizing radiations, and the radiation sensitivities of mammalian cells. *Progress in Nucleic Acid Research and Molecular Biology* 39: 305-352.

Cellular lethality, Direct action, Indirect action, Energy transfer, Single cell, Chemical protection

This review of the basis of cellular lethality caused by ionizing radiations opens with a discussion of transitions in the field of cellular radiation biology. The author contends that progress has stagnated, in part due to three unusual circumstances: First, theories of cellular radiation sensitivity that preclude post-irradiation modification of radiation damage by cellular metabolic processes continue to be taught, despite their being demonstrably unsound. Second, the lack of utility of one

of two phenomenological (operational) interpretations of cellular radiosensitivity first introduced more than 20 years ago has been stultifying for the reasons such abstractions often are, even on the grandest scale. The third circumstance concerns the notion of indirect action, that is, that most of the DNA damage responsible for cell death is caused indirectly by diffusing radicals, usually $\cdot\text{OH}$ resulting from the irradiation of bulk water, that are deposited neither in the macromolecule itself nor in adjacent molecules with which it is directly associated (bound). The author takes the view that energy deposited in DNA chromatin -- that is, *direct* action -- causes most of the biologically significant radiation damage, and presents it in this article, while remaining cognizant of the fact that, under special conditions, radiation damage not involving DNA could be of crucial importance. The case is made mainly in light of recent developments in the radiation chemistry of DNA (chromatin) and the probable role of such chemistry in a general theory of cellular radiosensitivity that overcomes the fundamental deficiencies outlined above. This review covers areas including single-cell survival curves, mechanisms of energy transfer, chemical protection and radical scavengers, and strand breaks in DNA, and offers general conclusions.

Lett, J. T., Cox, A. B., and Story, M. D. (1989) The role of repair in the survival of mammalian cells from heavy ion irradiation: Approximation to the ideal case of target theory. *Advances in Space Research* 9(10): 99-104.

Neon, Silicon, Argon, Iron, Niobium, Cell cycle dependence, Mouse lymphoblasts

Theories of cellular radiation sensitivity that preclude a significant role for cellular repair processes in the final biological expression of cellular damage induced by ionizing radiation are unsound. Experiments are discussed here in which the cell-cycle dependency of the repair deficiency of the S/S variant of the L5178Y murine leukemic lymphoblast was examined by treatment with the heavy ion, ^{20}Ne , ^{28}Si , ^{40}Ar , ^{56}Fe and ^{93}Nb . Evidence from those studies, which will be described in detail elsewhere, provide support for the notion that as the linear energy transfer (LET_∞) of the incident radiation increases the ability of the S/S cell to repair radiation damage decreases until effectively it is eliminated around $500 \text{ keV}/\mu\text{m}$. In the region of the latter LET_∞ value, the behavior of the S/S cell approximates the ideal case of target theory where post-irradiation metabolism (repair) does not influence cell survival. The expression of this phenomenon among different cell types and tissues will depend upon the actual repair systems involved and other considerations.

Lett, J. T., Cox, A. B., Story, M. D., Ehmann, U. K., and Blakely, E. A. (1989) Responses of synchronous L5178Y S/S cells to heavy ions and their significance for radiobiological theory. *Proc. Royal Soc. London* B237: 27-42.

Neon, Silicon, Argon, Iron, Niobium, RBE, Cell cycle dependence

Synchronous suspensions of the radiosensitive S/S variant of the L5178Y murine leukaemic lymphoblast at different positions in the cell cycle were exposed aerobically to segments of heavy-ion beams (^{20}Ne , ^{28}Si , ^{40}Ar , ^{56}Fe and ^{93}Nb) in the Bragg plateau regions of energy deposition. The incident energies of the ion beams were in the range of $460 \pm 95 \text{ MeV u}^{-1}$, and the calculated values of linear energy transfer (LET_∞) for the primary nuclei in the irradiated samples were 33 ± 3 , 60 ± 3 , 95 ± 5 , 213 ± 21 and $478 \pm 36 \text{ KeV um}^{-1}$, respectively; 280 kVp X-rays were used as the baseline radiation. Generally, the maxima or inflections in relations between relative biological effectiveness (RBE) and LET_∞ were dependent upon the cycle position at which the cells were irradiated. Certain of those relations were influenced by post-irradiation hypothermia.

Irradiation in the cell cycle at mid- G_1 to mid- $G_1 + 3 \text{ h}$, henceforth called G_1 to $G_1 + 3 \text{ h}$, resulted in survival curves that were close approximations to simple exponential functions. As the LET_∞ was increased, the RBE did not exceed 1.0, and by 478 keV um^{-1} it had fallen to 0.39. Although

similar behaviour has been reported for inactivation of proteins and certain viruses by ionizing radiations, so far the response of the S/S variant is unique for mammalian cells. The slope of the survival curve for X-photons (D_0 : 0.27 Gy) is reduced in G_1 to $G_1 + 3$ h by post-irradiation incubation at hypothermic temperatures and reaches a minimum (D_0 : 0.51 Gy) at 25 °C. As the LET_∞ was increased, however, the extent of hypothermic recovery was reduced progressively and essentially was eliminated at 478 keV μm^{-1} .

At the cycle position where the peak of radioresistance to X-photons occurs for S/S cells. $G_1 + 8$ h, increases in LET_∞ elicited only small increases in RBE (at 10% survival), until a maximum was reached around 200 keV μm^{-1} . At 478 keV μm^{-1} , what little remained of the variation in response through the cell cycle could be attributed to secondary radiations (δ rays) and smaller nuclei produced by fragmentation of the primary ions.

Schimmerling, W., Alpen, E. L., Powers-Risius, P., Wong, M., DeGuzman, R. J., and Rapkin, M. (1987) The relative biological effectiveness of 670 MeV/A neon as a function of depth in water for a tissue model. *Radiation Research* 112: 436-448.

Spermatogonial cell killing, RBEs, Heavy ions, HZE, RBE, Mouse testes

Linear energy transfer (LET_∞) spectra of identified charged fragments and primaries, produced by nuclear interactions of 670 MeV/A neon in water, were measured along the unmodulated Bragg curve of the neon beam. The relative biological effectiveness (RBE) values for spermatogonial cell killing, as reported on the basis of weight loss assay of mouse testes irradiated with beams of approximately constant single LET_∞ , were summed over the particle LET_∞ spectra to obtain an effective RBE for each charged-particle species, as a function of water absorber thickness. The resultant values of effective RBE were combined to obtain an effective RBE for the mixed radiation field. The RBE calculated in this way was compared with experimental RBEs obtained for spermatogonial cell killing in the mixed radiation field produced by neon ions traversing a thick water absorber. Discrepancies of 10-40% were observed between the calculated RBE and the RBE measured in the mixed radiation field. Part of this discrepancy can be attributed to undetected low-Z fragments, whose contribution is not included in the calculation, leading to an overestimated value for the calculated RBE. On the other hand, calculated values 10% greater than the measured RBE are explained as track structure effects due to the higher radial ionization density near neon tracks relative to the ionization density near the silicon tracks used to fit the RBE vs LET_∞ data.

Yang, T. C., Gruenert, D. C., Holley, W. R., and Curtis, S. B. (1990) Response of cultured human airway epithelial cells to X-rays and energetic α particles. *International Journal of Radiation Biology* 58: 509-518.

Alpha particles, Human epithelial cells, X-rays, RBE, Cell inactivation

Radon and its progeny, which emit α particles during decay, may play an important role in inducing human lung cancer. To gain a better understanding of the biological effects of α -particles in human lung we studied the response of cultured human airway epithelial cells to X-rays and monoenergetic helium ions. Our experimental results indicated that the radiation response of primary cultures was similar to that for airway epithelial cells that were transformed with a plasmid containing an origin-defective SV40 virus. The RBE for cell inactivation determined by the ratio of $D_{0\alpha}$ for X-rays to that for 8 MeV helium ions was 18-22. The cross-section for helium ions,

calculated from the D_0 value, was about $24 \mu\text{m}^2$ for cells of the primary culture. This cross-section is significantly smaller than the average geometric nuclear area ($\sim 180 \mu\text{m}^2$), suggesting that an average of 75 α -particles (8 MeV helium ions) per cell nucleus are needed to induce a lethal lesion.

Yang, T. C., Stampfer, M. R., and Tobias, C. A. (1989) Radiation studies on sensitivity and repair of human mammary epithelial cells. *International Journal of Radiation Biology* 56: 605-609.

Human mammary epithelial cells, Heavy ions, Repair, Radiosensitivity

For radiation risk assessment and cancer radiotherapy it is important to know how human cells, especially epithelial cells, respond to ionizing radiation. In our laboratory we have a large collection of normal and tumor cells of human mammary tissue and have developed techniques to grow these cells in culture (Stampfer and Bartley 1986). In the past several years we have studied the radiosensitivity and repair of human mammary epithelial cells from normal and tumor tissue following low- and high-LET irradiation. For a better understanding of radiation responses of premalignant cells to radiation, our studies also include epithelial cells immortalized *in vitro* and from tissue peripheral to the tumor.

2.2.2 LETHALITY, SURVIVAL

REPORTS/MEETINGS

Lett, J. T. (1990) The end of a hiatus in cell survival theory and its significance for radiation therapy. *Journal of Cancer Research and Clinical Oncology* 116 (Suppl): 844 (abstract).

Cell survival, Target theory, L5178Y S/S

For 50 years sustained efforts have been made to explain cellular radiosensitivity with general target theory. Although its two major progenitors, Lea and Zimmer, warned that the theory was inapplicable if radiation damage was altered by subsequent metabolic activity, efforts to use it for mammalian cells have continued long after the discovery of cellular and molecular repair mechanisms, and in spite of Zimmer's efforts to reverse the trend until his recent death. Experiments that examined the responses of the cell-cycle dependent, repair-deficient, L5178Y S/S variant x-photons and heavy ions have shown that any theory of cellular radiosensitivity that neglects post-irradiation repair mechanisms is unsound. Target theory is applicable only if repair systems are absent or rendered ineffective. Thus Zimmer was correct, his efforts were not in vain, and an unusual period in the history of modern science has now ended. Certain notions derived conceptually from target theory such as "sublethal damage" also are untenable. There is no scientific definition of sublethal damage in the literature; and the concept of the repair of sublethal damage likewise neglects basic scientific principles. The radiation damage that leads to cell death is all "potentially lethal" damage. Problems arising from prolonged use of unscientific abstractions are eliminated by rigorous use of extant scientific terminology and cell survival curves are explicable in terms of damage to cellular deoxyribonucleoprotein and its repair. This advance is important for the future development of radiation therapy, as will be discussed.

Story, M. D., Sanchez, F. J., Cox, A. B., and Lett, J. T. (1989) Factors influencing recovery and cellular survival of the L5178Y S/S cell from irradiation. Abstract presented at the 37th Annual Meeting of the Radiation Research Society, Seattle, WA, March 18-23, 1989.

L5178Y S/S, Hypothermia, HZE particles, X-rays, Nutrient effect

The very radiosensitive L5178Y S/S cell has been used to examine factors influencing cellular recovery and ultimately cellular survival via hyper(hypo)thermia, exposure to HZE particles, and changes in the protein components of growth media after X-irradiation. Exposure to HZE particles of LET up to 500 keV/u progressively altered the radiation substrate, making it unrecognizable to, or unmanageable by, the relevant repair systems. When cells were incubated at 23°C for various times after heavy-ion irradiation, cellular recovery was diminished and eliminated at 478 keV/u. After X-irradiation, increases in hyperthermic temperature for which cell killing was less than 50% systematically reduced the D_0 (0.27 Gy) of G_1 cells to 0.135 Gy by 41.5°C, and at G_1+8 hrs, the shoulder was progressively eliminated. For 25 years, the cell has been grown in media containing particular protein fractions, because it had been shown that variations in sera components, and hence the nutritional status of the cell, could change the survival curve. Recently, the advent of more highly purified protein components has caused another increase in radioresistance at G_1+8 hrs without changing karyotype. Over time, the changes in the purity of these fractions have resulted in defined alterations in D_0 from 0.38, via 0.50, to 0.65 Gy, thus substantiating the very early observation in 1963.

2.2.3. DNA DAMAGE AND REPAIR

JOURNALS

Lett, J. T., Keng, P. C., Bergtold, D. S., and Howard, J. (1987) Effects of heavy ions on rabbit tissues: Induction of DNA strand breaks in retinal photoreceptor cells by high doses of radiation. *Radiation and Environmental Biophysics* 26: 23-36.

New Zealand white rabbits, Alkaline sucrose gradients, Strand breakage, Heavy ions, HZE, RBE, Neon ions, Argon ions

Excised retinas from New Zealand white (NZW) rabbits were irradiated at 0°C with 9-260 Gy (depending on the type of radiation) of 300 kVp X-rays, or the first 5 cm (range: ~14 cm in water) of 365 MeV/u Ne ions or 530 MeV/u Ar ions (LET_{∞} 's: ~1, 35 ± 3 and 90 ± 5 keV/ μ m, respectively). Other positions (LET_{∞} 's) in the Ne-ion beam (Bragg curve) were employed in more limited experiments. The retinas were frozen and stored in liquid nitrogen until analysis.

Total strand breakage in the DNA of retinal photoreceptor (sensory) cells was determined from sedimentation profiles obtained by velocity sedimentation through reoriented alkaline sucrose gradients under conditions free from anomalies related to rotor speed. For the radiation doses employed: the reciprocal of the number average molecular weight, M_n , was related linearly to dose for each radiation quality and extrapolation to zero dose in each case gave positive intercepts for which the mean unirradiated molecular weight, M_0 , was $6.1 \pm 1.0 \times 10^8$ daltons; the efficiencies of total strand breakage for the different radiations were 50 ± 3 , 110 ± 2 and 240 ± 6 eV/strand break, respectively. For the heavy ions, accurate analogous calculations for other positions in the Bragg curves were precluded by beam degeneration due to fragmentation of the primary particles, etc.

Overall, the experimental results support the concept that ionizing radiations damage cellular DNA by two general processes. One process causes localized damage, which under our experimental conditions is revealed as strand breaks and/or alkali-labile bonds in regions between molecules of size *circa* 10^9 daltons (subunits); the other causes essentially random damage. Base damage caused by either process would not have been delineated in our experiments.

Peak, M. J., Peak, J. G., and Blazek, E. R. (1988) Symposium report: Radiation-induced DNA damage and repair. *International Journal of Radiation Biology* 54: 513-519.

Argonne National Laboratory, Symposium, Radioprotectants

The Argonne National Laboratory Symposium brought together 109 scientists from five countries to discuss the molecular effects of radiation on DNA and the responses of cells to radiation exposure. Six speakers covered three general areas: (1) DNA damages caused by radiations; (2) repair of these damages in prokaryotes and eukaryotes; and (3) aminothiols as radioprotectors. In addition, a roundtable discussion chaired by J. W. Ward dealt with alkaline and neutral elution methodology.

Yamamoto, O., Fuji, I., Yoshida, T., Cox, A. B., and Lett, J. T. (1988) Age dependency of base modification in rabbit liver DNA. *Journal of Gerontology: Biological Sciences* 43: B132-136.

Liver, DNA, New Zealand white rabbits, Age dependence

Age-related modifications of DNA bases have been observed in the liver of the New Zealand white (NZW) rabbit (*Oryctolagus cuniculus*), a lagomorph with a median life-span in captivity of 5-7 years. The ages of the animals studied ranged from 6 weeks to 9 years. After the DNA had been extracted from the liver cell nuclei and hydrolyzed with acid, the bases were analyzed by column chromatography with Cellulofine gels (GC-15-m). Two peaks in the chromatogram, which eluted before the four DNA bases, contained modified bases. Those materials, which were obtained in relatively large amounts from old animals, were highly fluorescent, and were shown to be crosslinked base products by mass spectrometry. The yield of crosslinked products versus rabbit age (>0.5 yr) can be fitted by an exponential function (correlation coefficient: 0.76 ± 0.09).

Yang, T. C., Craise, L. M., Mei, M-T., and Tobias, C. A. (1989) Neoplastic cell transformation by high-LET radiation: Molecular mechanisms. *Advances in Space Research* 9(10): 131-140.

Neoplasia, Mouse embryo cells, C3H10T1/2, DNA strand breaks, RBE, HZE, Cell transformation

Experimental data on molecular mechanisms are essential for understanding the bioeffects of radiation and for developing biophysical models, which can help in determining the shape of dose-response curves at very low doses, e.g., doses less than 1 cGy. Although it has been shown that ionizing radiation can cause neoplastic cell transformation directly, that high-LET heavy ions in general can be more effective than photons in transforming cells, and that the radiogenic cell transformation is a multi-step processes, we know very little about the molecular nature of lesions important for cell transformation, the relationship between lethal and transformational damages, and the evolution of initial damages into final chromosomal aberrations which alter the growth control of cells. Using cultured mouse embryo cells (C3H10T1/2) as a model system, we have collected quantitative data on dose-response curves for heavy ions with various charges and energies. An analysis of these quantitative data suggested that two DNA breaks formed within

80Å may cause cell transformation and that two DNA breaks formed within 20Å may be lethal. Through studies with restriction enzymes that produce DNA damages at specific sites, we have found that DNA double strand breaks, including both blunt- and cohesive-ended breaks, can cause cell transformation *in vitro*. These results indicate that DNA double strand breaks can be important primary lesions for radiogenic cell transformation and that blunt-ended double strand breaks can form lethal as well as transformational damages due to misrepair or incomplete repair in the cell. The RBE-LET relationship is similar for HGPRT gene mutation, chromosomal deletion, and cell transformation, suggesting common lesions may be involved in these radiation effects. The high RBE of high-LET radiation for cell killing and neoplastic cell transformation is most likely related to its effectiveness in producing DNA double strand breaks in mammalian cells. At present the role of oncogenes in radiation cell transformation is unclear.

2.2.3. DNA DAMAGE AND REPAIR

REPORTS/MEETINGS

Atwell, W. and Hardy, A. C. (1989) The solar proton event radiation hazard to high-inclination Space Shuttle missions. Abstract presented at the 6th Scientific Assembly of the International Association of Geomagnetism and Aeronomy (IAGA), Exeter University, United Kingdom, July 24-Aug. 4, 1989.

Shuttle, Protons, Computerized anatomical man model

The solar proton events that have occurred during the last three solar cycles are reviewed. The free-space spectra for the large events were computed and geomagnetically attenuated to orbital inclinations of 57 and 90 (polar) degrees. Using a shielding model of the Space Shuttle and a computerized anatomical man model, biological dose data are presented for the skin, eye, and blood-forming organs and are compared with the current NASA astronaut dose limits.

2.3. TISSUE, ORGANS AND ORGANISMS

JOURNALS

Ainsworth, E. J. (1986) Early and late mammalian responses to heavy charged particles. *Advances in Space Research* 6(11): 153-165.

Mouse lethality, CFU-S, Testes weight loss, Life-span shortening, Heavy ions, Neutrons, RBE

This overview summarizes murine results on acute lethality responses, inactivation of marrow CFU-S and intestinal microcolonies, testes weight loss, life-span shortening, and posterior lens opacification in mice irradiated with heavy charged particles. RBE-LET relationships for these mammalian responses are compared with results from *in vitro* studies. The trend is that the maximum RBE for *in vivo* responses tends to be lower and occurs at a lower LET than for inactivation of V79 and T-1 cells in culture. Based on inactivation cross sections, the response of CFU-S *in vivo* conforms to expectations from earlier studies with prokaryotic systems and mammalian cells in culture. Effects of heavy ions are compared with fission spectrum neutrons, and the results are consistent with the interpretation that RBEs are lower than for fission neutrons at about the same LET, probably due to differences in track structure. Issues discussed focus on challenges associated with assessments of early and late effects of charged particles based on dose, RBE and LET, and with the concordance or discordance of results obtained with *in vivo* and *in vitro* model systems. Models for radiation damage/repair and misrepair should consider effects observed with *in vivo* as well as *in vitro* model systems.

Butler, T. M. (1990) Program review: The lifetime effects of space radiation in rhesus monkeys. USAFSAM-TR-90-3.

Program review, Rhesus monkeys

This report summarizes findings from a select panel of scientists charged with reviewing the quality and productivity of the USAFSAM 24-year in-house study of the lifetime effects of space radiation in the rhesus monkey. The panel also had the responsibility of assessing the value of the study in both military and civilian scientific applications and making recommendations for maximizing the yield of relevant data as the animals near the end of their life-span. The panelists reviewed results presented by project scientists during a 2-day conference in San Antonio, TX (March 9-10, 1989). They were unanimous in their endorsement of the study as a uniquely important resource of information on the late effects of space radiation and the interaction of late effects with the normal aging processes. In asserting that the study should be continued for at least another 5 years, the panel made specific recommendations for additional work to be carried out in collaboration with scientists at other laboratories who could provide the breadth of technical expertise required to fully exploit the potential of this project. The scientific proceedings of the conference will be published as separate journal articles.

2.3. TISSUE, ORGANS AND ORGANISMS

REPORTS/MEETINGS

Ainsworth, E. J., Afzal, S. M. J., Crouse, D. A., Hanson, W. R., and Fry, R. J. M. (1989) Tissue responses to low protracted doses of high LET radiations or photons: early and late damage relevant to radio-protective countermeasures. *Advances in Space Research* 9(10): 299-313.

Tissue response, Low doses, Heavy charged particles, Gamma rays

Early and late murine tissue responses to single or fractionated low doses of heavy charged particles, fission-spectrum neutrons or gamma rays are considered. Damage to the hematopoietic system is emphasized, but results on acute lethality, host response to challenge with transplanted leukemia cells and life-shortening are presented. Low dose rates per fraction were used in some neutron experiments. Split-dose lethality studies (LD 50/30) with fission neutrons indicated greater accumulation of injury during a 9 fraction course (over 17 days) than was the case for g-radiation. When total doses of 96 or 247 cGy of neutrons or g rays were given as a single dose or in 9 fractions, a significant sparing effect on femur CFU-S depression was observed for both radiation qualities during the first 11 days, but there was not an earlier return to normal with dose fractionation. During the 9 fraction sequence, a significant sparing effect of low dose rate on CFU-S depression was observed in both neutron and g-irradiated mice. CFU-S content at the end of the fractionation sequence did not correlate with measured LD 50/30. Sustained depression of femur and spleen CFU-S and a significant thrombocytopenia were observed when a total neutron dose of 240 cGy was given in 72 fractions over 24 weeks at low dose rates. The temporal aspects of CFU-S repopulation were different after a single versus fractionated neutron doses. The sustained reduction in the size of the CFU-S population was accompanied by an increase in the fraction in DNA synthesis. The proliferation characteristics and effects of age were different for radial CFU-S population closely associated with bone, compared with the axial population that can be readily aspirated from the femur. In aged irradiated animals, the CFU-S proliferation/redistribution response to typhoid vaccine showed both an age and radiation effect. After high single doses of neutrons or g-rays, a significant age- and radiation-related deficiency in host defense mechanisms was detected by a shorter mean survival time following challenge with transplantable leukemia cells. Comparison of dose-response curves for life shortening after irradiation with fission-spectrum neutrons or high energy silicon particles indicated high initial slopes for both radiation qualities at low doses, but for higher doses of silicon, the effect per Gy decreased to a value similar to that for g-rays. The two component life-shortening curve for silicon particles has implications for the potential efficacy of radioprotectants. Recent studies on protection against early and late effects by amino thiols, prostaglandins, and other compounds are discussed.

2.3.1. IN VIVO/IN VITRO SYSTEMS

JOURNALS

Geard, C. R. and Worgul, B. V. (1987) The lens and cataract: Clastogenic responses in epithelial cells of the organ-cultured rat lens. *Environmental Mutagenesis* 9: 111-122.

Cataracts, Rat lens cultures, Chromosome aberrations, Gamma rays, Mutagen-carcinogens, SCE, Lenses

The epithelial cells of the vertebrate lens have an unique character and a probable involvement in cataract formation, which could be initiated by exogenous stimuli.

Individual rat lenses were organ-cultured, and the effects of mitomycin C and gamma rays on sister chromatid exchanges (SCE), chromosomal aberrations, and cellular kinetics assessed in cells from the epithelial monolayer. SCE showed about a 5.5-fold increase over the mitomycin C dose range (0, 17, 83, 170 nM), while chromosomal aberrations increased 38-fold. In cells from untreated lenses, SCE were 1,600 times more frequent than aberrations and at a level consistent with *in vivo* assessments in other cell types. Gamma rays (up to 4 Gy) had a greater inhibiting effect on cellular progression, while 17 nM mitomycin C and 1 Gy induced similar clastogenic responses.

This first demonstration of such changes in lens epithelial cells expands on the cell types available for monitoring potential mutagen-carcinogens. Additionally chromosomal changes resulting from lens cellular challenge could be the basis of later cytopathological changes in the lens, of which cataract is the primary concern to humans. Potential cataractogens warrant monitoring, and the study outlined may aid in this endeavor, as well as contributing to an understanding of cataract etiology.

2.3.1. IN VIVO/IN VITRO SYSTEMS

REPORTS/MEETINGS

Wigle, J. C. (1989) Aberrant PLD repair as a late radiation effect. Abstract presented at the 37th Annual Meeting of the Radiation Research Society, Seattle, WA, March 18-23, 1989.

Rhesus monkeys, Skin cell cultures, PLD repair, Trait effects

The Chronic Radiation Colony at the USAF School of Aerospace Medicine is a lifetime study of late effects in rhesus monkeys exposed to simulated space radiation. Radiobiological studies of primary skin cell cultures from these aged monkeys indicate that cells from 55 MeV proton irradiated monkeys are more sensitive to *in vitro* cell killing by cobalt-60 gamma rays and 55 MeV protons than cells from age-matched controls. Preliminary data suggest these differences in radiosensitivity could be related to differences in repair kinetics after irradiation. For initial surviving fractions greater than 1%, cells from control monkeys irradiated *in vitro* with 55 MeV protons accomplish little or no PLD repair (measured by colony formation) during the first 6 hrs after irradiation, followed by a gradual increase in survival over the next 18 hrs. At initial surviving fractions between 0.1% and 1%, survival increases gradually during the first 6 hrs after irradiation. 55 MeV proton irradiated CHO cells, on the other hand, show "classical" biphasic PLD repair kinetics within the first 6 hrs after irradiation and a slower phase occurring during the next 18 hrs. These repair kinetics correlate with observed RBE measurements.

2.3.2. CARCINOGENESIS AND LIFE SHORTENING

JOURNALS

Wood, D. H., Hardy, K. A., Cox, A. B., Salmon, Y. L., Yochmowitz, M. G., and Cordts, R. E. (1989) Delayed effects of proton irradiation in *Macaca mulatta* (22-year summary). Presented at the Conference on High Energy Radiation Background in Space (CHERBS 87), Sanibel Island, FL, November 3-5, 1987. American Institute of Physics Conference Proceedings No. 186, eds. A. C. Rester, Jr. and J. I. Trombka. New York: American Institute of Physics, pp. 381-392.

Rhesus monkeys, Protons, Life shortening, Cataracts, Glucose tolerance

Lifetime observations on a group of rhesus monkeys indicate that life expectancy loss from exposure to protons in the energy range encountered in the Van Allen belts and solar proton events can be correlated with the dose and energy of radiation. The primary cause of life shortening is nonleukemic cancers. Radiation also increased the risk of endometriosis (an abnormal proliferation of the lining of the uterus in females). Other effects associated with radiation exposures are lowered glucose tolerance and increased incidence of cataracts. Calculations of the relative risk of fatal cancers in the irradiated subjects reveal that the total body surface dose required to double the risk of death from cancer over a 20-year post-exposure period varies with the linear energy transfer (LET) of the radiation. The ability to determine the integrated dose and LET spectrum in space radiation exposures of humans is, therefore, critical to the assessment of lifetime cancer risk.

Wood, D. H., Yochmowitz, M. G., Hardy, K. A., and Salmon, Y. L. (1986) Animal studies of life shortening and cancer risk from space radiation. *Advances in Space Research* 6(11): 275-283.

Life shortening, Cancer risk, Total-body exposures, Rhesus monkeys, Cancer, Endometriosis

The U.S. Air Force study of the delayed effects of single, total-body exposures to simulated space radiation in Rhesus monkeys is now in its 21st year. Observations of 301 irradiated and 57 age-matched control animals indicate that life expectancy loss from exposure to protons in the energy range encountered in the Van Allen belts and solar proton events can be expressed as a logarithmic function of the dose. The primary causes of life shortening are cancer and endometriosis (an abnormal proliferation of the lining of the uterus in females). Life shortening estimates permit comparison of the risk associated with space radiation exposures to be compared with that of other occupational and environmental hazards, thereby facilitating risk/benefit decisions in the planning and operational phases of manned space missions. Calculations of the relative risk of fatal cancers in the irradiated subjects reveal that the total body surface dose required to double the risk of death from cancer over a 20-year post-exposure period varies with the linear energy transfer (LET) of the radiation. The ability to determine the integrated dose and LET spectrum in space radiation exposures of humans is, therefore, critical to the assessment of lifetime cancer risk.

2.3.3. CATARACTOGENESIS

JOURNALS

Holsclaw, D. S., Merriam, G. R., Jr., Medvedovsky, C., Rothstein, H., and Worgul, B. V. (1989) Stationary radiation cataracts: An animal model. *Experimental Eye Research* 48: 385-398.

Radiation cataracts, Bullfrogs, X-rays, Restitution, Transparency

The restitution of normal fibrogenesis that occurs in stationary radiation cataracts provides a unique opportunity to study the cytopathomechanism of radiocataractogenesis. Previous attempts at investigating this phenomenon have been limited by the lack of an appropriate animal model. This report describes the induction of stationary radiation cataracts in postmetamorphic bullfrogs following ocular irradiation with a 10 Gy (1 Gy = 100 rads) dose of X-rays. The eyes of non-irradiated animals and animals irradiated with 25 Gy (an established dose known to induce progressive cataracts in frogs) served as controls. Animals were followed biomicroscopically and histopathologically over 79 weeks. As previously described, the cataracts developed in a dose-dependent manner. The 25 Gy irradiated lenses rapidly progressed to complete opacification (4+) by 26 weeks, while lenses exposed to 10 Gy advanced to the 2.5+ stage by 35 weeks and progressed no further. In the lower dose lenses, transparent cortex began to appear anteriorly and posteriorly between the capsule and opaque fibers at 45 weeks. As the clear fibers accumulated, the disrupted region came to occupy increasingly deeper cortex. Histologically, opacities in both groups were preceded by disorganization of the bow cytoarchitecture, meridional row disorganization, and the appearance in the lens epithelium of nuclear polymorphism, fragmented nuclei, micronuclei, clusters of nuclei, and abnormal mitotic figures. In the lenses exposed to the 25 Gy dose, this damage continued to worsen, so that the 4+ stage was characterized by extensive epithelial cell death, absence of the lens bow, degenerated fiber masses, and liquefied substrata. In contrast, prior to the appearance of transparent cortex in the 10 Gy group, the lens epithelial aberrations arc of the bow, and meridional row disorganization were all observed to improve. Further, by 69 weeks, the lens epithelium appeared as a largely homogenous population and the meridional rows and the arc of the bow had become reestablished. The details of these observations and their possible relationship to the cytopathomechanism of radiation cataract formation are discussed.

Lett, J. T., Cox, A. B., and Lee, A. C. (1986) Cataractogenic potential of ionizing radiations in animal models that simulate man. *Advances in Space Research* 6(11): 295-303.

New Zealand white rabbits, Rhesus monkeys, Beagle dog, Animal models, Heavy ions, HZE

Aspects of experiments on radiation-induced lenticular opacification during the life-spans of two animal models, the New Zealand White rabbit and the Rhesus monkey, are compared and contrasted with published results from a life span study of another animal model, the beagle dog, and the most recent data from the ongoing study of the survivors from radiation exposure at Hiroshima and Nagasaki. An important connection among the three animal studies is that all the measurements of cataract indices were made by one of the authors (A.C.L.), so variation from personal subjectivity was reduced to a minimum.

The primary objective of the rabbit experiments (radiations involved: ^{56}Fe , ^{40}Ar and ^{20}Ne ions, and ^{60}Co g photons) is an evaluation of hazards to astronauts from galactic particulate radiations. An analogous evaluation of hazards from solar flares during space flight is being made with monkeys exposed to 32, 55, 138 and 400 MeV protons.

Conclusions are drawn about the proper use of animal models to simulate radiation responses in man and the levels of radiation-induced lenticular opacification that pose risks to man in space.

Odrich, S., Medvedovsky, C., Merriam, G. R., and Worgul, B. V. (1988) Micronucleation in the lens epithelium following *in vivo* exposure to physical and chemical mutagens. *Lens Research* 5(384): 203-216.

Rat lens, Lens epithelium, Micronuclei, Cataracts, Mutagenicity

Rats were exposed to cataractogenic doses of known physical and chemical genotoxic agents in order to study the efficacy of using micronuclei to monitor mutagenicity in the lens epithelium. The total numbers of micronuclei were counted in lens epithelia from rats exposed to graded doses of either 250kVp X-rays or the antileukemic drug, 1,4 dimethanesulfonylbutane (Myleran®). The results indicate a dose-dependent incidence of micronucleation in the lens epithelium following exposure. The findings are consistent with the hypothesis that the cataractogenicity of certain agents may be related to their effect on the genome of lens epithelial cells.

Worgul, B. V. (1988) Accelerated heavy particles and the lens: V. Theoretical basis of cataract enhancement by dose fractionation. *Ophthalmic Research* 20: 143-148.

Fractionation, Track structure, Lens epithelium, Inverse dose-rate effect, Cataracts

That accelerated heavy ions are highly cataractogenic is indisputable. The basis of heavy particle effectiveness and the augmentation by fractionation, as recently demonstrated, remains less clear. There is no question, however, that these are tied to the "track structure" and densely ionizing nature of the radiation. The unique energy deposition characteristics relating to charge and "track structure" are now being explored to begin to dissect the cellular response of the lens epithelium to radiation exposure. The elucidation of the basis of the cataractogenic effect of accelerated heavy ions is important not only to risk assessment, but also in the consideration of theories of radiation action and the mechanism of cortical opacification arising from a myriad of cataractotoxic agents.

Worgul, B. V., Merriam, G. R., Jr., Medvedovsky, C., and Brenner, D. J. (1989) Accelerated heavy particles and the lens. III. Cataract enhancement by dose fractionation. *Radiation Research* 118: 93-110.

Cataractogenesis, Fractionation, Rats, Ar ions, X-rays, Inverse dose-rate effect, Lens

For a number of biological end points it has been shown that, in contrast to low linear energy transfer (LET) radiation, dose fractionation of high-LET radiation does not result in a reduction in overall effectiveness. Studies were conducted to determine the effect of fractionating the exposures to heavy ion doses on the development of cataracts. Rat eyes were exposed to single doses of 1, 5, and 25 cGy of 570 MeV/amu ⁴⁰Ar ions and to 2, 4, and 10 Gy or 250 kVp X rays. These were compared to unirradiated controls and eyes that were exposed to the same total dose delivered in four fractions over 12 hours. While in all cases fractionation of the exposure to X rays produced significant reduction in cataractogenic potential, fractionating doses of ⁴⁰Ar ions caused a dose- and stage-dependent enhancement in the development of cataracts.

2.3.3. CATARACTOGENESIS

REPORTS/MEETINGS

Calvin, H. I., Medvedovsky, C., Hess, J. L., David, J., and Worgul, B. V. (1988) Rapid cataractogenesis in glutathione-depleted preweanling mice. *Investigative Ophthalmology and Visual Science* 29: 29 (abstract).

Mice cataractogenesis, Glutathione, Age dependence

The inhibitor of glutathione biosynthesis, L-buthionine sulfoximine (L-BSO), induces age-dependent dense corticonuclear cataracts in mice. Further studies have shown that consistent induction of lenticular pathology occurs after 6 injections of the drug (4 mmol/kg) over a 2-day period at 8-10 days of age. The earliest abnormalities, evident by 48 h after the initiation of treatment, include swollen fibers in the superficial anterior and posterior cortex, nucleated fibers in the deep cortex, fragmented nuclei, and disorganization of the bow. In some lenses, disappearance of fiber boundaries and granular degeneration are seen. Concomitantly, glutathione is depleted to less than 5% of control values. Between 48 and 72 h, lens wet weight increases, dry weight diminishes, glutathione becomes essentially undetectable, and Ca attains very high levels. Meanwhile, fiber swelling, rupture and degeneration have become more pronounced and extend into the deep cortex and lens nucleus. The densest opacities are seen at 16-21 days of age. Further pathological changes include: disorganization of the epithelium (gaps and stratification), large vacuoles in the anterior and posterior cortex, and scattered aggregates of fragmented nuclei. Pathology is least severe in the bow. During subsequent weeks, partial recovery takes place, as the degenerated tissue is replaced by new fibers and displaced into the deep cortex and lens nucleus. In summary, depletion of lens glutathione in preweanling mice leads to profound age-dependent damage to lens fiber cell membranes and widespread disruption of lens cytoarchitecture.

Cox, A. B., Lett, J. T., and Lee, A. C. (1990) Late cataractogenesis in primates exposed to protons. Abstract presented at the 38th Annual Meeting of the Radiation Research Society, New Orleans, LA, April 7-12, 1990.

Rhesus monkeys, Protons, Dose threshold

Rhesus monkeys (*Macaca mulatta*) irradiated in the 1960s with low acute doses of protons ranging in energy from 10-2300 MeV are demonstrating late progressive radiation cataractogenesis 20 to 25 years following exposure. Comparable late ocular changes in humans would represent significant radiation sequelae for astronauts exposed to showers of protons associated with periods of intense solar activity. At the current stage of the investigation, it appears that the dose threshold for excess cataracts attributable to radiation will be less than 2 Gy in rhesus monkeys surviving to ages in the region of the median life-span of the species.

Holsclaw, D., Worgul, B. V., Rothstein, H., and Medvedovsky, C. (1988) Modification of clinical and cytopathological changes in irradiation induced cataracts: effects of hypophysectomy and hormone replacement therapy. *Investigative Ophthalmology and Visual Science* 29: 428 (abstract).

Hypophysectomy, Hormones, Replacement therapy, Lens epithelium, Cataractogenesis, Slit-lamp microscopy, Radiation cataracts

Lens epithelial mitosis has long been implicated in the cytopathomechanism of radiation-induced cataractogenesis. It has been proposed that radio-cataractogenesis depends upon the mitosis-driven formation of aberrant fibers from epithelial cells damaged by ionizing radiation. We investigated

the role of lenticular mitosis in the cytopathogenesis of radiocataracts directly by manipulating the cell cycle of the lens epithelium in frogs by hypophysectomy (known to halt mitotic activity) and pituitary hormone administration (known to stimulate mitosis and reverse hypophysectomy-induced mitotic suppression). An additional objective was to establish an animal model within which aspects of radiocataractogenesis could be modulated.

Postmetamorphic bullfrogs were hypophysectomized, irradiated and given pituitary hormone replacement. Irradiated animals, irradiated animals + hormone replacement, and irradiated hypophysectomized animals served as controls. Cataract development was evaluated clinically by slit-lamp biomicroscopy (Merriam/Focht method) and histologically by lens epithelial whole mounts.

While irradiated hypophysectomized animals failed to develop opacities, as previously demonstrated, irradiated hypophysectomized animals with hormonal replacement (mitosis reinstated) developed cataracts; furthermore, the incidence and severity of the radiation-induced lens changes exceeded the levels of controls. These findings support a central role for lenticular mitosis in the cytopathomechanism of radiocataracts. Further, the ability to successfully modulate cataractogenesis by manipulating lenticular mitosis offers a biological system that greatly facilitates the mechanistic study of radiocataractogenesis. Applications of this system, including titrating cataractogenesis and characterizing the behavior and consequences of DNA repair in radiation-induced injury, will also be discussed.

Kung, J. S., Worgul, B. V., David, J., and Rini, F. (1987) The effects of exogenous genotoxic agents on the amphibian lens. *Investigative Ophthalmology and Visual Science* 28: 86 (abstract).

Mutagens, Benzo-a-pyrene, Ethyl-methane sulphonate, Rana pipiens, Lens epithelium, Cell cycle, Cataracts

It has been postulated that agents which are genotoxic to the lens epithelium should also be cataractogenic. A question which arises is whether incidental exposure to mutagens in the environment can affect the lens. Therefore, the genotoxic effects of the well known environmental mutagens Benzo-a-pyrene (BP) and Ethyl-methanesulphonate (EMS) on the lens epithelia of *Rana pipiens* were assessed. Four groups of frogs were immersed in 2.5, 5.0, 10.0, and 20.0 micrograms/ml of BP for one week. Four additional groups of frogs were placed into 25, 50, 100, and 200 micrograms/ml of EMS for the same period. Following sacrifice of the animals, lens epithelial whole-mounts were prepared. The epithelia were stained by the Feulgen technique to permit visualization and quantitative analysis of nuclear DNA content. The lens epithelia of frogs exposed to EMS showed evidence of genotoxicity as manifested by the appearance of micronucleated cells. More striking, however, was a marked increase in the pre-mitotic, G2, population in the lens epithelium. A concomitant decrease in mitoses suggests an arrest in the cell cycle. In contrast, micronuclei were not present in the epithelia of frogs immersed in BP and the cell cycle appeared unaffected. It is unclear whether this reflects an insensitivity of lens cells to the mutagen or that the BP and its genotoxic metabolites failed to cross the blood aqueous barrier. In any case, the experience with EMS strongly suggests that exposure to certain environmental mutagens can adversely affect the lens.

Medvedovsky, C., Merriam, G. R., Jr., David, J., Rosskothien, H., and Worgul, B. V. (1989) An integrative scoring system for experimental cataract assessment. *Investigative Ophthalmology and Visual Science* (Suppl.) 30:144 (abstract).

Scoring system, Scheimpflug-based, Experimental cataracts

Until the advent of Scheimpflug-based slitlamp camera systems (SLCs), experimental cataract assessment has been hampered by its subjectivity, lack of linearity, and unstandardized scoring criteria. While previous studies in this laboratory have shown that SLC analysis is not suitable for determining cataract onset, it does provide for linear quantification of the loss of transparency once opacification has begun. We therefore have developed a methodology whereby conventional slitlamp biomicroscopy is employed to monitor the earliest lens changes. When first noted, the cataracts are considered to have a value of one. Thereafter, progression is followed using a Zeiss SLC modified for experimental use. As opacification proceeds, it is scored by the following formula:

$$\text{Cataract stage} = 1.0 + (I_t - I_i) / I_i$$

where I_i = Intensity 0 Time, and I_t = Intensity Exptl. The scores accumulate until readings become unreliable due to very severe anterior changes preventing light from reaching the cortex. At that point the conventional slitlamp is again used to monitor for complete opacification -- Stage 4 cataracts. The intensities (I) are the pooled average measurements from four 45° meridians. The methodology and possible refinements for accurate inter- and intra-experimental comparisons will be presented.

Medvedovsky, C., Merriam, G. R., Jr., and Worgul, B. V. (1988) Nonsubjective assessment of radiation cataract development by Scheimpflug image analysis. Abstract presented at the 36th Annual Meeting of the Radiation Research Society, Philadelphia, PA, April 16-21, 1988, p. 128.

Scheimpflug image analysis, X-rays, Cataract scoring, Lens opacities, Cataracts

Historically the major impediment to radiation cataract studies, both clinical and experimental, has been the necessarily subjective nature of assessing the transparency of the lens. This has spurred the development of instruments which produce photographic or video images amenable to digital analysis.

Our laboratory has incorporated the video-based Zeiss Scheimpflug Slit-Lamp System (SLS) into our ongoing studies of radiation cataractogenesis. In order to evaluate the utility of the instrument we employed the SLS in X-ray cataract studies in rats. As a benchmark and an indicator for future comparisons we used the Merriam/Focht (M/F) method of scoring opacification by classical slit-lamp analysis. It was found that conventional slit-lamp biomicroscopic surveys by skilled observers are without question the most sensitive and reproducible means to detect and score the initial appearance of radiation cataracts (M/F scale $\leq 1+$). Once cortical involvement becomes more extensive, however (M/F scale $> 1+$ and $< 4+$), the SLS allows for a much greater resolution reflected in a continuously incremental record. The usefulness of the assay diminishes as the anterior cortex becomes more severely compromised. These findings as well as the potential of using the SLS for interpreting radiation effects on the lens, will be presented.

Medvedovsky, C. P., Seidenberg, K., David, J. Broglio, T., and Worgul, B. V. (1990) The histopathological basis of focal radiation damage to the lens epithelium. Abstract presented at the 38th Annual Meeting of the Radiation Research Society, New Orleans, LA, April 7-12, 1990 (p. 111).

Lens epithelium, Serial section, Reconstructions, Cataracts, Heavy ions, Focal damage

Recent observations of discrete focal damage to the lens epithelial population following accelerated heavy ion exposure raised the possibility of a biological effect unique to particle radiation. Extensive analysis of epithelia exposed to a variety of both low and high LET radiations has shown

this not to be the case. The development of foci in the lens epithelium appears to be a ubiquitous, albeit extremely late, response to ionizing radiation. In epithelial flat-mount preparations, the foci appear as areas of stratification, each surrounding a central low-density region containing one to several large cells. Their number, size, and onset time are dependent on dose and radiation quality. Serial section reconstructions reveal that the organization of the cortex subjacent to individual foci is always atypical. Histochemical studies found that the large central cells produce basement membrane without regard to orientation. It is believed that the lens fibers that differentiate after radiation fail to provide proper scaffolding for the overlying epithelial cells to maintain their normal spatial relationships.

Seidenberg, K., Medvedovsky, C., David, J., Broglio, T., and Worgul, B. V. (1990) Lens epithelial focal damage due to ionizing radiation. *Investigative Ophthalmology and Visual Science* 31: 204 (abstract).

Focal damage, Cataracts, Lens epithelium, Heavy ions

Recently a unique radiation pathology was described in the lens epithelia of animals exposed to accelerated heavy ions. It was typified by discrete focal areas of stratified spindle-shaped cells surrounding a low-density zone containing one to several large cells covering the normal monolayered cuboidal lens epithelium. Because the damage had not been described previously, it was thought that the foci were pathognomonic lesions specific to heavy ion exposure. Extensive analysis has shown this not to be the case. The appearance of foci in the lens epithelium appears to be a common late response to radiation. Serial sectioning and histochemical studies help further define the architecture and demonstrated the intimate involvement of degenerated cortex and new capsular material in the foci.

It is suspected that radiation injury induces a nonspecific process, which may be initiated by other cataractogenic causes that result in foci-like pathology. Anterior subcapsular cataracts caused by mechanical trauma or noxious injury to the lenses have striking similarities to the foci. Thus anterior changes in cataracta complicata (a group that includes radiation cataracts) often involve clusters of spindle-shaped cells that produce capsular material in locations not normally found to contain it. In the case of radiation-caused foci, the problem is probably due to the abnormal deposition of cortical fibers after exposure, resulting in the areas of lost architectural integrity, in turn allowing epithelial cells to invade the cortical space. While a common pathogenesis cannot be ascribed unequivocally to the other agents that produce similar focal disorganization, it is not unlikely that they all are tied to primary alterations in the substrata, i.e., the cortex.

Worgul, B. V. (1988) The theoretical basis of cataract enhancement by dose fractionation of accelerated heavy ions. *Investigative Ophthalmology and Visual Science* 29: 317 (abstract).

Dose fractionation, Cataractogenesis, Heavy ions, Inverse dose-rate effect, Cell cycle, Lens

Augmentation caused by fractionation or protraction of heavy particle doses has been reported for a number of systems, including cell transformation, cell killing, mutagenesis, life shortening and, most recently, cataractogenesis. Its mechanism, however, remains unknown. Currently one popular hypothesis is that the fractionation regimen has a synchronizing effect on the cell populations, e.g., the early fractions may place hit cells in a more vulnerable position in the cell cycle. There is very compelling evidence that the potentiation effect of split doses of heavy ions, at least for cell killing *in vitro*, is characterized by 2 distinct steps - sensitization and synchronization. Data from our laboratory indicate that for endpoints which require a surviving population, such as cataractogenesis (and perhaps tumorigenesis), synchronization and desensitization are critical. In other words, by delivering a heavy particle dose in fractions, the cells may find themselves in a less vulnerable portion of the cell cycle.

It is hypothesized that the synchronization is produced by the low linear-energy transfer component of the particle track. Studies dissecting the cellular response of the lens epithelium reveal a dependence on charge and track structure of the ions. These relationships and their relevance to cataract enhancement will be discussed.

Worgul, B. V. (1990) Quantifying genotoxicity in the lens. *Internat. Soc. Ocul. Tox.* 2: 30 (abstract).

Genotoxicity, Cataracts, Micronuclei, Cellular differentiation

The association of aberrant differentiation of the lens epithelium and a number of cortical cataracts suggests a causal relationship. If so, then any agent capable of disrupting normal morphogenesis and differentiation should by definition be cataractogenic. Inasmuch as it is generally recognized that differentiation is a function of a cascade of gene expression, one can predict that an agent capable of disrupting the genome by definition must also be cataractogenic. In our effort to examine this possibility, we have applied a variety of techniques to assay and quantify genomic instability in the lens. A variety of factors singular to the lens have proved problematic, not least of which is the limited population of epithelial cells available for study.

Of the many cytogenic techniques that we have tested, micronuclear frequency assay is the method of choice to assess mutagenesis in this population. The micronucleus is a readily discernable expression of the failure of the chromosome or chromosomal fragment to be included in the daughter cell's nuclei following cell division. The technique, its limitations, and the results of our experimental studies will be discussed. We will also present preliminary results of the application of the methodology to the human population.

Worgul, B. V., Medvedovsky, C., Powers-Risius, P., and Alpen, E. L. (1987) Cataractogenesis and cytopathological changes in mouse lenses exposed to 600 MeV/amu iron ions. *Investigative Ophthalmology and Visual Science* 28: 282 (abstract).

Mice, Fe ions, Cataracts, RBE, Micronucleation, Lens epithelium

The lenses of mice exposed to 600 MeV/amu iron ions were evaluated by slit-lamp biomicroscopy and cytopathological analyses. The doses ranged from 0.05 to 1.6 Gy and the lenses were assessed at 5, 10, and 16 months post-irradiation.

Cataracts which developed in a dose and time dependent manner were significantly more advanced in all of the exposed mice when compared to the unirradiated controls. The great difference between the severity of the cataracts caused by 0.05 Gy and those present in the control animals indicates that the lowest dose used in the study far exceeds the threshold dose for the production of cataracts by accelerated iron ions. These data, when considered in light of previous low LET radiation cataract studies on the mouse lens, suggest that at very low doses the Relative Biological Effectiveness (RBE) for iron will prove comparable to those seen for argon in the rat lens. In the rat studies RBEs in excess of 40 were observed.

The cytopathological studies demonstrated a similar dose dependence for a number of endpoints, including micronucleation, interphase death, and meridional row (MR) disorganization. X-ray cataracts and MR disorganization have been shown to correlate quantitatively. A similar correlation was seen in the present study. The microscopic changes, taken together, once again support the view that the mechanism of heavy ion-induced cataractogenesis is the same as that for cataracts caused by low LET radiation.

Worgul, B. V., Medvedovsky, C., Powers-Risius, P., and Alpen, E. L. (1988) Changes in the mouse lens caused by 600 MeV/amu accelerated iron ions. Abstract presented at the 36th Annual Meeting of the Radiation Research Society, Philadelphia, PA, April 16-21, 1988, p. 109.

Mouse lens, Iron, RBE, Cataracts, Cellular pathology

The lenses of mice were evaluated by slit-lamp biomicroscopy and cytopathological analysis following doses of 600 MeV/amu iron ions ranging from 0.05 to 1.6 Gy. The examinations were conducted at 5, 10 and 16 months post-irradiation. Cataracts were present in all irradiated animals although the severities were dose- and time-dependent. The degree of opacification observed in the 0.05 Gy dose group indicated that the threshold dose for cataractogenesis must be significantly lower. Furthermore, when compared to results from previous low-LET radiation studies in the mouse lens, a relatively high RBE is suggested for iron ions.

In addition to the overt loss of transparency, histopathological analyses revealed a strong dose dependence for a number of endpoints. These included micronucleation, interphase death, and meridional row disorganization. Previous studies have shown that X-ray cataracts and meridional row disorganization correlate quantitatively. Taken together, the microscopic changes support the view that the mechanism of heavy ion induced cataractogenesis is the same as that for cataracts caused by low-LET radiation. The damage incurred in the lens by heavy particles while quantitatively dissimilar, is qualitatively indistinguishable from that caused by X-rays.

Worgul, B. V., Medvedovsky, C., Powers-Risius, P., and Alpen, E. L. (1989) Accelerated Heavy Ions and the lens. IV. Biomicroscopic and cytopathological analyses of the lenses of mice irradiated with 600 MeV/amu ^{56}Fe ions. *Radiation Research* 120: 280-293.

Fe ions, Mice, Slit-lamp, Cataracts, Cytopathology, Lens epithelium

The lenses of mice exposed to 600 MeV/amu iron ions were evaluated by slit-lamp biomicroscopy and cytopathological analyses. The doses ranged from 0.05 to 1.6 Gy, and the lenses were assessed at several intervals post-irradiation.

Cataract, the development of which is dependent on both time and dose, is significantly more advanced in all of the exposed mice when compared to the unirradiated controls. The great difference between the severity of the cataracts caused by 0.05 Gy (the lowest dose used) and those that developed spontaneously in the control animals is an indication that 0.05 Gy may far exceed the threshold dose for the production of cataracts by accelerated iron ions.

Cytopathologically, a similar dose dependence was observed for a number of endpoints including micronucleation, interphase death, and meridional row disorganization. In addition, the exposure to the ^{56}Fe ions produced a long-term effect on the mitotic population and a pronounced "focal" loss of epithelial cytoarchitecture. The microscopic changes support the view that the mechanism of heavy-ion-induced cataractogenesis is the same as that for cataracts caused by low-LET radiation.

2.3.4. OTHER EFFECTS

JOURNALS

Cox, A. B. and Lett, J. T. (1989) The quantification of wound healing as a method to assess late radiation damage in primate skin exposed to high-energy protons. *Advances in Space Research* 9(10): 125-130.

Late radiation damage, Protons, Rhesus monkeys, Wound healing

In an experiment examining the effects of space radiations on primates, different groups of rhesus monkeys (*Macaca mulatta*) were exposed to single whole-body doses of 32- or 55-MeV protons. Survivors of those exposures, together with age-matched controls, have been monitored continuously since 1964 and 1965. Late effects of nominal proton doses ranging from 2-6 Gray have been measured *in vitro* using skin fibroblasts from the animals. A logical extension of that study is reported here, and it involves observations of wound healing after 3-mm diameter dermal punches were removed from the ears (pinnae) of control and irradiated monkeys. Tendencies in the reduction of competence to repair cutaneous wounds have been revealed by the initial examinations of animals that received doses greater than 2 Gy more than 2 decades earlier. These trends indicate that this method of assessing radiation damage to skin exposed to high-energy radiations warrants further study.

Krebs, W., Krebs, I., Merriam, G. R., Jr., and Worgul, B. V. (1988) The effect of accelerated argon ions on the retina. *Radiation Research* 115: 192-201.

Argon ions, Retina, Microlesions, Electron microscopy

It has been postulated that high energy heavy ions cause a unique form of damage in living tissue, which results from the high linear energy transfer of accelerated single particles. We have searched for these single-particle effects, so-called "microlesions," in composite electron micrographs of retinas of rats which had been irradiated with a dose of 1 Gy of 570 MeV/amu argon ions. The calculated rate of energy deposition of the radiation in the retina was about 100 keV/ μm and the fluence was four particles per 100 μm^2 . Different areas of the irradiated retinas which combined would have been expected to be traversed by approximately 2400 particles were examined. We were unable to detect ultrastructural changes in the irradiated retinas distinct from those of controls. The spatial cellular densities of pigment epithelial and photoreceptor cells remained within the normal range when examined at 24 hours and at 6 months after irradiation. These findings suggest that the retina is relatively resistant to heavy-ion irradiation and that under the experimental conditions the passage of high energy argon ions does not cause retinal microlesions that can be detected by ultrastructural analysis.

Krebs, W., Krebs, I., and Worgul, B. V. (1990) Effect of accelerated iron ions on the retina. *Radiation Research* 123: 213-219.

Rats, Fe ions, Photoreceptors, Retina, Choroid, Microlesions

The eyes of rats were exposed to doses of 0.1 and 2.5 Gy of 450-MeV/amu ^{56}Fe particles (LET ~ 195 keV/ μm). The beam axes were oriented perpendicular to the central retina of the animals. Retinas were harvested immediately (<10 min), 24 h, 15 days, 136 days, and 186 days after the experiment. The retinas of animals of equivalent ages were sampled at the same intervals. By Day 15, the spatial densities of the pigment epithelial, photoreceptor, and bipolar cells in retinas irradiated with 2.5 Gy were 15 to 20% lower than those of the controls. The cellular density of the pigment epithelium returned to the control level by Day 186 while photoreceptor and bipolar cell

numbers remained depressed. One and fifteen days after irradiation, the choroidal vessels showed signs of radiation damage. Exposure to 0.1 Gy did not affect the cellular density within the retina at the interval specified (186 days). None of the retinas showed evidence of track-specific injury that could be interpreted as microlesions or tunnel lesions.

Todd, P. (1989) Stochastics of HZE-induced microlesions. *Advances in Space Research* 9: 31-34.

HZE, Microlesions, Single-particle effects

Fundamental biological experiments with bacteria, yeast, and mammalian cells irradiated with ions heavier than helium indicate that maximal probability of single-hit inactivation does not occur when the ion has LET below about 100-200 keV/ μ m. Theoretical treatments of cell inactivation data and the radiation chemistry in particle tracks are consistent with this finding. If a "microlesion" is defined as a linear array, within a tissue, of cells inactivated with maximum probability, surrounded by non-lethally damaged cells, then, by this definition, there must be an LET below which "microlesion" damage cannot be expected. In a retrospective survey of experimental literature in which single-particle effects in tissues were sought, it was found that little or no evidence has been reported supporting single-particle effects in tissues when LET was below 200 keV/ μ m, while some experimenters who irradiated tissues with particles having LET greater than 200 keV/ μ m reported effects that could be attributed to single particle tracks.

2.3.4. OTHER EFFECTS

REPORTS/MEETINGS

Cox, A. B. (1989) Cutaneous tissue repair in irradiated primates. Abstract presented at the 37th Annual Meeting of the Radiation Research Society, Seattle, WA, 1989.

Protons, Rhesus monkeys, Wound healing

Protons will be a major radiation hazard to humans on lengthy missions in space. Even if radiation exposures are not lethal, some doses will compound effects of normal aging in individuals at risk. For this reason, late radiation effects are being studied in a group of primates known as the Chronic Radiation Colony. Following single whole-body doses of 32 or 55 MeV protons in 1964 and 1965, rhesus monkeys have been maintained as part of a long-term study. The removal of small skin biopsies for cellular studies has not compromised the health of the animals, but primates that received proton doses greater than 2.5 Gy more than 20 years ago exhibit diminished ability to heal 3-mm diameter holes in their pinnae when they are compared with age-matched controls. Trends in the results of the *in vivo* wound-healing studies parallel those seen when skin fibroblasts have been grown to senescence *in vitro*. In the latter studies, proton doses greater than 2.5 Gy tended to reduce the numbers of generations produced by skin fibroblasts in culture. Data from *in vivo* and *in vitro* experiments now indicate that late radiation effects following low or intermediate radiation doses can manifest themselves in primate skin more than 20 years after exposure when a challenge (e.g., a minor surgical treatment) is experienced.

Krebs, I., Krebs, W., Merriam, G. R., Jr., and Worgul, B. V. (1987) Irradiation of the retina with high-LET (100 KeV/ μ m) argon ions does not cause overt ultrastructural damage. *Investigative Ophthalmology and Visual Science* 28: 264 (abstract).

High-LET, Ar ions, Microlesions, Electron microscopy, Eye

The high linear energy transfer (LET) and charge of accelerated heavy ions has caused some to postulate that the passage of such particles through tissues may produce a unique form of damage, so-called "microlesions". Studies using scanning electron microscopy have suggested that tunnels or holes seen in the tissue after irradiation were in fact manifestations of such injuries. Since these studies remain largely unconfirmed and because of the importance of the microlesion concept in attempts at the assessment of risk to exposure to heavy particle irradiation, we examined the retinas of rat eyes exposed to 1 Gy of 570 MeV/amu argon ions. The ions were delivered in the plateau region of the Bragg curve. Thus, the average energy deposition of the particles throughout the retina was approximately 100 KeV/ μ m² and the dose delivered was equivalent to an average fluence of 1 particle traverse/25 μ m². The analysis was conducted using composite electron micrographs of *en face* sections of the retina from animals killed 24 hours or 6 months after irradiation, each of which covered an area of approximately 100 x 100 μ m at the level of the pigment epithelium, the rod outer segments, and the inner nuclear layer. In none of these were we able to detect ultrastructural changes distinct from those of the controls. We therefore could not confirm the existence of holes or tunnels produced by argon particles of this energy. Our studies are consistent with observations following X-irradiation of the eye which concluded that the neural elements of the retina are far less radiation-sensitive than are other ocular tissues such as the lens.

Krebs, W., Krebs, I. P., and Worgul, B. V. (1989) Ultrastructural changes in the retina and choroid due to irradiation with high energy iron ions. *Investigative Ophthalmology and Visual Science* (Suppl.) 30: 351 (abstract).

Heavy ions, HZE, Cosmic rays, Rats, Choroid, Retina, Iron

The heavy ion component (HZE) of cosmic radiation remains problematic to the assessment of risk in manned space flight. The biological effectiveness of such radiation has yet to be established, particularly in regard to nervous tissue. This has been complicated by the suggestion that a heavy particle with a charge number (Z) of 20 or more, and with a linear energy transfer (LET) of approximately 200 keV/ μ m or greater, causes a unique injury - the microlesion. We have analyzed retinas of rats irradiated with 450 keV/amu of iron ions (⁵⁶Fe, Z=26, LET=195 keV/ μ m) at doses ranging from 0.1 to 2.5 Gy. Electron micrographs of tangential sections of choroid and retina of irradiated (2.5 Gy) and control animals revealed early vascular damage in the choroid and retina. Twenty-four hours after irradiation, the densities of photoreceptor and pigment epithelial cells were decreased by about 15%, after 2 weeks by 23%, and after 19 weeks by 38%. No further reduction of cell number was seen 26 weeks after the experiment. There was no morphological evidence for microlesion damage. These findings suggest that -- as with low LET radiation -- the primary damage had been to the vascular system of choroid and retina. The resultant reduced blood flow secondarily caused the destruction of retinal cells.

Worgul, B. V. (1988) Radiation damage to the eye. Abstract presented at the 36th Annual Meeting of the Radiation Research Society, Philadelphia, PA, April 12-16, 1988, p. 149.

Lyrical biology, Lens, Cornea, Retina, Eye

*Streaming through the stratum corneum
a wondrous wetted window to within;
and traversing the lens called crystallin
that isolated singular sibling of skin;
to finally come upon retina oculi,
a brazenly brandished bit of brain,
course the photons with which we see,
as well those too tempestuous to tame.*

*And while the calmer are image bound
the latter loose a legacy lethal;
leaving we with tissue sound
to conjure constructs cosmically causal.
For though global study at first sight
provides possibilities too puny to pry;
it takes only comprehension slight
to learn far more than meets the eye.*

Worgul, B. V., Krebs, W., and Krebs, I. (1989) Ultrastructural damage in the retina and choroid of rat eyes exposed to iron ions. Abstract presented at the 37th meeting of the Radiation Research Society, Seattle, WA, March 18-23, 1989.

HZE particles, Microlesions, Rats, Fe, Retina, Choroid, Eye

The heavy ion component of cosmic radiation remains problematic to the assessment of risk in manned space flight. The biological effectiveness of HZE particles has yet to be established, particularly with regard to nervous tissue. This has been complicated by the suggestion that a heavy ion with a charge of 20 or more, and with an LET approximately 200 keV/um or greater, causes a unique injury -- the microlesion. We have analyzed retinas of rats irradiated with 450 MeV iron ions ($Z=26$; $LET=195$ keV/um) at doses ranging from 0.1 to 2.5 Gy. Electron microscopy of tangential sections of the choroid and retina of 2.5 Gy irradiated rat eyes revealed relatively early vascular damage in both tissues. Twenty-four hours after exposure, the densities of the photoreceptor and pigment epithelial cells were reduced by 15% when compared to controls. At 19 weeks after irradiation, the cell numbers were about 3/4 that of controls and remained unchanged at 26 weeks. The time course and nature of the damage to these cell populations was consonant with a primary injury to the vascular systems of the choroid and retina. Such is the case following low-LET radiation -- the destruction of retinal cells resulting secondarily from ischemia.

2.4. RADIOPROTECTANTS

REPORTS/MEETINGS

Frank, P., Medvedovsky, C., Haik, B., Rini, F., and Worgul, B. V. (1987) Radioprotection of ocular tissues by WR-2721. Abstract presented at the 35th Annual Meeting of the Radiation Research Society, p. 121.

Ocular tissues, WR-2721, X-rays, Rats

The compound WR-2721 is a derivative of mercaptoethylamine, which is currently undergoing clinical trials as a radioprotective agent. Because of the apparent inability of WR-2721 to cross the blood-aqueous-retina barrier, it is felt to minimize the possibility that the drug might interfere with the tumoricidal effect of radiation of intraocular tumors. Studies were conducted on the rat to determine if the WR-2721 might be useful in ameliorating the damage to superficial tissues following radiotherapy for intraocular and orbital tumors.

A WR-2721 (20 mg/ml) solution in normal saline was administered topically prior to irradiating rat eyes with 20 Gy of 250 kVp X-rays. The full range of controls consisted of eyes which received the saline alone, saline with radiation, radiation alone and drug given post-irradiation. The administration of WR-2721 prior to radiation significantly reduced the onset and severity of blepharoconjunctivitis. The onset of the acute stage of radiokeratitis was delayed but late corneal effects and permanent keratopathy were almost completely eliminated.

2.5. PLANTS

JOURNALS

Anikeeva, I. D., Akatov, Y. A., Vaulina, E. N., Kostina, L. N., Marenny, A. M., Portman, A. I., Rusin, S. V., and Benton, E. V. (1990) Radiobiological experiments with plant seeds aboard the biosatellite KOSMOS 1887. *Nucl Tracks Radiat Meas* 17(2): 93-97 (*Int J Radiat Appl Instrum, Part D*).

COSMOS 1887, Arabidopsis thaliana, Crepis capillaris, Shielding, Biological dosimeter, Mutation effects, Fertility

The effects of space-flight factors on the seeds of *Arabidopsis thaliana* and *Crepis capillaris* were studied provided with various protective measures: The seeds were located inside the satellite and in open space, protected with aluminum foil and also exposed without the foil, cover. When the seeds were in open space without any protection, their viability was found to be suppressed; the survival rate and fertility of plants grown from these seeds were also diminished. An increase in the frequency of chromosome aberrations (CA) and in the number of multiple injuries was registered in this case. Experiments with the aluminum foil shielding showed a decrease in the suppression of the seeds' viability, but mutational changes were found to be even more increased, while the survival rate and fertility of the plants decreased. An increase in the thickness of shielding resulted in a decrease in the effects up to the level of the control, except for the effects connected with CA and fertility of the plants. Analysis of the results shows that these impairments can be ascribed to the action of single heavy charged particles (HCP). The seeds can be thus regarded as an integral biological "dosimeter" that allows estimation of the total effects of radiation, ecological, and biological factors.

3. RISK ASSESSMENT

3.1. RADIATION HEALTH AND EPIDEMIOLOGY

JOURNALS

Sinclair, W. K. (1988) Trends in radiation protection -- a view from the National Council on Radiation Protection and Measurements (NCRP). *Health Physics* 55: 149-157.

Chernobyl, Neutrons, Radon, Quality factors, Age dependence, Occupational exposure, Risk systems

The present status of ionizing radiation protection in our society, with the exception of extraordinary events such as the Chernobyl accident, can be considered reasonably satisfactory. Occupationally, average exposures have risks no greater than accident rates in "safe" industries and show a downward trend in concert with results of safety practices in other occupations; higher exposures are being addressed specifically, and a new NCRP guideline may prove useful. An important concern relating to the quality factor for neutrons is at least partially accounted for by recent International Commission on Radiological Protection (ICRP) and NCRP recommendations. Among public exposures, the most important by far is exposure to indoor Rn. However, this problem is being addressed on all fronts, and its magnitude and the means to deal with it will soon be better known.

For the near future, we should see a stabilizing of risk estimates, albeit at levels very probably higher than formerly. There may also be an increasing tendency to use incidence rather than mortality for calculating these estimates. These changes may require some adjustment in our perspective on limits. As the difference in risk between the sexes becomes more definite, we may wish to adopt a policy of equal risk rather than one of equal dose. Age data also emphasize, more and more, the decline of risk with age; consequently, using older workers when feasible in radiation-exposure circumstances becomes more desirable.

For the longer-term future, various developments can be expected, including, possibly, a more suitable climate for a risk system, a more appropriate way to express differences in radiation quality, further knowledge of the role probabilities of causation may play in radiation control, the effect of mitigating and enhancing factors, and progress in fundamental oncology. All of these are exciting possibilities which may provide a variety of options for the most effective radiation protection in the future.

Wood, D. H., Pickering, J. E., Yochmowitz, M. G., Hardy, K. A., and Salmon, Y. L. (1988) Radiation risk assessment for military space crews. *Military Medicine* 153(6): 298-303.

Cancer risk, Occupational exposure, Radiation exposure

Space crews on Department of Defense missions may be required to accept greater radiation risks than their civilian counterparts. Data accumulated over a 20-year period on nonhuman primates exposed to simulated space radiation now make it possible to estimate life expectancy loss and cancer risk for space radiation events. The numeric risk estimated facilitate risk versus gain decisions and support more conservative radiation protection standards for non-emergency operations, especially for females.

Worgul, B. V., Krebs, W., and Koniarek, J. P. (1989) Microlesions: Theory and reality. *Advances in Space Research* 9(10): 315-323.

Microlesions, HZE particles, Fe ions, Galactic cosmic rays, Quality factors, Rats

Efforts to assess radiation risk in space have been complicated by the considerable unknowns regarding the biological effects of the heavy ion component (HZE particles) of the cosmic rays. The attention has focused primarily on the assignment of a quality factor (Q) which would take into account the greater effectiveness of heavy ions vis-a-vis other forms of ionizing radiation. If, however, as the so-called "Microlesion Theory" allows, the passage of HZE particles through living tissue produces unique biological damage, the traditional use of Q becomes meaningless. Therefore, it is critical to determine if microlesions, in fact, do exist.

While the concept does not necessarily require detectable morphological damage, "tunnel-lesions" or holes in ocular tissues have been cited as evidence of microlesions. These data, however, are open to reinterpretation. On-going light, scanning, and transmission electron microscopic studies of the corneas, lenses, and retinas of rat eyes exposed to 450 MeV/amu ⁵⁶Fe ions thus far have not revealed tunnel-lesion damage. The morphological effects of the heavy ions have been found to be qualitatively similar to the changes following other kinds of ionizing radiation.

Worgul, B. V., Merriam, G. R., Jr., and Medvedovsky, C. (1989) Cortical cataract development - an expression of primary damage to the lens epithelium. *Lens and Eye Toxicity Research* 6(4): 559-571.

Cortical cataract, Cataractotoxic load, Cell differentiation, Lens epithelium

Inasmuch as cortical opacities constitute the majority of senile cataracts their pathogenesis has been a matter of investigative concern for over a century. Evidence has been accumulating indicating a primary role for the lens epithelium in the loss of transparency of the cortex. Data from experimental work and clinical experience are consistent with a primary damage to the genome of the lens epithelial cell. The damage is mediated by the aberrant differentiation of the lens fiber cells which collectively express as a cataract. The present paper reviews some of that evidence and offers preliminary analysis of the contributing aspects of cellular parameters associated with the pathology. Also, the concept of the "cataractotoxic load" and its applicability to the development of human senile cortical cataracts is discussed.

3.1. RADIATION HEALTH AND EPIDEMIOLOGY

REPORTS/MEETINGS

Lett, J. T., Atwell, W., and Golightly, M. J. (1990) Radiation hazards to humans in deep space: a summary with special reference to large solar particle events. Presented at the National Oceanic and Atmospheric Administration (NOAA) Space Environment Services Center Users Conference, Boulder, CO, May 15-17, 1990.

Solar particle events, Radiation hazards

For didactic purposes, an adumbration is given here of the health risks faced by astronauts from radiation hazards during extended missions in deep space. Special emphasis is given, by way of the examples provided by very recent solar activity, to biological consequences of large solar proton events and the need for accurate prediction of such events. The circumstances pertaining to missions within the protection of the magnetosphere of the Earth are relatively well understood and recently they have been documented in detail.

Nachtwey, D. S. (1989) Radiological health risks. Presented at the 19th Intersociety Conference on Environmental Systems (ICES), San Diego, CA, July 24-26, 1989. SAE Technical Paper Series #891432.

HZE, Heavy ions, Doses, Dose equivalent, Quality factors, Galactic cosmic rays

The crew of a manned Mars mission will be unavoidably exposed to galactic cosmic ray (GCR) flux. If one employs conventional radiological health practices involving absorbed dose (D), dose-equivalents (H), and LET-dependent quality factors (Q), the Mars mission crew shielded by 2 g/cm² Al could receive about 0.7 Sv in a 460-day mission at solar minimum. However, three-fourths of this dose-equivalent in free space is contributed by high LET heavy ions ($Z \geq 3$) and target fragments with average Q of 10.3 and 20, respectively. Such high quality factors for these particles may be inappropriate. Moreover, in a 460-day mission, less than half of the nuclei in the body of an astronaut will have been traversed by a single heavy particle. The entire concept of D/Q/H as applied to GCR must be reconsidered.

Silberberg, R., Tsao, C. H., Adams, J. H., Jr., and Letaw, J. R. (1987) Radiation hazards in space. *Aerospace America*, October 1987, p. 38.

Radiation dose, Shielding, Space exploration

In order to understand the radiation hazards associated with space flight, one must consider the shielding necessary to protect space travellers who venture outside of the Earth's magnetic field. This article describes the three types of radiation of concern, explains radiation dose units and recommended limits by the National Council on Radiation Protection, and reviews mathematical models for calculating risk associated with different types of shielding.

Sinclair, W. K. (1990) Risk estimates for human exposure to galactic radiation. Presented at the 20th Annual Intersociety Conference on Environmental Systems (ICES), Williamsburg, VA, July 9-12, 1990. SAE Technical Paper Series #901344.

Low doses, NCRP, ICRP, Galactic cosmic rays

The probability of cancer induction is the main concern in the exposure of individuals to low doses of ionizing radiation. Estimates of the risk of cancer induction formerly (1977-1980) about 1×10^{-2} Sv⁻¹ have recently been increased to $3-5 \times 10^{-2}$ Sv⁻¹ for low doses. These increased estimates are mainly the result of changes in the assessment of the Japanese survivors of the A-bombs in 1945. They result from the accumulation of 11 years or more of data on solid tumors, changes in the statistical projection methods, and revisions in the dosimetry of those exposed. The dosimetry revisions are the result of a very comprehensive U.S.-Japan study that defines the doses more precisely than before. The high dose, high dose rate exposures in Japan result in risks higher than those due to low doses and dose rate. Thus these risks must be reduced by a dose rate effectiveness factor, which is derived mainly from laboratory information.

These changes in cancer risk estimates will affect NCRP and ICRP recommendations on protection limits for low-LET radiation. For high-LET radiations such as those encountered in space, the risks are known relative to low-LET radiation effects; therefore a quality factor must be applied that introduces additional uncertainty.

Sinclair, W. K. Recent estimates of cancer risk from low-LET ionizing radiation and radiation protection limits. Adv. Space Research, 1990

ICRP, NCRP, Low-LET, Low doses

Estimates of the risk of cancer induction, formerly about 1%/Sv, formed the basis of ICRP radiation protection limits in 1977. They have now increased to about 4-5%/Sv for low doses. These increases are based mainly on new data for the Japanese survivors of the A-bombs of 1945. They result from the accumulation of 11 years more of data on solid tumors, the revisions in the dosimetry of those exposed, and improvement in statistical methods and projections. The application of a dose rate effectiveness factor between effects at high dose rate and those at low dose and dose rate is also an important consideration. Not only has the total risk changed, but also the distribution of risk among organs. Thus the effective dose equivalent may require modification. These changes are modifying ICRP and NCRP thinking about recommendations on protection limits, especially for radiation workers.

Worgul, B. V., David, J., Odrich, S., Merriam, J., Merriam, G. R., Jr., and Geard, C. (1990) An evaluation of *in situ* mutagenic damage in the lens epithelia of cataract patients. Investigative Ophthalmology and Visual Science 31: 435 (abstract).

Lens epithelium, Cataracts, Micronuclei, Cataract patients, Mutagens

Utilizing fragments (tags) of lens epithelium recovered during the extracapsular cataract extraction procedure, we have been able to assess cytogenic changes in the epithelial population that reflect genomic instability. Epithelial tags comprising 30,000 to 90,000 cells were obtained from patients without prior regard to the type of cataract or the age of individuals. Thirty of such tags were prepared as flat mounts and stained by the Feulgen method or with chromomycin A₃. Both stain DNA stoichiometrically and therefore allow quantitative determination of a variety of nuclear parameters including size, distribution, and relative number, as well as DNA content.

A high percentage of the tags contain a population of micronucleated cells. A micronucleus (MN) is typically the consequence of a deletion of the centromere region preventing spindle attachment to the chromosome or chromosomal fragment during mitosis. MN frequency has been shown to be a correlative measure of genomic instability in a number of tissues. Experimentally, studies on the lens have established a dose-response relationship between MN frequency and exposure to genotoxins.

The presence of micronuclei in the epithelia of cataract patients appears to be independent of age. The data is less clear for the type of cataract or past exposure to mutagens due to the anecdotal nature of the assessment. However, the number of MNs in the epithelial cells of some individuals strongly suggest a history of compromised genomic integrity.

3.2. SPACE FLIGHT RADIATION HEALTH PHYSICS

JOURNALS

Akatov, Y. A., Dudkin, V. E., Kovalev, E. E., Benton, E. V., Frank, A. L., Watts, J. W. Jr., and Parnell, T. A. (1990) Depth distribution of absorbed dose on the external surface of COSMOS 1887 biosatellite. *Nuclear Tracks Radiation Measures* 17(2): 105-107 (*Int J Radiat Appl Instrum, Part D*).

COSMOS 1887, Thermoluminescent detectors, Depth distribution, Absorbed dose, Shielding thickness, Vette model

Significant absorbed dose levels exceeding 1.0 Gy per day have been measured on the external surface of the Cosmos 1887 biosatellite as functions of depths in stacks of thin thermoluminescent detectors (TLDs) of USSR and USA manufacture. The dose was found to decrease rapidly with increasing absorber thickness, thereby indicating the presence of intensive fluxes of low-energy particles. Comparison between the USSR and US results and calculations based on the Vette model environment are in satisfactory agreement. The major contribution to the dose under thin shielding thickness is shown to be from electrons. The fraction of the dose due to protons and heavier charged particles increases with shielding thickness.

Akopova, A. B., Magradze, N. V., Dudkin, V. E., Kovalev, E. E., Potapov, Y. V., Benton, E. V., Frank, A. L., Benton, E. R., Parnell, T. A., and Watts, J. W. Jr. (1990) Linear energy transfer (LET) spectra of cosmic radiation in low Earth orbit. *Nucl Tracks Radiat Meas* 17(2): 93-97 (*Int J Radiat Appl Instrum, Part D*).

Integral LET spectra, Low Earth-orbit, U.S.S.R.-U.S., COSMOS biosatellite, PNTD, Thermoluminescent detectors, Fission foils, Nuclear emulsions

Integral linear energy transfer (LET) spectra of cosmic radiation (CR) particles were measured on five Cosmos series spacecraft in low Earth orbit (LEO). Particular emphasis is placed on results of the Cosmos 1887 biosatellite, which carried a set of joint USSR-USA radiation experiments involving passive detectors that included thermoluminescent detectors (TLDs), plastic nuclear track detectors (PNTDs), fission foils, nuclear photoemulsions, etc., which were located both inside and outside the spacecraft. Measured LET spectra are compared with those theoretically calculated. Results show that there is some dependence of LET spectra on orbital parameters. The results are used to estimate the CR quality factor (QF) for the Cosmos 1887 mission.

Atwell, W., Beever, E. R., and Hardy, A. C. (1989) A parametric study of space radiation exposures to critical body organs for low Earth orbit missions. *Advances in Space Research* 9(10): 243-245.

Shuttle, Anatomical man models, Low Earth-orbit

The geomagnetically-trapped and galactic cosmic radiation environments are two of the major sources of naturally-occurring space radiation exposure to astronauts in low Earth orbit. The exposure is dependent primarily on altitude, spacecraft shielding, crew stay-times, and solar cycle effects for a 28.5° orbital inclination. Based on Space Shuttle experience, the calculated results of a parametric study are presented for several mission scenarios using a computerized anatomical man model and are compared with the NASA crew exposure limits for several critical body organs.

Atwell, W., Beever, E. R., Hardy, A. C., Richmond, R. G., and Cash, B. L. (1989) Space radiation shielding analysis and dosimetry for the Space Shuttle Program. Presented at the Conference on High Energy Radiation Background in Space (CHERBS 87), Sanibel Island, FL, November 3-5, 1987. American Institute of Physics Conference Proceedings No. 186, Eds. A. C. Rester, Jr. and J. I. Trombka. New York: American Institute of Physics, pp. 289-296.

Active dosimeters, Passive dosimeters, Shuttle, Anatomical man models, Missions, Radiation dose

Active and passive radiation dosimeters have been flown on every Space Shuttle mission to measure the naturally occurring, background Van Allen and galactic cosmic radiation doses that astronauts and radiation-sensitive experiments and payloads receive. A review of the various models utilized at the NASA/Johnson Space Center, Radiation Analysis and Dosimetry is presented. An analytical shielding model of the Shuttle was developed as an engineering tool to aid in making pre-mission radiation dose calculations and is discussed in detail. The anatomical man models are also discussed. A comparison between the onboard dosimeter measurements for the 24 Shuttle missions to date and the dose calculations using the radiation environment and shielding models is presented.

Benton, E. V. (1986) Summary of radiation dosimetry results on U. S. and Soviet manned spacecraft. *Advances in Space Research* 6(11): 315-328.

Passive radiation detectors, Active radiation detectors, U.S. spacecraft, Soviet spacecraft, Low Earth-orbit, Spacelabs

Measurements of the radiation environment aboard U.S. and Soviet manned spacecraft are reviewed and summarized. Data obtained mostly from passive and some active radiation detectors now exist for the case of low Earth-orbit missions. Major uncertainties still exist for space exposure in high altitude, high inclination, geostationary orbits, in connection with solar effects and that of shielding. Data from active detectors flown in Spacelabs 1 and 2 suggest that a variety of phenomena must be understood before the effects of long-term exposure at the space-station type of orbit and shielding can be properly assessed.

Benton, E. V. and Parnell, T. A. (1988) Space radiation dosimetry on U. S. and Soviet manned missions. In: *Terrestrial Space Radiation and Its Biological Effects*, Proceedings of the NATO Advanced Study Institute, Vol. 154, eds. P. D. McCormack, C. E. Swenberg, and H. Buecker. New York: Plenum Press, pp. 729-794.

U.S. spacecraft, Soviet spacecraft, Low Earth-orbit, Plastic nuclear track detectors, Thermoluminescent dosimeters, CR-39, Polycarbonate, Cellulose-nitrate sheets, Shuttle, Spacelab, Shielding

Radiation measurements obtained on board U.S. and Soviet spacecraft are presented and discussed. A considerable amount of data has now been collected and analyzed from measurements with a variety of detector types in low Earth orbit. The objectives of these measurements have been to investigate the dose and LET spectra within the complex shielding of large spacecraft. The shielding modifies the external radiation (trapped protons, electrons, cosmic ray nuclei) which, in turn, is quite dependent on orbital parameters (altitude, inclination). For manned flights, these measurements provide a crew exposure record and a data base for future spacecraft design and flight planning. For the scientific community, they provide useful information for planning and analyzing data from experiments with high sensitivity to radiation. In this paper, results of measurements by both passive and active detectors are described. High-LET spectra measurements were obtained by means of plastic nuclear track detectors (PNTDs) while

thermoluminescent dosimeters (TLDs) measured the dose. A few flights carried active detectors--tissue equivalent ion chambers (TEICs), particle spectrometers (generally to measure the LET distribution), and particle rate counters. On some flights, thermal and epithermal neutrons were measured with the use of fission foils, and metal samples analyzed by gamma ray spectroscopy measured low levels of several activation lines. PNTDs consisting of different combinations of CR-39, polycarbonate, and cellulose-nitrate sheets have proved to be an effective means of measuring the high-LET spectra. To date, they have been used on all the Space Shuttle flights, including Spacelabs 1 and 2, and the earlier missions of the Gemini, Apollo, and Skylab series. The assembly of various types of detectors, especially the large numbers deployed in the crew compartments, modules, access tunnels, and pallets of Spacelabs 1 and 2, have provided the most comprehensive mapping yet available of the radiation environment of a large spacecraft in low Earth orbit. They demonstrate the efficiency and advantages of coordinated measurements with passive and active detectors. The dosimetric results accumulated for over twenty-five years indicate the difficulty of accurately predicting the total picture of radiation phenomena as it will be encountered by space station crews and other future missions. Understanding the effects of different types and configurations of shielding is also of particular importance. Detailed results of the measurements and comparison with calculated values are described.

Curtis, S. B., Atwell, W., Beever, R., and Hardy, A. (1986) Radiation environments and absorbed dose estimations on manned space missions. *Advances in Space Research* 6(11): 269-274.

Radiation risk, Radiation environment, Space mission scenarios, Space Station, Geosynchronous orbit, Lunar mission, Low Earth-orbit

In order to make an assessment of radiation risk during manned missions in space, it is necessary first to have as accurate an estimation as possible of the radiation environment within the spacecraft to which the astronauts will be exposed. Then, with this knowledge and the inclusion of body self-shielding, estimations can be made of absorbed doses for various body organs (skin, eye, blood-forming organs, etc.). A review is presented of our present knowledge of the radiation environments and absorbed doses expected for several space mission scenarios selected for our development of the new radiation protection guidelines. The scenarios selected are a 90-day mission at an altitude (450 km) and orbital inclinations (28.5°, 57° and 90°) appropriate for NASA's Space Station, a 15-day sortie to geosynchronous orbit, and a 90-day lunar mission. All scenarios chosen yielded dose equivalents between five and ten rem to the blood-forming organs if no large solar particle event were encountered. Such particle events could add considerable exposure particularly to the skin and eye for all scenarios except the one at 28.5° orbital inclination.

Dudkin, V. E., Potapov, Y. V., Akopova, A. B., Melkumyan, L. V., Benton, E. V., and Frank, A. L. (1990) Differential neutron energy spectra measured on spacecraft in low Earth orbit. *Nucl Tracks Radiat Meas* 17(2): 87-91 (*Int J Radiat Appl Instrum, Part D*).

Neutrons, Plastic nuclear track detectors, Photographic emulsions, Radiation dose, Fission foils

Two methods for measuring neutrons in the range from thermal energies to dozens of MeV were used. In the first method, alpha-particles emitted from the ${}^6\text{Li}(n, \alpha)\text{T}$ reaction are detected with the help of plastic nuclear track detectors, yielding results on thermal and resonance neutrons. Also, fission foils are used to detect fast neutrons. In the second method, fast neutrons are recorded by nuclear photographic emulsions (NPE). The results of measurements on board various satellites are presented. The neutron flux density does not appear to correlate clearly with orbital parameters. Up to 50% of neutrons are due to albedo neutrons from the atmosphere while

the fluxes inside the satellites are 15-20% higher than those on the outside. Estimates show that the neutron contribution to the total equivalent radiation dose reaches 20-30%.

Letaw, J. R., Silberberg, R., and Tsao, C. H. (1987) Radiation hazards on space missions. *Nature* 330: 709-710 (commentary).

Shielding, Space exploration

On the ambitious forays into space currently being contemplated, astronauts would encounter unfamiliar radiation environments. The risk of undue exposure would be diminished by spacecraft shielding.

Letaw, J. R., Silberberg, R., and Tsao, C. H. (1988) Galactic cosmic radiation doses to astronauts outside the magnetosphere. In: *Terrestrial Space Radiation and Its Biological Effects*, Proceedings of the NATO Advanced Study Institute, Vol. 154, Eds. P. D. McCormack, C. E. Swenberg, and H. Bucker. New York: Plenum Press, pp. 663-673.

GCR, Dose equivalent, Shielding, Space Station, HZE, Radiation dosimeter

The dose and dose equivalent from galactic cosmic radiation outside the magnetosphere have been computed. Each of the principal radiation components were considered. These include primary cosmic rays, spallation fragments of the heavy ions, and secondary products (protons, neutrons, alphas, and recoil nuclei) from interactions in tissue. Conventional quality factors were used in converting from dose to dose equivalent.

Three mission environments have been considered: free space, the lunar surface, and the Martian surface. The annual dose equivalents to the blood-forming organs in these environments are approximately 500 mSv, 250 mSv, and 120 mSv, respectively (1 mSv - 0.1 rem). The dose on the lunar surface is one-half of free space because there is only a single hemisphere of exposure. The dose on the Martian surface is half again the dose on the moon because of the shielding provided by a thin carbon dioxide atmosphere.

Dose versus aluminum shielding thickness functions have been computed for the free space exposure. Galactic cosmic radiation is energetic and highly penetrating. 30 cm of aluminum shielding reduces the dose equivalent 25% to 40% (depending on the phase of the solar cycle). Aiming for conformity with the draft NCRP annual dose limit for Space Station crew members, which is 500 mSv yr⁻¹, we recommend 7.5 cm of aluminum shielding in all habitable areas of spacecraft designed for long-duration missions outside Earth's magnetosphere. This shielding thickness reduces the galactic cosmic ray dose and diminishes the risk to astronauts from energetic particle events.

Letaw, J. R., Silberberg, R., and Tsao, C. H. (1989) Radiation hazards on space missions outside the magnetosphere. *Advances in Space Research* 9(10): 285-291.

Dose equivalent, Shielding materials, Doses, Solar energetic particles

Future space missions outside the magnetosphere will subject astronauts to a hostile and unfamiliar radiation environment. An annual dose equivalent to the blood-forming organs (BFOs) of ~0.5 Sv is expected, mostly from heavy ions in the galactic cosmic radiation. On long-duration missions, an anomalously large solar energetic particle event may occur. Such an event can expose astronauts to up to ~25 Gy (skin dose) and up to ~2 Sv (BFO dose) with no shielding. The

anticipated radiation exposure may necessitate spacecraft design concessions and some restriction of mission activities. In this paper we discuss our model calculations of radiation doses in several exo-magnetospheric environments. Specific radiation shielding strategies are discussed. A new calculation of aluminum equivalents of potential spacecraft shielding materials demonstrates the importance of low-atomic-mass species for protection from galactic cosmic radiation.

Letaw, J. R., Silberberg, R., Tsao, C. H., and Benton, E. V. (1989) Model analysis of Space Shuttle dosimetry data. *Advances in Space Research* 9(10): 257-260.

Plastic track detector, Shuttle, STS-51F, STS-51J, STS-61C, Radiation dosimeter

An extensive model analysis of plastic track detector measurements of high-LET particles on the Space Shuttle has been performed. Three shuttle flights, STS-51F (low-altitude, high-inclination), STS-51J (high-altitude, low-inclination), and STS-61C (low-altitude, low-inclination), are considered. The model includes contributions from trapped protons and galactic cosmic radiation as well as target secondary particles. Target secondaries, expected to be of importance in thickly shielded space environments, are found to be a significant component of the measured LET (linear energy transfer) spectra.

Parnell, T. A., Watts, J. W., Jr., Fishman, G. J., Benton, E. V., Frank, A. L., and Gregory, J. C. (1986) The measured radiation environment within Spacelabs 1 and 2 and comparison with predictions. *Advances in Space Research* 6(12): 125-134.

Spacelab, Passive radiation detectors, Active radiation detectors, Thermoluminescent dosimeters, Ion chambers, South Atlantic Anomaly, Proportional counters

To measure the radiation environment in the Spacelab (SL) module and on the pallet, a set of passive and active radiation detectors was flown as part of the Verification Flight Instrumentation (VFI). SL1 carried 4 passive and 2 active detector packages which, with the data from the 26 passive detectors of Experiment INS006, provided a comprehensive survey of the radiation environment within the spacecraft. SL2 carried 2 passive VFI units on the pallet. Thermoluminescent dosimeters (TLDs) measured the low linear energy transfer (LET) dose component; the HZE fluence and LET spectra were mapped with CR-39 track detectors; thermal and epithermal neutrons were measured with the use of fission foils; metal samples analyzed by gamma ray spectroscopy measured low levels of several activation lines. The TLDs registered from 97 to 143 mrad in the SL1 module. Dose equivalents of 330 ± 70 mrem in the SL1 module and 537 ± 37 mrem on the SL2 pallet were measured. The active units in the SL1 module each contained an integrating tissue-equivalent ion chamber and two differently-shielded xenon-filled proportional counters. The ion chambers accumulated 125 and 128 mrad for the mission with 17 and 12 mrad accumulated during passages through the South Atlantic Anomaly (SAA). The proportional counter rates (~ 1 cps at sea level) were ~ 100 cps in the middle of the SAA (mostly protons), ~ 35 cps at large geomagnetic latitudes (cosmic rays), and ~ 100 cps in the South Horn of the electron belts (mostly bremsstrahlung). Detailed results of the measurements and comparison with calculated values are described.

Richmond, R. G., Badhwar, G. D., Cash, B., and Atwell, W. (1987) Measurement of differential proton spectra onboard the Space Shuttle using a thermoluminescent dosimetry system. *Nuclear Instruments and Methods in Physics Research* A256: 393-397.

Shuttle, Thermoluminescent dosimeters, Low-inclination orbits, Low Earth-orbit

An experimental technique that permits the extraction of orbit-averaged, differential energy spectra of trapped radiation belt protons using simple passive detectors is described. An inversion technique is used for the data analysis. The basic principle of the described system is the measurement of the energy deposited in six thermoluminescent (TLD) detector assemblies behind various spherical absorbers. The technique has been applied to a detector assembly flown on four Shuttle flights. Although severe restraints were placed on the flight package, the differential energy spectra derived from these measurements are in good agreement with analytical results using a modified trapped proton environment model. The technique shows good promise for measuring the spectra in low inclination orbits where the flux of high energy galactic cosmic ray protons is small. Modifications to the detector assembly to improve the accuracy and to extend the range of the system to higher energies are suggested.

Simonsen, L. C., Nealy, J. E., Townsend, L. W., and Wilson J. W. (1990) Space radiation dose estimates on the surface of Mars. *Journal of Spacecraft and Rockets* 27: 353-354.

Radiation dose, Mars, Galactic cosmic rays, Solar energetic particles

A future goal of the U.S. space program is a commitment to the manned exploration and habitation of Mars. An important consideration of such missions is the exposure of crewmembers to the damaging effects of ionizing radiation from high-energy galactic cosmic ray fluxes and solar proton flares. The crew will encounter the most harmful radiation environment in transit to Mars from which they must be adequately protected. However, once on the planet's surface, the Martian environment should provide a significant amount of protection from free-space radiation fluxes.

In the current Mars scenario descriptions, the crew flight time to Mars is estimated to be anywhere from 7 months to over a year each way, with stay times on the surface ranging from 20 days to 2 years. To maintain dose levels below established astronaut limits, dose estimates need to be determined for the entire mission length. With extended crew durations on the surface anticipated, the characterization of the Mars radiation environment is important in assessing all radiation protection requirements. This synopsis focuses on the probable doses incurred by surface inhabitants from the transport of galactic cosmic rays and solar protons through the Mars atmosphere.

Townsend, L. W., Nealy, J. E., Wilson, J. W., and Atwell, W. (1989) Large solar flare radiation shielding requirements for manned interplanetary missions. *Journal of Spacecraft and Rockets* 26: 126-128.

Solar flare, Radiation shielding, Transport codes, Dose equivalent, Organic polymers

As the 21st century approaches, there is an ever-increasing interest in launching manned missions to Mars. A major concern to mission planners is exposure of the flight crews to highly penetrating and damaging space radiations. Beyond the protective covering of the Earth's magnetosphere, the two main sources of these radiations are galactic cosmic rays and solar particle events. Preliminary analyses of potential exposures from galactic cosmic rays (GCRs) were presented elsewhere. In this Note, estimates of shielding thicknesses required to protect astronauts on interplanetary missions from the effects of large solar flare events are presented. The calculations use integral proton fluences for the February 1956, November 1960, and August 1972 solar particle events as inputs into the NASA Langley Research Center nucleon transport code BRYNTRN. This deterministic computer code transports primary protons and secondary protons and neutrons through any number of layers of target material of arbitrary thickness and composition. Contributions from target nucleus breakup (fragmentation) and recoil are also included. The results for each flare are presented as estimates of dose equivalent [in units of roentgen equivalent

man (rem)] to the skin, eye, and blood-forming organs (BFO) behind various thicknesses of aluminum shielding. These results indicate that the February 1956 event was the most penetrating; however, the August 1972 event, the largest ever recorded, could have been mission- or life-threatening for thinly shielded (≤ 5 g/cm²) spacecraft. Also presented are estimates of the thicknesses of water shielding required to reduce the BFO dose equivalent to currently recommended astronaut exposure limits. These latter results suggest that organic polymers, similar to water, appear to be a much more desirable shielding material than aluminum.

Townsend, L. W., Wilson, J. W., and Cucinotta, F. A. (1987) A simple parameterization for quality factor as a function of linear energy transfer. *Health Physics* 5: 531-532.

Quality factors

In a recent report of a Joint Task Group of the International Commission on Radiological Protection (ICRP) and the International Commission on Radiation Units and Measurements (ICRU) to these same organizations (ICRU86), the problem of radiation quality and its quantitative treatment in protection studies was addressed. The conclusions of the report, although intended as input to these two commissions and not as recommendations from them, have nevertheless been endorsed in principle by the ICRU and subsequently published. The ICRP is currently reviewing its general recommendations about Q , the radiation quality factor, but has not yet altered them (ICR486).

Wilson, J. W., Shinn, J. L., and Townsend, L. W. (1990) Nuclear reaction effects in conventional risk assessment for energetic ion exposure. *Health Physics* 58: 749-752.

Quality factors, Nuclear reaction effects

Biological risks are related to the local energy deposited by the passage of energetic ions. The ionization energy loss is of the order of $0.2 Z^2$ keV/ μ for a passing high-energy ion of charge Z . Some of the ions produce nuclear reactions in which 10 to 100 MeV are released (per event) locally as secondary nuclear fragments. The average energy transfer rate is $0.05 A^{2/3}$ keV/ μ , where A is the ions' atomic weight. Since the quality factor of the fragments is usually taken as 20, the risk associated with direct atomic ionization is on the order of risk associated with the nuclear events for incident low-charge ions ($Z < 5$), while the risk is dominated by the direct ionization for high charge ($Z > 5$). At a sufficiently low energy, the direct ionization always dominates the biological risk independent of the ion charge and mass. In the present note, we quantify these various contributions to biological risk using quality factors presently in force (ICRP 1977) and evaluate the effects of newly proposed quality factors (ICRU 1986).

3.2. SPACE FLIGHT RADIATION HEALTH PHYSICS

REPORTS/MEETINGS

Atwell, W. (1989) Space radiation exposures to critical body organs for low Earth orbit missions. Invited paper presented at the 60th Annual Meeting of the Aerospace Medical Association, Washington DC, May 7-11, 1989.

Anatomical man models, Organ dose equivalent

The geomagnetically trapped, galactic cosmic, and solar particle event radiation environments are the three major sources of naturally occurring space radiation exposure to astronauts in low Earth orbit. The degree of radiation exposure is dependent on mission altitude, inclination and duration, spacecraft and spacesuit shielding, and solar cycle effects. Using a computerized anatomical man model, critical body organ dose equivalent data are presented for several mission scenarios. These results are compared with the current NASA crew exposure limits.

Atwell, W. (1990) Astronaut exposure to space radiation: Space Shuttle experience. Invited paper presented at the 20th Intersociety Conference on Environmental Systems (ICES), Williamsburg, VA, July 9-12, 1990. SAE Technical Paper Series #901342.

Shuttle, Exposure estimates, Radiation dosimeter

Space Shuttle astronauts are exposed to both the "trapped" and the galactic cosmic radiation environments. In addition, the sun periodically emits high-energy particles that could pose a serious threat to flight crews. NASA adheres to federal regulations and recommended exposure limits for radiation protection and has established a radiological health and risk assessment program. Using models of the space radiation environment, a Shuttle shielding model, and an anatomical human model, crew exposure estimates are made for each Shuttle flight. The various models are reviewed. Dosimeters are worn by each astronaut and are flown at several fixed locations to obtain in-flight measurements. The dosimetry complement is discussed in detail. A comparison between the pre-mission calculations and measurements is presented. Extrapolation of Shuttle experience to long-duration exposure is explored.

Atwell, W., Beever, E. R., and Hardy, A. C. (1987) Radiation shielding analysis for the Space Shuttle Program: An overview. Proceedings, Theory and Practices in Radiation Protection and Shielding, American Nuclear Society, Knoxville, TN, April 22-24, 1987, pp. 271-280 (ISBN: 0-89448-132-0).

Dose calculations, Shielding models, Shuttle dosimeter

An overview of the capabilities and methodologies utilized at the National Aeronautics and Space Administration (NASA)/Johnson Space Center (JSC) to perform pre-mission and real-time space radiation dose calculations for the Space Shuttle program is presented. The three sources of naturally occurring space radiation, a) geomagnetically trapped (Van Allen belts) protons and electrons, b) galactic cosmic radiation (GCR), and c) solar flare particles (predominantly protons), are discussed. Analytical tools, such as environment models, spacecraft shielding models and radiation dose computer programs, are also discussed. Pre-mission radiation dose calculations are compared with onboard Space Shuttle dosimeter measurements.

Atwell, W., Hardy, A. C., Beever, E. R., Richmond, R. G., and Cash, B. L. (1987) A comparison of space radiation dose calculations with onboard dosimeter measurements for Space Shuttle missions. Presented at the NASA Workshop, High Energy Accelerator and Space Radiation, Berkeley, CA, February 17-19, 1987.

Shielding model, Passive dosimeters, Active dosimeters, Thermoluminescent dosimeters, Shielding measurements

Utilizing an analytical shielding model of the Space Shuttle and the natural space radiation environment models, pre-mission dose calculations are made prior to each Shuttle mission. Passive dosimeters are flown at six fixed locations in the Shuttle, and active dosimeters are onboard to support extra-vehicular activity and contingency situations for every flight. In addition,

each crewman wears a passive thermoluminescent dosimeter. The dosimeters are read out shortly after landing. The comparison of pre-mission calculations with the measurements is discussed in detail. Results indicate a good agreement between the calculations and measurements and provide confidence in the shielding and environment models.

Golightly, M. J., Atwell, W., Hardy, A. C., Hardy, K., Quam, W., and Riehl, K. (1990) Time-resolved dose and dose equivalent measurements during high inclination shuttle missions made with the U.S. Air Force radiation monitoring equipment (RME)-III. Abstract presented at the 61st Annual Meeting of the Aerospace Medical Association, New Orleans, LA, May 13-17, 1990.

Radiation dosimetry, RME-III, Shuttle

INTRODUCTION. Routine ionizing radiation dosimetry aboard the U.S. Space Shuttle is done with simple passive and active dosimeters. A significant improvement is achieved by using a tissue-equivalent instrument that provides time-correlated radiation quality, integral dose and instantaneous dose rate information. **METHODS.** The RME-III is a portable active dosimeter developed by EG&G for the U.S. Air Force. It features a 3-channel tissue-equivalent proportional counter that measures particle fluence and dose and computes dose equivalent at operator-selected time intervals. The data and time of each reading are stored in memory modules for future analysis. The RME-III was flown in a middeck locker aboard Shuttle missions STS-27 and STS-28; these missions featured 57° inclination orbits at altitudes of 242 nm and 160 nm, respectively. Time-resolved measurements were correlated with spacecraft position. **RESULTS.** 102 hours and 116 hours of data, measured at 10-second intervals, were collected during STS-27 and STS-28, respectively. Total dose and dose equivalent measured were 1580 μGy and 2473 μSv (STS-27) and 636 μGy and 1094 μSv (STS-28). The dose was separated into trapped proton, Galactic Cosmic Radiation (GCR), and solar particle event (SPE) proton components. The dose/dose equivalent measured during STS-27 was dominated by trapped protons, while measurements from STS-28 were dominated by GCR. Additionally, the dose inside the crew module from the SPE that occurred during STS-28 was determined. **CONCLUSIONS.** The RME represents a significant improvement in manned space flight radiation dosimetry; time-resolved data permits separation of the dose into major sources of exposure. A similar measurement of source terms is not possible with current Shuttle dosimetry.

Hardy, K. A., Atwell, W., Golightly, M. J., Hardy, A. C., Quam, W. (1990) Real-time and time-resolved dose measurements on Space Shuttle missions with the radiation monitoring equipment (RME)-III. Presented at the 35th Annual Meeting of the Health Physics Society, Anaheim, CA, June 24-28, 1990 (Paper No. TAM-B9).

Active dosimeters, Shuttle, Tissue equivalent proportional counter, Doses, Dose equivalent

The RME-III is a self-contained portable active dosimeter system developed by EG&G for the US Air Force and modified for use on the Space Shuttle. It features a three-channel tissue equivalent proportional counter that measures particle fluence and computes dose and dose equivalent at operator-selected time intervals. The total accumulated dose and dose equivalent are displayed real time on a liquid crystal display while the data and time of the interval dose readings are stored in memory modules for future analysis. Analysis of the time-resolved data permits correlation of the radiation exposure with Shuttle position and altitude.

The RME-III was flown in a middeck locker aboard STS-27, STS-28, and STS-33. STS-27 and STS-28 featured 57° inclination circular orbits at 448 km (242 NM) and 296 km (160 NM), respectively, while STS-33 flew at a 28.5° inclination elliptical orbit (perigee: 231 km [125 NM]; apogee: 563 km [304 NM]). Total dose and dose equivalent measured were 1580 μGy /2473 μSv

on STS-27, 636 $\mu\text{Gy}/1094 \mu\text{Sv}$ on STS-28, and 3706 $\mu\text{Gy}/4827 \mu\text{Sv}$ on STS-33. Analysis of the time-resolved data indicated that doses on STS-27 and STS-33 were dominated by the trapped Van Allen Belt protons, while the dose on STS-28 was primarily due to galactic cosmic rays. A solar proton event also occurred on STS-28 that was measured with the RME-III. Time-resolved data from each mission are presented.

Keith, J. E. and Richmond, R. G. (1987) Neutrons in space: Measurements aboard the Space Shuttle. Proceedings, theory and practices in radiation protection and shielding, American Nuclear Society, Knoxville, TN, April 22-24, 1987, pp. 281-286 (ISBN 0-89448-132-0).

Neutron flux, Space Shuttle, Shielding measurements

One of the most complex and challenging problems of measuring radiation levels in manned spacecraft has been the characterization of the neutron flux within the vehicle. Recently it has been suggested that the quality factor for neutrons should be raised, resulting in larger dose-equivalents. A simple, initial experiment to measure the time-averaged neutron fluxes within the Space Shuttle has been completed. This paper describes the technique, reports the results, evaluates the necessary assumptions, and discusses the implications.

Konradi, A., Richmond, R. G., Hardy, A. C., and Atwell, W. (1986) Space Shuttle dosimeters as indicators of long-term inner belt stability. Abstract presented at the Fall Meeting of the American Geophysical Union, San Francisco, CA, December 1986. *Eos* 67: 1154.

Thermoluminescent dosimeter, Shuttle, Radiation dosimeter

Between 1983 and 1986 thermoluminescent dosimeters were carried on 20 shuttle flights at a variety of orbital altitudes corresponding to the region of the atmospheric cutoff of the South Atlantic Anomaly. Shielded by the Space Shuttle structure, these dosimeters respond to any penetrating inner belt protons and galactic cosmic rays. The measured orbit averaged dose was compared to dose calculations based on radiation belt models for solar maximum and solar minimum derived from data centered around 1970 and 1964, respectively. The results show that after two solar cycles the observations agree with the predictions of the solar minimum model to better than a factor of two. This difference falls within the accuracy of the model.

Richmond, R. G., Badhwar, G. D., Cash, B. L., and Atwell, W. (1987) Measurement of orbit-averaged, differential energy spectra of trapped protons using thermoluminescent dosimeter techniques. Proceedings, Theory and Practices in Radiation Protection and Shielding, American Nuclear Society, Knoxville, TN, April 22-24, 1987, pp. 264-270 (ISBN: 0-89448-132-0).

Thermoluminescent dosimeters, Shuttle, Low-inclination orbits, Low Earth-orbit

A unique detector assembly consisting of six thermoluminescent detector (TLD) stacks under different thicknesses of spherical absorbers, has been flown on four Shuttle flights. The TLD detectors provide a measure of the total energy deposited by the charged particles (protons) that penetrate the absorbers. An inversion technique has been developed to extract the orbit-averaged, differential energy spectra of the trapped radiation belt protons from these measurements. For low-inclination orbits, the extracted spectra are in good agreement with the spectra calculated using trapped radiation models. The technique offers good promise for estimating differential proton spectra on a routine basis inside the Shuttle for low-inclination missions. The system/technique is not recommended for higher (greater than 30 degrees) inclination missions for spacecraft altitudes less than 300 nm. The reasons are discussed.

Shinn, J. L., Wilson, J. W., and Nealy, J. E. (1990) Reliability of the Equivalent Sphere Model in Blood-Forming Organ Dose Estimation. NASA Technical Memorandum 4178.

Dose equivalent, Sphere model, Mars

The radiation dose equivalents to blood-forming organs (BFOs) of astronauts on the Martian surface due to major solar flare events are calculated using the detailed body geometry of Langley and Billings. The solar flare spectra of February 1956, November 1960, and August 1972 events are employed instead of the idealized Webber form. The detailed geometry results are compared with those based on the 5-cm sphere model, which has been used often in the past to approximate BFO dose and dose equivalent. Larger discrepancies are found for the later two events, possibly due to the lower numbers of highly penetrating protons. It is concluded that the 5-cm sphere model is not suitable for quantitative use in connection with future NASA deep-space, long-duration mission shield design studies.

Silberberg, R., Tsao, C. H., Adams, J. H., Jr., and Letaw, J. R. (1989) High-energy radiation environment during manned space flights. Presented at the Conference on High Energy Radiation Background in Space (CHERBS 87), Sanibel Island, FL, November 3-5, 1987. AIP Conference Proceedings No. 186, eds. A. C. Rester, Jr. and J. I. Trombka (American Institute of Physics, New York, 1989), pp. 146-158.

Galactic cosmic rays, Long-duration space missions, Shielding

Radiation doses from cosmic rays on long-duration space missions, at solar minimum, with 4 g/cm² Al shielding and 5 g/cm² tissue self-shielding exceed by a factor of about 60 the allowable dose of 0.5 rem/year to the general public and by a factor of about 6 the dose of 5 rem/year allowable to radiation workers. The annual dose of 30 rem nearly equals the allowable dose to a few volunteer astronauts which is 40 rem/year. Rare solar flare particle events would deliver doses of about 200 to 300 rem, in a period of about one day (like the 1956 and 1972 flares) for the above conditions of shielding. These doses are lethal to about 20 percent and 40 percent of the recipients, respectively.

We shall present here detailed flux and dose calculations with shielding, using the fluxes and energy spectra of all the nuclei from hydrogen to iron, nuclear spallation cross sections, and our NRL propagation code for cosmic ray nuclei, and the HETC and MCNP codes developed at Oak Ridge for protons, mesons and neutrons. Radiation quality factors, appropriate to the rate of ionization of various cosmic-ray and secondary nuclei and of nuclear recoils, will be included in the dose calculations.

Our calculations show that both the cosmic-ray and solar particle doses can be brought down to acceptable levels. For thin shielding, the contribution of heavy nuclei to the dose dominates since the rate of ionization is proportional to Z^2 , and for heavy ions, the quality factor $Q=20$. For thick shielding, the dose from neutron-generated nuclear recoils dominates.

Simonsen, L. C., Nealy, J. E., Townsend, L. W., and Wilson, J. W. (1990) Radiation exposure for manned Mars surface missions. NASA Technical Paper 2979.

Mars, BRYNTRN, Galactic cosmic rays, Solar energetic particles, Transport codes

The Langley cosmic ray transport code and the Langley nucleon transport code (BRYNTRN) are used to quantify the transport and attenuation of galactic cosmic rays (GCR) and solar proton flares through the Martian atmosphere. Surface doses are estimated using both a low-density and a high-density carbon dioxide model of the atmosphere which, in the vertical direction, provide a total of 16 g/cm² and 22 g/cm² of protection, respectively. At the Martian surface during the solar minimum cycle, a blood-forming organ (BFO) dose equivalent of 10.5 to 12 rem/yr due to galactic cosmic ray transport and attenuation is calculated. Estimates of the BFO dose equivalents that would have been incurred from the three large solar flare events of August 1972, November 1960, and February 1956 are also calculated at the surface. Results indicate surface BFO dose equivalents of approximately 2-5, 5-7, and 8-10 rem per event, respectively. Doses are also estimated at altitudes up to 12 km above the surface where the atmosphere will provide less total protection.

Townsend, L. W., Nealy, J. E., Wilson, J. W., and Simonsen, L. C. (1990) Estimates of galactic cosmic ray shielding requirements during solar minimum. NASA Technical Memorandum 4167.

Galactic cosmic rays, Transport codes, Shielding, Doses, Dose equivalent

Estimates of radiation risk from galactic cosmic rays are presented for manned interplanetary missions. The calculations use the Naval Research Laboratory cosmic ray spectrum model as input into the Langley Research Center galactic cosmic ray transport code. This code, which transports both heavy ions and nucleons, can be used with any number of layers of target material, consisting of up to five arbitrary constituents per layer. Calculated galactic cosmic ray fluxes, doses, and dose equivalents behind various thicknesses of aluminum, water, and liquid hydrogen shielding are presented for the solar minimum period. Estimates of risk to the skin and blood-forming organs (BFO) are made using 0-cm and 5-cm-depth dose and dose equivalent values, respectively, for water. These results indicate that at least 3.5 g/cm² (3.5 cm) of water, or 6.5 g/cm² (2.4 cm) of aluminum, or 1.0 g/cm² (14 cm) of liquid hydrogen shielding is required to reduce the annual exposure below the currently recommended BFO limit of 0.5 Sv. Because of large uncertainties in fragmentation parameters and the input cosmic ray spectrum, these exposure estimates may be uncertain by as much as a factor of 2 or more. The effects of these potential exposure uncertainties or shield thickness requirements are analyzed.

Townsend, L. W., Wilson, J. W., and Nealy, J. E. (1989) Space radiation shielding strategies and requirements for deep space missions. Paper presented at the 19th Intersociety Conference on Environmental Systems (ICES), San Diego, CA, July 24-26, 1989. SAE Technical Paper Series #891433.

Space radiation, Shielding strategies, Dose equivalent

The ultimate limitation to manned exploration of the solar system will likely be cumulative exposure of the crews to penetrating space radiations. The two major sources of these radiations during deep-space missions are solar particle events (flares) and galactic cosmic rays. Methods to estimate crew exposures and to evaluate concomitant shield requirements for these radiation sources are currently under development. Consisting of deterministic space radiation transport computer codes and accurate models of their nuclear interaction inputs, these calculational tools are employed to estimate the composition and thicknesses of candidate shield materials required for spacecraft equipment and crew protection. In this paper, the current status of model and code development is summarized, preliminary estimates of deep-space shield requirements are presented, and an assessment of radiation protection as a potential "showstopper" for manned deep-space missions will be made.

3.3. INTER- AND INTRASPECIES EXTRAPOLATION

JOURNALS

Dalrymple, G. V., Nagle, W. A., Moss, A. J., Cavin, L. A., Broadwater, J. R., McGuire, E. L., Eason, C. S., Mitchell, J. C., Hardy, K. A., Wood, D. H., Salmon, Y. A., and Yochmowitz, M. G. (1989) The protons of space and brain tumors: 1. Clinical and dosimetric considerations. In: High Energy Radiation Background in Space, Eds. A. C. Rester, Jr. and J. I. Trombka. New York: American Institute of Physics, pp. 407-411.

Rhesus monkeys, Protons, RBE, Glioblastoma, Brain tumors, Radiation therapy

Almost 25 years ago a large group of rhesus monkeys were irradiated with protons (32-2300 MeV). The experiments were designed: (1) to estimate the RBE of protons *per se*, and (2) to provide some estimate of the hazards of the radiation environment of space. The initial results showed the RBE to be about 1.0 for acute radiation effects (mortality, hematologic changes, etc.). The colony has been maintained at Brooks AFB, TX, since irradiation. The survivors of 55 MeV proton irradiation have developed a very high incidence of Glioblastoma multiforme, a highly malignant primary brain tumor. These tumors appeared 1-20 years after surface doses of 400-800 rads. Reconstruction of the dosimetry suggests that some areas within the brain may have received doses of 1500-2500 rads. More than 30 radiation-induced Glioblastomas have been reported in human patients who had received therapeutic head irradiation. The radiation doses required to induce Glioblastoma were of the same order of magnitude as required to induce Glioblastoma in the Rhesus monkey.

Cox, A. B., Lee, A. C., and Lett, J. T. (1988) Delayed effects of proton irradiation in the lens and integument: a primate model. In: *Terrestrial Space Radiation and Its Biological Effects*, Proceedings of the NATO Advanced Study Institute, Vol. 154, eds. P. D. McCormack, C. E. Swenberg, and H. Bucker. New York: Plenum Press, pp. 415-422.

Rhesus monkeys, Chronic Radiation Colony, Protons, Glioblastoma, Endometriosis

In 1964, the NASA Manned Spacecraft Center Biomedical Research Office and the USAF School of Aerospace Medicine inaugurated an experiment in Space Radiation Biology which now is approaching completion. Rhesus monkeys were irradiated "whole body" with X-rays (2 MeV), individual animals that received low and intermediate doses have been monitored for over 20 years, and those animals, together with age-matched controls, are known as the Chronic Radiation Colony (CRC). The CRC has provided exceptional information on late radiation effects of protons on primates. Highlights of the data from the colony include documentation of a high incidence of brain tumors (glioblastomas) in monkeys exposed to nominal surface doses of 55 MeV protons, ranging from 4.00 to 8.00 Gray (e.g., Wood et al. 1986 a and b). Also of interest is a high frequency of endometriosis in irradiated female (monkeys e.g., Wood et al., 1983). As the CRC population decreases in size, complete physical examinations of all animals will continue to be scheduled semiannually. In addition, however, we are looking for signs of more subtle (less devastating) late radiation damage which might provide insight into the realistic limits of exposure to be defined for humans participating in future space missions.

Lett, J. T., Cox, A. B., and Lee, A. C. (1988) Selected examples of degenerative late effects caused by particulate radiations in normal tissues. In: *Terrestrial Space Radiation and Its Biological Effects*, Proceedings of the NATO Advanced Study Institute, Vol. 154, Eds. P. D. McCormack, C. E. Swenberg, and H. Bucker. New York: Plenum Press, pp. 393-413.

Late effects, HZE, Minilesions, Neon, Argon, Iron, Cataractogenesis, Neoplasia

When astronauts undertake lengthy missions in outer space, they will receive extended (chronic) exposure to a spectrum of cosmic radiations that contains a substantial component of highly energetic particles, including heavy ions. That aspect of space flight was illustrated by the flicker-flash phenomenon observed by "dark-adapted" members of the crews of the lunar (Apollo) missions. Many of the heavy ions (HZE particles) are so penetrating that attempting to shield against them through space vehicle design is impractical at the present time. Fluxes of protons can become a major hazard if astronauts are caught during extravehicular activity (EVA) by the radiations associated with a major solar flare. To ensure the safety of astronauts and space workers, a scientific determination is needed of the health risks arising from anticipated exposures to space radiations during future space missions of long duration. From that information, an adequate risk/benefit analysis can be formulated. The best risk analysis available currently to NATO, which arose from the deliberations of subcommittee #75 of the National Council on Radiation and Protection, is but a step in the process.

Galactic heavy ions will destroy most of the cells traversed directly by their track cores, but in organized tissues adjacent cells will be exposed to the more sparsely ionizing radiations in the energy penumbrae surrounding the track cores, and minilesions could occur. Such penumbral effects could enhance the long-term expression of tissue damage caused by the track cores of heavy ions since, in general terms, late tissue damage from sparsely ionizing radiations develops more slowly than that caused by densely ionizing radiations. For example, the volumes of incipient minilesions could increase over extended periods of time. Significant formation of minilesions was not anticipated, however, in the ground-based experiments discussed here because they involved the heavy ions ^{20}Ne , ^{40}Ar , ^{56}Fe at relativistic energies, protons of different energies, and $g(X)$ -photons. The heavy ion ^{56}Fe was included in the studies not simply because it represented a useful way of providing a level of linear energy transfer (LET_{∞}) near $200 \text{ keV}/\mu\text{m}$, which is the anticipated borderline LET_{∞} for minilesion formation (Todd, 1983), but rather because it is potentially the most dangerous component of the spectrum of galactic heavy ions in terms of flux and relative biological effectiveness (RBE) (Silberberg et al., 1984).

Late sequelae resulting from chronic exposure to ionizing radiations long have been a subject of concern for human health, and poignant illustrations of them are occurring now in the survivors from the atomic explosions at Hiroshima and Nagasaki. Although neoplastic sequelae currently represent the most dangerous risks to human health from chronic radiation exposure, late degenerative, nonmalignant sequelae also present their problems. The responses of normal tissues in a previously irradiated individual also may influence the outcome of therapies for subsequent malignancies or other late sequelae. A 20% loss of hair follicles expressed as partial baldness (alopecia) could be a risk worth taking under certain circumstances, but analogous damage to other parts of the skin could be more serious if it reduced the efficacy of post-irradiation therapy (surgery). Furthermore, even success of that treatment could still leave the need for other therapies to stem further late progressive degeneration in the normal tissues. For whom is there an acceptable benefit for the risk of a potentially inoperable cataract causing loss of vision late in life? Significant losses of post-mitotic cells (neurons) from the central nervous system (CNS) surely would cause an impairment of nervous function that is unacceptable under all but the most extreme circumstances.

The most plausible experimental method for evaluating radiation risks to humans is to obtain results from animate or inanimate model systems and "extrapolate them to man"; but then the question is: how valid are the extrapolations? This simple question is of such overriding importance that it must be examined in depth here in conjunction with an assessment of late degenerative effects caused by heavy ions and protons in the normal tissues of model animal systems. The latter assessment is achieved by the use of selected examples and should be considered as complementary to treatments of radiation carcinogenesis given elsewhere in this publication; but the major emphasis will be upon cataractogenesis, because important comparisons among the cataractogenic responses of higher mammals now are becoming possible.

Lett, J. T., Lee, A. C., Cox, A. B., and Wood, D. H. (1989) Late cataractogenesis caused by particulate radiations and photons in long-lived mammalian species. *Advances in Space Research* 9(10): 325-331.

Late cataractogenesis, New Zealand white rabbits, Beagle dog, Rhesus monkeys, Life-span

Radiation cataractogenesis induced by small acute doses of particulate radiations and photons in the New Zealand white (NZW) rabbit (*Oryctolagus cuniculus*), the beagle dog (*Canis familiaris*), and the Rhesus monkey (*Macaca mulatta*) is discussed in the context of the use of animal models to assess the radiation hazards faced by humans during lengthy sojourns in deep space. Attention is paid to: 1) the importance of life-span studies with long-lived species the above animals have median lifespans in captivity of 5-7, 13-14, and ~25 years, respectively; 2) the magnitudes of possible dose thresholds for cataractogenesis from sparsely ionizing radiations and the modifications of those thresholds of the late degenerative phase of the phenomenon.

Nagle, W. A., Moss, A. J., Jr., Dalrymple, G. V., Cox, A. B., Wigle, J. F., and Mitchell, J. C. (1989) The protons of space and brain tumors: II. Cellular and molecular considerations. Presented at the Conference on High Energy Radiation Background in Space (CHERBS 87), Sanibel Island, FL, November 3-5, 1987. American Institute of Physics Conference Proceedings No. 186, eds. A. C. Rester, Jr. and J. I. Trombka. New York: American Institute of Physics.

Gliomas, Rhesus monkeys, Radiation therapy, Genetic abnormalities, Patient

An increased incidence of highly malignant gliomas, termed glioblastoma multiforme, has been observed in Rhesus monkeys irradiated with 55 MeV protons and in humans treated with therapeutic irradiation to the head. The results suggest a radiation etiology for these tumors. In this paper, we review briefly some characteristics of glioma tumors and summarize the genetic changes associated with malignant gliomas in experimental animals and in humans. The genetic abnormalities include cytogenetic alterations and changes in the structure and expression of specific oncogenes. We discuss the potential for these genetic changes to contribute to several putative mechanisms leading to aberrant growth stimulation and, ultimately, to tumorigenesis. In addition, we review briefly some recent data concerning the molecular nature of radiation-induced somatic cell mutation and oncogene activation and discuss the significance of these results for the radiation etiology of malignant gliomas. Finally, some implications of these results are discussed in relation to human radiation exposure in space.

3.3. INTER- AND INTRASPECIES EXTRAPOLATION

REPORTS/MEETINGS

Cox, A. B. and Lett, J. T. (1987) Quantitation of late radiation damage in the skin of the Rhesus monkey (abstract). In: *Radiation Research, Proceedings of the 8th International Congress of Radiation Research, Edinburgh, July 19-24, 1987*. Eds. E. M. Fielden, J. F. Fowler, J. H. Hendry, and D. Scott. New York: Taylor & Francis, Volume 1, p. 279.

Late radiation damage, Rhesus monkeys, Stem cell survival, Protons

Estimates of the survival of stem cells in the skin of the rabbit can be obtained by propagating primary cultures of skin fibroblasts to terminal senescence by use of the Hayflick technique. The procedure has been extended successfully to monkeys exposed some 20 years ago to protons of different energies (32-400 MeV) and hence of different penetrations (from approximately 1 cm to whole body). Examples of stem cell survival from animals irradiated in the range 2-4 Gy will be presented together with results of experiments designed to simplify the technique and to explore the effects of different modes of transportation of biopsies between the sampling site and the laboratory. Results from biopsies selected from different sites on the primate body also will be discussed. In initial studies, biopsies taken either from the ear or from the thorax of the rhesus monkey gave similar results. Not only are these studies of importance for evaluating the radiation risks of space flight, but also the potential of this analytical system for assessing late damage in the skins of radiotherapy patients is obvious.

Dalrymple, G. V., Nagle, W. A., Moss, A. J. Jr., Wood, D. H., Wigle, J. C., Cox, A. B., Salmon, Y. L., Yochmowitz, M. G., and Hardy, K. A. (1988) Brain tumors induced by protons and x-rays. Abstract presented at the 36th Annual Meeting of the Radiation Research Society, Philadelphia, PA, April 16-21, 1988.

Brain tumors, Protons, X-rays, Electrons, RBE, Central nervous system, Leukemia

Twenty-five years ago (1963-1969), some 2000 rhesus monkeys were irradiated with X-rays, electrons, and protons as part of a study designed to establish the RBE of the radiations of space. The survivors of the acute effects of 55-MeV protons developed significant numbers of malignant gliomas. Tumors of this type have not been seen in any other surviving irradiated or control monkeys. Other types of central nervous system (CNS) tumors (extra-axial meningioma, pituitary tumor, etc.) have appeared in the higher-energy proton groups.

Review of the reports of radiation therapy-induced brain tumors in patients (1953-1987) indicates that partial- and whole-head irradiation has the potential to induce a spectrum of CNS tumors ranging from highly malignant gliomas and sarcomas to benign meningiomas. Whole-head exposure (as used for acute leukemia) reduced the dose required and shortened the time between irradiation and tumor appearance, as compared with localized irradiation for lesions such as pituitary tumor and craniopharyngioma.

We will contrast the tumor induction by protons in monkeys with the human patient experience. Also, the status of the USAF/VA Collaborative Medical Research Project will be presented; this effort is concerned with the mechanisms of induction of brain tumors by protons and X-rays.

3.4. RADIATION LIMITS AND STANDARDS

JOURNALS

Fry, R. J. M. and Lett, J. T. (1988) Radiation hazards in space put in perspective. *Nature* 335: 305-306 [letter].

Galactic cosmic rays, Career risk, Late effects, GCR, Dose equivalent

In this response to the Commentary by Letaw *et al.* concerning the radiation hazards of space travel, the authors challenge Letaw's estimates of comparative deposition of energy for galactic cosmic rays, and estimates of dose equivalents for large solar particle events. NCRP recommendations on career risk and the differences between acute and stochastic late effects in developing quality factors are also discussed.

Sinclair, W. K. (1987) Risk, research, and radiation protection. *Radiation Research* 112, 191-216

Radiation protection, Late effects, NCRP

Radiation protection concerns the risk of stochastic late effects, especially cancer, and limits on radiation exposure both occupationally and for the public tend to be based on these risks. The risks are determined, mainly by expert committees, from the steadily growing information on exposed human populations, especially the survivors of the atomic bombs dropped in Japan in 1945. Risks of cancer estimated up to the early 1980s were in the range of 1 to $5 \times 10^{-2}/\text{Sv}$, but recent revisions in the dosimetry of the Japanese survivors and additional cycles of epidemiological information suggest values now probably at the high end of this range. These are likely to require an increase in the values used for radiation protection. A major problem with risk estimation is that data are available only for substantial doses and must be extrapolated down to the low-dose region of interest in radiation protection. Thus the shape of the dose-response curve is important, and here we must turn to laboratory research. Of importance are studies involving (1) *dose rate*, which affects the response to low-LET radiation and often to high-LET radiation as well; (2) *radiation quality*, since the shapes of the dose-response curves for high- and low-LET radiation differ and thus the RBE, the ratio between them, varies, reaching a maximum value RBE_M at low doses; and (3) *modifiers* of the carcinogenic response, which either enhance or reduce the effect of a given dose. Radiation protection depends both on risk information, and especially also on comparisons with other occupational and public risks, and on research, not only for extrapolations of risk to low doses but also in areas where human information is lacking such as in effects of radiation quality and in modifications of response.

Sinclair, W. K. (1990) Quality factor, concepts and issues. *Radiation Protection Dosimetry* 31(1/4):355-359.

Quality factors, NCRP, ICRU, Radiation weighting factors, Effective quality factors

Three issues in quality factor assignment arise from Report 40 of the ICRU. These include the validity of the observation of the high RBE values for high-LET radiation at low doses, the question of reference radiation, X or g rays, and the 'effective' quality factor in the body compared with the nominal value of Q. On the first item, high values of RBE at low doses are becoming generally accepted, see a recent report from the NCRP. On the second, a survey of past recommendations of both ICRP and NCRP indicate that both organizations have, for protection purposes, always set all low-LET radiations equal to 1 and accepted the differences (of 2-3 times) between them. However, for radiobiological purposes high energy g rays are to be preferred as

the reference radiation. Third, the 'effective quality factor' or radiation weighting factor W_R , for a variety of whole body exposure circumstances can be estimated from $H_E = W_R \sum w_T D_T$ where the effective dose equivalent is the summation of tissue weighing factors w_T times the absorbed dose D_T for the organ, multiplied by an average 'radiation weighing factor' W_R . W_R values can be calculated for a variety of exposure circumstances and are always less than Q . Maximum values, for fission neutrons, for example, are not greatly less however. These issues are under further consideration by the ICRP.

3.4. RADIATION LIMITS AND STANDARDS

REPORTS/MEETINGS

Sinclair, W. K. (1989) Radiation protection policy: implications for the future. In: *Radiation Protection Today: The NCRP at Sixty Years*. Proceedings of the 25th Annual Meeting of the National Council on Radiation Protection and Measurements, Washington, DC, April 5-6, 1989, pp. 343-355.

Radiation standards, Radiation limits, Radiation protection, NCRP

This audience has been treated in the last day and a half to a remarkable survey of progress in radiation protection, from its early beginnings soon after the discovery of radiation in 1895, to the present time. A few glimpses of the future have also been provided in the earlier papers in these Proceedings. In this paper, some of the subjects that have been discussed in this meeting will be recapped briefly, with special regard to the most recent results, because where we have been and what we have learned has much to do with where we can go in the future. Furthermore, in the process of this recap, some of the problems that the NCRP (and others) must address in the future will be indicated.

Wilson, J. W., Townsend, L. W., and Cucinotta, F. A. (1987) On the Potential Impact of the Newly Proposed Quality Factors on Space Radiation Protection. NASA Technical Memorandum 89055.

Quality factors, Near-Earth environment, Low Earth-orbit

The recently proposed changes in the defined quality factor hold great potential for easing some of the protection requirements in protection from the electron and proton environments of the near Earth environment. At the same time, the high Linear Energy Transfer (LET) components play an even more important role, which must be further evaluated. Several recommendations are made that need to be addressed before these new quality factors can be implemented into space radiation protection practice.

4. MICROGRAVITY

4.1. MICROGRAVITY

JOURNALS

Cassanto, J. M., Holemans, W., Moller, T., Todd, P., Stewart, R. M., and Korszun, Z. R. (1990) Low-cost low-volume carrier (Minilab) for biotechnology and fluids experiments in low gravity. *Space Commercialization: Platforms and Processing, Progress in Astronautics and Aeronautics* 127: 199-213.

Flight hardware, Fluid experiment, Low gravity, Biotechnology

Research opportunities in biotechnology and fluid technology under conditions of microgravity can be made available to research workers from developing countries through relevant research projects and low-cost access to microgravity environments. Examples of such projects include polymeric film formation, purification methodology, liquid-liquid diffusion, and growth of organic and protein crystals. An example of a low-cost research device is the Materials Dispersion Apparatus (MDA) which can be used to conduct important low-volume experiments in an automated fashion wherever pairs, or groups of pairs, of liquids must interact. Pairs of samples of 1.0 ml or less can be brought together surface to surface, separated by membrane, or as vapors. Studies of miscibility, cell motility, film formation, and crystal growth are possible; and multiple samples, more than 100 per MDA unit, can be used. The MDA is designed to be compatible with several carriers: shuttle middeck lockers, Get-Away Special canisters, Hitchhiker, LifeSat, recoverable re-entry vehicles, low-gravity aircraft flights, and sounding rockets. The MDA consists of a pair of sliding blocks, in which wells in one block move into contact with wells in the other block under electronic command. Requirements for power, including temperature control, are minimal. Experiments related to biotechnology have been designed for a single flight of the MDA in which the carrier will be a sounding rocket that provides approximately 6 min of low gravity. Examples of experiments to be conducted include the nucleation of organic crystals in aqueous solution, behavior of immiscible aqueous solutions, solid-liquid surface phenomena at high surface-tension gradients, and the formation of thin polymeric membranes.

Cassanto, J. M., Ziserman, H. I., Chapman, D. K., Korszun, Z. R., and Todd, P. (1988) Simulation of launch and reentry acceleration profiles for testing of shuttle and unmanned microgravity research payloads. *Advances in Space Research* 8(12): 141-146.

Low-cost payloads, Re-entry acceleration, Protein crystals, Unmanned flight, Low gravity, Microgravity

Microgravity experiments designed for execution in Get-Away Special canisters, Hitchhiker modules, and Reusable Re-entry Satellites will be subjected to launch and re-entry accelerations. Crew-dependent provisions for preventing acceleration damage to equipment or products will not be available for these payloads during flight; therefore, the effects of launch and re-entry accelerations on all aspects of such payloads must be evaluated prior to flight. A procedure was developed for conveniently simulating the launch and re-entry acceleration profiles of the Space Shuttle (3.3 and 1.7 x g maximum, respectively) and of two versions of NASA's proposed Reusable Re-entry Satellite (RRS) (8 x g maximum in one case and 4 x g in the other). By using the 7 m centrifuge of the Gravitational Plant Physiology Laboratory in Philadelphia, it was possible to simulate the time dependence of 5 different acceleration episodes for payload masses up to 59 kg. A commercial low-cost payload device, the "Materials Dispersion Apparatus" (MDA) was tested for (1) integrity of mechanical function, (2) retention of fluid in its compartments, and (3) integrity of products. In particular, the sharp rise from 0 g to maximum g-loading that occurs during re-

entry in various unmanned vehicles was successfully simulated, conditions were established for reliable functioning of the MDA, and crystals of 5 proteins suspended in compartments filled with mother liquor were subjected to these acceleration loads.

Hymer, W. C., Barlow, G. H., Blaisdell, S. J., Cleveland, C., Farrington, M., Feldmeier, M., Grindeland, R., Hatfield, J. M., Lanham, J. W., Lewis, M. L., Morrison, D. R., Olack, N., Richman, D. W., Rose, J., Scharp, D. W., Snyder, R. S., Swanson, C. A., Todd, P., and Wilfinger, W. (1987) Continuous flow electrophoretic separation of proteins and cells from mammalian tissues. *Cell Biophysics* 10: 61-85.

Continuous flow electrophoretic separation, Electrophoresis, Polystyrene microspheres, Cultured human embryonic cells, Canine cells, Rat cells, Microgravity, Low gravity

A new continuous flow electrophoretic separator for cells and macromolecules was built and tested in laboratory experiments and in the microgravity environment of space flight. Buffer flows upward in a 120-cm long flow chamber, which is 6 cm wide x 1.5 mm thick in the laboratory version and 16 cm wide x 3.0 mm thick in the microgravity version. Electrophoretic subpopulations are collected in 197 fractions spanning 16 cm at the upper end of the chamber. The electrode buffer is recirculated through front and back cooling chambers, which are also electrode chambers. Ovalbumin and rat serum albumin were used as test proteins in resolution and throughput tests; resolution of these two proteins at 25% total w/v concentration in microgravity was the same as that found at 0.2% w/v concentration in the laboratory. Band spreading caused by Poiseuille flow and conductance gaps was evaluated using polystyrene microspheres in microgravity, and these phenomena were quantitatively the same in microgravity as in the laboratory. Rat anterior pituitary cells were separated into subpopulations enriched with cells that secrete specific hormones; growth-hormone-secreting cells were found to have high electrophoretic mobility, whereas prolactin-secreting cells were found to have low electrophoretic mobility. Cultured human embryonic kidney cells were separated into several electrophoretic subfractions that produced different plasminogen activators; a medium-high-mobility subpopulation and a medium-low-mobility subpopulation each produced a different molecular form of urokinase, whereas a high- and an intermediate-mobility subpopulation produced tissue plasminogen activator. Canine pancreatic islets of Langerhans cells were separated into subpopulations, which, after reaggregation into pseudoislets, were found to be enriched with cells that secrete specific hormones; insulin-secreting beta cells were found in lowest mobility fractions, whereas glucagon-secreting alpha cells were found in the highest mobility fractions.

Results of particle electrophoresis experiments were comparable in microgravity and in the laboratory, since cell densities that overloaded the carrier buffer (resulting in zone sedimentation) were avoided, and a 500-fold increase in protein throughput was achieved without compromising resolution in microgravity.

Todd, P. (1989) Gravity-dependent phenomena at the scale of the single cell. *American Society for Gravitational and Space Biology Bulletin* 2: 95-113.

Gravitational cell biology, Single cell functions, Low gravity, Hydrostatic pressure, Sedimentation, Microgravity

Progress in gravitational cell biology research will depend on the continuing evaluation of a wide variety of physical phenomena affected by gravity and their roles in extracellular, intercellular, and intracellular processes. This paper examines those responses of organisms to gravity which depend on functions at the single cell level. Single cell functions are affected by perturbations in their internal and external environment by a variety of factors, one of which is the effect of gravity. Physical phenomena that could influence cell function include sedimentation, buoyancy-driven

convection, streaming potential, hydrostatic pressure, and interactions among physical transport processes. Thermal motion and fluid viscosity play a significant role in all transport processes at the cellular level. The sedimentation of intracellular organelles tends to be counteracted by the cytoskeleton. Intracellular convective transport may be possible in large plant cells. In a microgravity environment extracellular solutes must be transported by diffusion or active circulatory processes in the absence of density gradient-driven convection, and flocculation and coalescence are reduced by the lack of motion of aggregates.

Todd, P., Hymer, W. C., Morrison, D. R., Goolsby, C. L., Hatfield, J. M., Kunze, M. E., and Motter, K. (1988) Cell bioprocessing in space: applications of analytical cytology. *The Physiologist* 31 (Suppl): 552-555.

Cell bioprocessing, Electrophoresis, Analytical cytology, Microgravity, Low gravity, Cells

Cell bioprocessing in space consists of the preparation, cultivation, purification, and investigation of cells and their products in the microgravity environment of orbital space flight. Inertial acceleration is used as an independent variable to explore the limits of specific bioprocessing functions, such as cell growth and secretion, gravity-dependent phenomena in cell bioreactors, cell fusion, the influence of thermal convection on processes at cellular dimensions, the electrophoretic separation of cell subpopulations and subcellular particles, and two-phase partitioning of cells, bioparticles, and macromolecules. Analytical cytology techniques are under development for on-orbit application to future cell growth and separation experiments, such as those anticipated in the Space Station era.

4.1. MICROGRAVITY

REPORTS/MEETINGS

Hymer, W. C., Grindeland, R., Hayes, C., Lanham, J. W., Cleveland, C., Todd, P., and Morrison, D. (1988) Heterogeneity in the growth hormone pituitary gland "system" of rats and humans: Implications to microgravity based research. In: *Microgravity Science and Applications Flight Programs: Selected Papers*, NASA Technical Memorandum 4069, Vol. 1, 47-88.

Growth hormone, Bioassays, Muscle and bone metabolism, Cell function, Microgravity, Low gravity

Since its discovery over 50 years ago, growth hormone (GH) has attracted the attention of both clinical and basic research. The hormone accounts for 20% of the total protein contained in the anterior pituitary gland. Further, some 35-50% of the six different hormone producing cell types are committed specifically to the synthesis of GH. Milligram quantities of GH are present in the human pituitary gland, whereas only microgram quantities of the five other peptide hormones are contained in this 500 mg, bean-shaped structure. Why should there be such a disproportionate amount of GH?

As the techniques to study cells and hormone molecules became more sensitive, it also became clear that heterogeneity was a landmark of pituitary GH: Several variant forms of the hormone molecule exist within the gland as well as in the bloodstream. Further, these variant forms possess unique biological activities. Finally, there is evidence to suggest that GH-producing cells are also functionally heterogeneous. Our NASA-sponsored research deals directly with these issues in both the human and rat pituitary gland. We believe that the large percentages of cells committed to GH production, taken together with the sizeable numbers of variant forms of GH, offer great

flexibility to the "GH system." It is tempting to speculate that this flexibility helps the body meet the varied metabolic demands placed on it. Textbooks describe how GH increases muscle mass, increases breakdown of fat, decreases uptake of carbohydrate into cells, and increases cell division. In light of these numerous activities, the recent claim that synthetic human GH "will soon be used to make short children taller and, possibly, help dieters lose fat and make aging people look young" is therefore not surprising.

Space flight provides a unique environment which impacts the GH system on several levels. First, GH controls muscle and bone metabolism, two tissues known to be negatively affected in flight. Second, cellular "life" as we know it has obviously evolved under the constant force of gravity. Evidence is beginning to accumulate that cell function, in the absence of gravity, is altered. Third, space bioprocessing takes advantage of the lack of convective forces in production of materials of medical relevance. Our NASA-sponsored researches on GH touch on all three of these levels.

The underlying theme of the work described in this paper centers around the difference between bioassayable and immunoassayable GH first recognized over 10 years ago. While the cellular and molecular basis for this dichotomy remain unresolved, our efforts show that it unquestionably exists.

Morrison, D. R., Hymer, W. D., Todd, P., and Grindeland, R. E. (1987) Mammalian cell culture methods in microgravity. Abstract presented at the Annual Meeting of the American Society for Gravitational and Space Biology, Logan, UT, October 18-21, 1987.

Mammalian cell culture, STS-8, BSTA, Biorack, Bioprocessing, Microgravity, Low gravity, RISM

Microgravity experiments on cultured cells pose unique design considerations for flight hardware. With the exception of growth studies on WI-38 lung fibroblasts in the Biological Specimen Test Apparatus on Skylab and the Cell Attachment Test on STS-8, cell culture experiments performed in space have been confined to small (5-10 ml) growth or holding chambers in basic incubators. Anchorage dependent cells were grown to confluence prior to flight and maintained on orbit. Experiments were necessarily simple permitting only basic observations and sample fixation on orbit for postflight analysis back on Earth. Since 1978 several conferences have identified many areas where cell culture experiments in microgravity may provide unique insight into basic cell biology mechanisms and potential advantages in process technology for growth and maintenance of fragile mammalian cells. A summary of the various mammalian cell culture systems which have been flown in space is presented. The requirements and approach for several new cell culture flight experiments are reviewed along with adaptations of the BSTA, the Biorack culture chambers, the Carry-on Incubator chambers, and the Refrigerator/Incubator Storage Module. Advantages and disadvantages are discussed for various conventional systems which could be modified and for new systems being developed for bioprocessing or basic cell biology studies in micro-g.

Todd, P. (1989) Physical phenomena and the microgravity response. *Cells in Space*, Eds. J. D. Sibonga, R. C. Mains, T. N. Fast, P. X. Callahan and C. M. Winget, NASA Conference Publication 10034: 103-116.

Microgravity, Low gravity, Statolith, Cytoskeleton

The living biological cell is not a sack of Newtonian fluid containing systems of chemical reactions at equilibrium. It is a kinetically-driven system, not a thermodynamically-driven system. While the cell as a whole might be considered isothermal, at the scale of individual macromolecular events there is heat generated, and presumably sharp thermal gradients exist at the submicron level. Basic physical phenomena to be considered when exploring the cell's response to inertial acceleration

include particle sedimentation, solutal convection, thermal convection, electrokinetics, motility, cytoskeletal work and hydrostatic pressure. Protein crystal growth experiments, for example, illustrate the profound effects of convection currents on macromolecular assembly. Reaction kinetics in the cell vary all the way from diffusion-limited (very fast) to life-time limited (very slow). Transport processes vary from free diffusion, to facilitated and active transmembrane transport, to contractile-protein-driven motility, to crystalline immobilization. At least four physical states of matter (phases) exist in the cell: Aqueous, non-aqueous, solid, and immiscible-aqueous. Levels of order vary from crystalline to free solution. The relative volumes of these states profoundly influence the cell's response to inertial acceleration. Such subcellular phenomena as stretch-receptor activation, microtubule re-assembly, synaptic junction formation, chemotactic receptor activation, and statolith sedimentation have been studied recently with respect to both their basic mechanisms and their responsiveness to inertial acceleration. From such studies a widespread role of cytoskeletal organization is becoming apparent.

Todd, P., Morrison, D. R., Barlow, G. H., Lewis, M. L., Lanham, J. W., Cleveland, C., Williams, K., Kunze, M. E., and Goolsby, C. L. (1988) Kidney cell electrophoresis in space flight: Rationale, methods, results and flow cytometry applications. In: *Microgravity Science and Applications Flight Programs: Selected Papers*, NASA Technical Memorandum 4069, Vol. 1, 89-118.

Human kidney, Human embryonic cell, Cell electrophoresis, Apollo-Soyuz, STS-3, Cytology, CFES, STS-8, Microgravity, Low gravity

The human kidney performs an incredible number of different functions. Individual cells are responsible for the production of renin, erythropoietin, enzymes of vitamin D metabolism, plasminogen activators of at least 3 types, granulocyte conditioning factor, the maintenance of electrolyte balance, and the clearance of soluble wastes from the blood, to mention a few. The sharing of these functions among cells will take decades to fully characterize, and many of these functions, if they could be isolated, are also of commercial importance to biotechnology. For example, the kidney is perhaps the second most prolific tissue with respect to plasminogen activator production, which is one of today's "hottest" biotechnology future market items.

The purpose of the research project described here was to develop a means of purifying subpopulations of cultured human embryonic kidney (HEK) cells to produce living subpopulations for study. Urokinase, a plasminogen activator found in urine, was the original product goal. Since primary cultures of differentiating epithelioid cells are not immortal, adequate numbers of cells could not be purified by cloning or cell sorting. Historically, Barlow and Kolin showed some three major subpopulations by "continuous belt" electrophoresis in a magnetic field. This finding was not pursued at the time of its discovery, but it was confirmed as an early goal in this project, and the original premise that electrophoretic subfractions would separate according to function was also confirmed.

A series of ground-based electrophoretic and enzymologic studies led to an experiment on the Apollo-Soyuz mission in which evidence for urokinase-rich cell subpopulations was found. The first objective of the present project was to reproduce this result with adequate statistical data and superior technique using the same apparatus. The "EEVT" experiment on STS-3 included two columns of fixed erythrocytes, which were photographed in flight. The remaining 6 tubes were dedicated to living kidney cells that were frozen for several weeks before and immediately after electrophoresis in space. Unfortunately, liquid nitrogen loss in a ground refrigeration unit destroyed all samples from this flight, and only photographic data from the fixed erythrocytes were usable. NASA then made time available on the Continuous Flow Electrophoresis System (CFES) aboard the Space Shuttle orbiters. Without the necessity of freezing cells, and without the influence of particle sedimentation or zone convection, it was then possible to separate cells by CFES in microgravity, as suggested by the discovery of a gravity-dependent component of

pituitary cell separation in free fluid electrophoresis methods. Thus far, it has been possible to separate only two samples of kidney cells, both on STS-8. Analytical results continue to be completed and published. In this paper, we describe the results of kidney cell electrophoresis apparatus and its testing; review results of kidney cell electrophoresis; and present results in the application of flow cytometry to kidney-cell electrophoresis in low gravity.

KEYWORD INDEX

KEYWORD INDEX

- ^{28}Si 12
 5-azacytidine 39
 ^{56}Fe nuclei 12

 Abrasion/Ablation 7
 Absorbed dose 72
 Absorptive cross sections 10, 11
 Accelerator beams 31
 Active dosimeters 73, 79, 80
 Active radiation detectors 73, 76
 Adiabatic approximation 4
 AE-8 17
 Affinity labelling 37
 Age dependence 47, 55, 68
 Alkaline sucrose gradients 46
 Alloy 4
 Alpha particles 9, 14, 44
 Alpha-alpha correlation 5
 Aluminum 28, 29
 Analytical cytology 94
 Analytical methods 24
 Analytical solution 23, 28
 Anatomical man models 72, 73, 78
 Animal models 53
 Antinuclei 8
 AP-8 17
 Apollo-Soyuz 96
 Ar ions 54, 63
Arabidopsis thaliana 66
 Argon 40, 43, 85
 Argon ions 46, 61
 Argonne National Laboratory 47

 Beagle dog 53, 86
 Benchmark 27
 Benchmark solution 22, 24
 Benzo-a-pyrene 56
 Bioassays 94
 Biological dosimeter 66
 Bioprocessing 95
 Biorack 95
 Biotechnology 92
 Boltzmann equation 22, 23, 27, 30
 Bone-tissue interface 20
 Bragg curve 30
 Brain tumors 34, 84, 87
 BRYNTRN 19, 25, 29, 30, 82
 BSTA 95
 Bullfrogs 53

C. elegans 39
 C3H10T1/2 40, 41, 42, 47
 Cancer 52
 Cancer risk 52, 68
 Canine cells 93
 Carcinogenesis 40
 Career risk 88
 Cascade 12
 Cataract patients 71
 Cataract scoring 57
 Cataractogenesis 54, 55, 58, 85
 Cataractotoxic load 69
 Cataracts 50, 52, 54, 56, 57, 58, 59, 60, 71
 Cell bioprocessing 94
 Cell culture 38
 Cell cycle 56, 58
 Cell cycle dependence 43
 Cell damage 37
 Cell differentiation 69
 Cell electrophoresis 96
 Cell function 94
 Cell inactivation 44
 Cell survival 45
 Cell transformation 41, 42, 47
 Cells 94
 Cellular differentiation 59
 Cellular lethality 42
 Cellular pathology 60
 Cellular radiosensitivity 36
 Cellular repair 38
 Cellulose-nitrate sheets 73
 Central collisions 13
 Central nervous system 87
 CFES 96
 CFU-S 49
 Charge changing cross sections 12
 Charge exchange 4
 Chemical protection 42
 Chernobyl 68
 Chinese hamster ovary cells 39
 CHO-K1 39
 Choroid 61, 63, 64
 Chromosome aberrations 37, 50
 Chronic Radiation Colony 84
 Cobalt decay lines 16
 Compton scattering 16
 Computerized anatomical man model 24, 48
 Continuous flow electrophoretic separation 93
 Cornea 63
 Correlations 8
 Cortical cataract 69
 Cosmic rays 63
 COSMOS 1887 66, 72
 COSMOS biosatellite 72
 Coulomb dissociation 6, 9
 Coulomb scattering 3

KEYWORD INDEX

- Coupled channel 9
Coupled-channel equations 5, 8
CR-39 73
Crepis capillaris 66
Cross sections 5, 6, 11, 15, 27, 28
Cultured human embryonic cells 93
Cultured mammalian cells 41
Cytology 96
Cytopathology 60
Cytoskeleton 95
- Data bases 22, 29
Depth distribution 72
Depth doses 19, 30
Differential cross sections 9, 11
Diogene 12, 13, 14
Dipole polarizabilities 2
Direct action 42
Direct and indirect action 36
DNA 47
DNA damage 37
DNA strand breaks 41, 47
Dose calculations 79
Dose equivalent 18, 19, 24, 25, 28, 70, 75, 77, 80, 82, 83, 88
Dose fractionation 58
Dose threshold 55
Doses 28, 70, 75, 80, 83
Dosimetry 31
Double strand breaks 36, 42
- Earth's atmosphere 23
Effective charge 2, 4
Effective quality factors 88
Eikonal approximation 8, 10
Eikonal optical model 8
Elastic scattering 6
Electric quadruple excitations 6
Electromagnetic dissociation 6, 11, 12
Electron microscopy 38, 61, 63
Electronic devices 4
Electronic excitation 3
Electronic transitions 3
Electrons 3, 17, 87
Electrophoresis 93, 94
Emulsion 12
Endometriosis 52, 84
Energy deposition 20
Energy levels 7
Energy transfer 42
Ethyl-methane sulphonate 39, 56
Evaporation model 12
Excitations 3
Excited states 8
- Experimental cataracts 56
Exposure 22
Exposure estimates 79
Eye 63, 64
- Fe 64
Fe ions 59, 60, 61, 69
Fertility 66
Fission foils 72, 74
Flight hardware 92
Flow cytometry 37
Fluence spectra 30, 31, 32
Fluid experiment 92
Focal damage 57, 58
Fractional charge 13
Fractionated doses 42
Fractionation 54
Fragment production 10
Fragment recoil 23
Fragmentation 12
Fragmentation experiments 32
Fragmentation model 5
- Galactic cosmic rays 8, 9, 20, 22, 25, 27, 28, 69, 70, 77, 82, 83, 88
Galactic cosmic rays transport 24
Gamma NKW 16
Gamma radiation 16
Gamma rays 50
Gamma-ray lines 16
Gas 4
GCR 26, 32, 75, 88
Genetic abnormalities 86
Genotoxicity 59
Geomagnetic field model 18
Geosynchronous orbit 74
Glioblastoma 84
Gliomas 86
Glucose tolerance 52
Glutathione 55
Gravitational cell biology 93
Growth hormone 94
- Hadronic transport 27
Harderian gland 40
Heavy charged particles 50
Heavy ion fragmentation 5, 7, 9
Heavy ion reactions 21
Heavy ion transport 22, 32
Heavy ions 14, 15, 23, 29, 38, 39, 40, 42, 44, 45, 46, 49, 53, 57, 58, 63, 70
Heavy-ion collisions 6, 11, 14
Helium 2
HGPRT mutation 42

KEYWORD INDEX

- High-energy nucleons 20
- High-LET 40, 41, 63
- Hormones 55
- Human embryonic cell 96
- Human epithelial cells 40, 41, 44
- Human keratinocytes 42
- Human kidney 96
- Human mammary epithelial cells 42, 45
- Hydrogen 4
- Hydrogen transitions 3
- Hydrogenic 3
- Hydrostatic pressure 93
- Hypophysectomy 55
- Hypothermia 46
- HZE 20, 23, 26, 29, 31, 38, 40, 44, 46, 47, 53, 62, 63, 70, 75, 85
- HZE interaction 20
- HZE particles 25, 32, 38, 46, 64, 69

- ICRP 70, 71
- ICRU 22, 88
- ICU 26
- Impulse approximation 10
- Inclusive cross section 10
- Indirect action 42
- Induced radioactivity 19
- Inelastic interactions 12
- Integral LET spectra 72
- Intranuclear cascade 22, 34
- Inverse dose-rate effect 54, 58
- Ion chambers 76
- Ionization 3
- Iron 40, 42, 43, 60, 63, 85
- Iron ions 39

- K-shell electrons 4
- Kaon 10

- L5178Y S/S 45, 46
- Late cataractogenesis 86
- Late effects 85, 88
- Late radiation damage 61, 87
- LDEF 19
- Lens 54, 58, 63
- Lens epithelium 54, 55, 56, 57, 58, 59, 60, 69, 71
- Lens opacities 57
- Lenses 50
- LET 19
- Leukemia 87
- Life shortening 52
- Life-span 86
- Life-span shortening 49
- Light fragments 12

- Liver 47
- Long-duration space missions 82
- Low dose-rate effect 40
- Low doses 50, 70, 71
- Low Earth-orbit 17, 18, 72, 73, 74, 76, 81, 89
- Low gravity 92, 93, 94, 95, 96
- Low rate effect 40
- Low-cost payloads 92
- Low-inclination orbits 76, 81
- Low-LET 34, 40, 71
- Lunar colony 25
- Lunar mission 74
- Lyrical biology 63

- Magnetic field models 17
- Magnetic shielding 28
- Mammalian cell culture 95
- Mars 26, 77, 82
- Material degradation 20
- Mesons 7
- Methods 22
- Mice 59, 60
- Mice cataractogenesis 55
- Microelectronic applications 34
- Microgravity 92, 93, 94, 95, 96
- Microlesions 8, 40, 61, 62, 63, 64, 69
- Micronucleation 59
- Micronuclei 54, 59, 71
- Minilesions 85
- Missions 73
- Model development 21
- Model verification 24
- Momentum transfer 4, 9, 10
- Monoenergetic beams 24
- Monte Carlo 22, 25
- Monte Carlo methods 22
- Mouse cells 38
- Mouse embryo cells 47
- Mouse lens 60
- Mouse lethality 49
- Mouse lymphoblasts 38, 43
- Mouse testes 44
- Multiple Coulomb scattering 14, 32
- Multiplicities 12
- Multipole polarizability 2
- Murine lymphoblast 36
- Muscle and bone metabolism 94
- Mutagen-carcinogens 50
- Mutagenicity 54
- Mutagens 56, 71
- Mutation effects 66
- Mutations 39

KEYWORD INDEX

- NCRP 70, 71, 88, 89
 Near-Earth environment 89
 Neon 13, 30, 31, 32, 43, 85
 Neon ions 39, 46
 Neon transport 30
 Neoplasia 42, 47, 85
 Neoplastic cell transformation 40
 Neutron albedo 17
 Neutron flux 81
 Neutron total cross sections 11
 Neutrons 11, 19, 49, 68, 74
 New Zealand white rabbits 38, 46, 47, 53, 86
 Niobium 43
 NKW transport 32
 NUCFRAG 10
 Nuclear emulsions 72
 Nuclear fragments 20
 Nuclear reaction effects 78
 Nucleon cross sections 7
 Nucleon knockout 9
 Nude mouse 41
 Numerical solutions 23
 Nutrient effect 46

 Occupational exposure 68
 Ocular tissues 65
 Optical models 5, 8
 Optical potential 10, 11
 Organ dose equivalent 78
 Organic polymers 77
 Oscillator strengths 2, 3, 4
 Oxygen 13
 Oxygen effect 36

 Partial cross sections 12
 Particle tracks 40
 Passive dosimeters 73, 79
 Passive radiation detectors 73, 76
 Patient 86
 PET 34
 Phase spaces 11
 Photographic emulsions 74
 Photonuclear reactions 11
 Photoreceptors 38, 61
 Pion production 13
 Plastic nuclear track detectors 12, 13, 73, 74
 Plastic track detector 76
 PLD repair 51
 PNTD 72
 Polycarbonate 73
 Polymers 3
 Polystyrene microspheres 93
 Positrons 14
 Positrons ionization 16
 Potential models 7
 Production cross sections 12
 Program review 49
 Projectile fragmentation 10, 15
 Projectile fragments 13
 Proline phototroph 39
 Proportional counters 76
 Protein crystals 92
 Proton production 14
 Proton-proton correlations 13
 Protons 3, 4, 6, 17, 22, 48, 52, 55, 61, 62, 84, 87

 Quality factors 17, 22, 68, 69, 70, 78, 88, 89
 Quarks 7

 Radial integrals 2, 3
 Radiation cataracts 53, 55
 Radiation dose 70, 73, 74, 77
 Radiation dosimeter 75, 76, 79, 81
 Radiation dosimetry 18, 20, 80
 Radiation environment 74
 Radiation exposures 18, 19, 68
 Radiation hazards 69
 Radiation limits 89
 Radiation protection 88, 89
 Radiation quality 32
 Radiation risk 74
 Radiation shielding 20, 77
 Radiation standards 89
 Radiation therapy 84, 86
 Radiation transport 27
 Radiation weighting factors 88
 Radioisotope imaging 34
 Radioprotectants 47
 Radiosensitivity 38, 45
 Radon 68
Rana pipiens 56
 Rat cells 93
 Rat lens 54
 Rat lens cultures 50
 Rats 54, 61, 63, 64, 65, 69
 RBE 36, 38, 39, 40, 43, 44, 46, 47, 49, 59, 60, 84, 87
 Re-entry acceleration 92
 Reaction cross sections 8
 Recoils 19
 Recombinant DNA 37
 Reconstructions 57
 Regolith 25, 26
 Relativistic heavy ion 9
 Relativity 5

KEYWORD INDEX

- Repair 36, 45
Replacement therapy 55
Restitution 53
Retina 61, 63, 64
Rhesus monkeys 34, 49, 51, 52, 53, 55, 61, 62, 84, 86, 87
Risk systems 68
RISM 95
RME-III 80
- SCE 50
Scheimpflug image analysis 57
Scheimpflug-based 56
Scoring system 56
Secondaries 19
Sedimentation 93
Sensitivity-analysis 27
SEP 19
Serial section 57
Shielding 18, 25, 26, 28, 29, 30, 32, 66, 70, 73, 75, 82, 83
Shielding materials 75
Shielding measurements 79, 81
Shielding models 79
Shielding strategies 83
Shielding thickness 72
Shuttle 18, 24, 29, 48, 72, 73, 76, 79, 80, 81
Shuttle dosimeter 79
Shuttle shielding model 24
Silicon 43
Silicon ions 39
Single cell 42
Single cell functions 93
Single event evaluation 26
Single-event upsets 20, 34
Single-particle effects 62
Skin cell cultures 51
Slit-lamp 60
Slit-lamp microscopy 55
Solar energetic particles 19, 75, 77, 82
Solar flare 16, 19, 77
Solar flare shielding 25
Solar maximum mission 16
Solar particle events 69
Solar periods 29
Soviet spacecraft 73
Space exploration 20, 70, 75
Space mission scenarios 74
Space radiation 83
Space Shuttle 81
Space Station 74, 75
Spacecraft shielding 20
Spacelab 73, 76
- Spallation products 19
Sparing 40
Spermatogonial cell killing 44
Sphere model 82
Stark effect 2
Statolith 95
Stem cell populations 38
Stem cell survival 87
Strand breakage 46
STS-3 96
STS-51F 76
STS-51J 76
STS-61C 76
STS-8 95, 96
SV40 40
Symposium 47
Synchronous cell cultures 38
- Target theory 45
Testes weight loss 49
Thermoluminescent detectors 72
Thermoluminescent dosimeters 73, 76, 79, 81
Tissue damage 38
Tissue response 50
Tissue-equivalent proportional counter 34, 80
Total cross sections 8, 10
Total reaction cross sections 6
Total-body exposures 52
Track structure 54
Trait effects 51
Transformation 42
Transparency 53
Transport 31
Transport calculations 6
Transport codes 7, 22, 23, 24, 25, 26, 27, 28, 29, 30, 32, 77, 82, 83
Transport methods 32
Transport model 20
Transport theory 30
Trapped protons 19, 34
Trapped radiation 17
Two-body relativistic equation 6
- U.S. spacecraft 73
U.S.S.R.-U.S. 72
Uncertainties 22, 28
Unmanned flight 92
- Validations 31, 32
Vette model 72
- Water 28, 30, 32
Weizsäcker-Williams method 9

KEYWORD INDEX

Wound healing 61, 62
WR-2721 65

X-ray production 4
X-rays 39, 44, 46, 53, 54, 57, 65, 87

AUTHOR INDEX

AUTHOR INDEX

- Adams, J. H., Jr. 70, 82
 Afzal, S. M. J. 50
 Ainsworth, E. J. 49, 50
 Akatov, Y. A. 66, 72
 Akopova, A. B. 72, 74
 Alard, J. P. 12, 13, 14
 Alpen, E. L. 32, 44, 59, 60
 Anderson, G. A. 34
 Anikeeva, I. D. 66
 Antonchik, V. A. 12
 Arnold, J. 12
 Atwell, W. 17, 24, 29, 48, 69, 72, 73, 74,
 76, 77, 78, 79, 80, 81
 Augerat, J. 12, 13, 14
- Babinet, R. 12, 13, 14
 Badavi, F. F. 5, 6, 7, 11, 22, 23
 Badhwar, G. D. 76, 81
 Barlow, G. H. 93, 96
 Bastid, N. 12, 13, 14
 Beever, E. R. 24, 72, 73, 74, 79
 Benton, E. R. 39, 72
 Benton, E. V. 12, 13, 19, 39, 66, 72, 73,
 74, 76
 Bergtold, D. S. 36, 38, 46
 Biagi, F. 12
 Blaisdell, S. J. 93
 Blakely, E. A. 43
 Blazek, E. R. 47
 Bogdanov, S. D. 12
 Braby, L. A. 34
 Brackenbush, L. W. 34
 Brechtmann, C. 12, 13
 Brenner, D. J. 54
 Broadwater, J. R. 84
 Brochard, F. 12, 13
 Broglio, T. 57, 58
 Buck, W. W. 8, 10, 11, 22, 23, 29, 30, 34
 Butler, T. M. 49
- Calvin, H. I. 55
 Cash, B. L. 24, 73, 76, 79, 81
 Cassanto, J. M. 92
 Cavin, L. A. 84
 Chapman, D. K. 92
 Charmensat, P. 12, 13
 Chun, S. Y. 11, 22, 23, 29, 30
 Chupp, E. L. 16
 Cleveland, C. 93, 94, 96
 Cordts, R. E. 34, 52
 Cox, A. B. 38, 43, 46, 47, 52, 53, 55, 61,
 62, 84, 85, 86, 87
 Craise, L. M. 39, 40, 41, 42, 47
 Crawford, H. J. 12, 15
- Crouau, M. 12
 Crouse, D. A. 50
 Cucinotta, F. A. 5, 6, 8, 9, 11, 18, 20, 25,
 29, 30, 78, 89
 Curtis, S. B. 14, 32, 74
- Dalrymple, G. V. 84, 86, 87
 David, J. 55, 56, 57, 58, 71
 De Marco, N. 13
 DeGuzman, R. J. 32, 44
 Delcourt, S. G. 37
 Demaison, P. 14
 Deutchman, P. A. 11
 Dudkin, V. E. 12, 72, 74
 Dupieux, P. 12, 13, 14
- Eason, C. S. 84
 Ehmann, U. K. 43
 Engelage, J. 15
- Fanet, H. 13
 Fanton, J. W. 34
 Farhat, H. 17, 28
 Farrington, M. 93
 Feldmeier, M. 93
 Fishman, G. J. 76
 Fodor, Z. 12, 13, 14
 Fogarty, T. N. 4, 34
 Forrest, D. J. 16
 Frank, A. L. 72, 74, 76
 Frank, P. 65
 Fraysse, L. 12, 13, 14
 Fry, R. J. M. 50, 88
 Fuji, I. 47
- Ganapol, B. D. 23, 24, 27, 28, 29, 30
 Geard, C. R. 50, 71
 Girard, J. 12, 13
 Golightly, M. J. 69, 80
 Goolsby, C. L. 94, 96
 Gorodetzky, P. 12, 13, 14
 Gosset, J. 12, 13, 14
 Gregory, J. C. 76
 Grindeland, R. E. 93, 94, 95
 Gross, F. 6
 Grubb, G. 3
 Gruenert, D. C. 44
 Guzik, T. G. 15
- Haik, B. 65
 Hajnal, F. 20
 Hanson, W. R. 50
 Hardy, A. C. 17, 24, 48, 72, 73, 74, 79, 80,
 81

AUTHOR INDEX

- Hardy, K. A. 52, 68, 80, 84, 87
 Harris, R. K. 34
 Hatfield, J. M. 93, 94
 Hayes, C. 94
 Heinrich, W. 12, 13, 19
 Hess, J. L. 55
 Hoffmann, A. 13
 Holemans, W. 92
 Holley, W. R. 44
 Holsclaw, D. S. 53, 55
 Hong, B. S. 10, 11, 30
 Howard, J. 30, 46
 Hymer, S. S. 37
 Hymer, W. C. 93, 94, 95

 Jarret, B. V. 30

 Keith, J. E. 81
 Keng, P. C. 36, 46
 Khan, F. 2, 3, 4, 9, 10, 14, 23, 29, 30
 Khandelwal, G. S. 2, 3, 4, 5, 8, 9, 10, 14, 18
 Kinzer R. L. 16
 Koniarek, J. P. 68
 Konradi, A. 17, 81
 Korszun, Z. R. 92
 Kostina, L. N. 66
 Kovalev, E. E. 12, 72
 Krebs, I. 61, 63, 64
 Krebs, W. 61, 63, 64, 68
 Kung, J. S. 56
 Kunze, M. E. 37, 94, 96

 L'Hote, D. 12, 13, 14
 Lamkin, S. L. 11, 23, 28, 29, 30
 Landis, D. A. 14
 Lanham, J. W. 93, 94, 96
 Laspalles, C. 12, 13
 Le Merdy, A. 12
 Lee, A. C. 53, 55, 84, 85, 86
 Leising, M. D. 16
 Lemaire, M. C. 12, 13, 14
 Letaw, J. R. 16, 26, 70, 75, 76, 82
 Lett, J. T. 36, 38, 42, 43, 45, 46, 47, 53, 55, 61, 69, 84, 85, 86, 87, 88
 Lewis, M. L. 93, 96
 Lindstrom, P. J. 15
 Long, S. A. T. 3
 Lucas, B. 12, 13
 Ludewigt, B. A. 14, 32

 Magradze, N. V. 72
 Marennny, A. M. 66
 Marroncle, J. 12, 13, 14

 Marshall, T. M. 39
 Maung, K. M. 6, 8, 10, 11
 McGuire, E. L. 84
 Meador, W. E. 5
 Medvedovsky, C. 53, 54, 55, 56, 57, 58, 59, 60, 65, 69
 Mei, M.-T. 39, 40, 47
 Melkumyan, L. V. 74
 Merriam, G. R., Jr. 53, 54, 56, 57, 61, 63, 69, 71
 Merriam, J. 71
 Miller, J. 30, 31
 Miller, M. 32
 Mitchell, J. C. 84, 86
 Mitchell, J. W. 15
 Moller, T. 92
 Montarou, G. 12, 13, 14
 Morrison, D. R. 93, 94, 95, 96
 Moss, A. J., Jr. 84, 86, 87
 Motter, K. 94
 Murphy, R. J. 16

 Nachtwey, D. S. 70
 Nagle, W. A. 84, 86, 87
 Nealy, J. E. 18, 19, 25, 26, 28, 29, 30, 77, 82, 83
 Nefedov, N. A. 12
 Nelson, G. A. 39
 Ngo, D. M. 34
 Norbury, J. W. 5, 6, 7, 8, 9, 10, 11

 Odrich, S. 54, 71
 Olack, N. 93
 Olsgaard, D. A. 3
 Ostroumov, V. I. 12

 Pandey, L. N. 3
 Parizet, M. J. 12, 13, 14
 Parnell, T. A. 72, 73, 76
 Peak, J. G. 47
 Peak, M. J. 47
 Phillips, M. H. 14, 32
 Pickering, J. E. 68
 Poitou, J. 12, 13, 14
 Portman, A. I. 66
 Potapov, Y. V. 72, 74
 Powers-Risius, P. 32, 44, 59, 60
 Pritchard, W. M. 3

 Qassoud, D. 12, 13
 Quam, W. 80

 Racca, C. 12, 13, 14
 Raha, S. 14

AUTHOR INDEX

- Rahmani, A. 12, 13, 14
Rapkin, M. 30, 31, 44
Rhim, J. S. 40, 41
Richman, D. W. 93
Richmond, R. G. 73, 76, 79, 81
Rieger, E. 16
Riehl, K. 80
Rini, F. 56, 65
Romo, D. 34
Rose, J. 93
Rosskoth, H. 56
Rothstein, H. 53, 55
Rusin, S. V. 66
Rustgi, M. L. 3
- Salmon, Y. A. 84
Salmon, Y. L. 52, 68, 87
Sanchez, F. J. 46
Scharp, D. W. 93
Schimmerling, W. 12, 13, 14, 15, 20, 21, 30, 31, 32, 44
Schubert, W. W. 39
Seidenberg, K. 57, 58
Share, G. H. 16
Shavers, M. R. 31, 32
Shinn, J. L. 18, 25, 28, 29, 78, 82
Silberberg, R. 16, 26, 70, 75, 76, 82
Simonsen, L. C. 18, 26, 28, 77, 82, 83
Sinclair, W. K. 68, 70, 71, 88, 89
Snyder, R. S. 93
Spieler, H. G. 30
Stampfer, M. R. 45
Stewart, R. M. 92
Story, M. D. 43, 46
Swanson, C. A. 93
Symons, T. J. M. 15
- Tamain, J. C. 13
Terrien, Y. 12, 13, 14
Tion, J. A. 6
Tobias, C. A. 40, 41, 42, 45, 47
Todd, P. 37, 40, 62, 92, 93, 94, 95, 96
Townsend, L. W. 5, 6, 7, 8, 9, 10, 11, 14, 17, 18, 19, 20, 21, 22, 23, 24, 25, 26, 27, 28, 29, 30, 32, 77, 78, 82, 83, 89
Tsao, C. H. 26, 70, 75, 76, 82
- Valero, J. 13
Valette, O. 12, 13, 14
Vaulina, E. N. 66
- Wallace, S. J. 6
Walton, J. T. 14
Watts, J. W., Jr. 72, 76
- Wefel, J. P. 15
Wigle, J. C. 51, 87
Wigle, J. F. 86
Wilfinger, W. 93
Williams, K. 96
Wilson, J. W. 2, 3, 4, 5, 6, 7, 8, 9, 10, 11, 14, 17, 18, 19, 20, 21, 22, 23, 24, 25, 26, 27, 28, 29, 30, 32, 34, 77, 78, 82, 83, 89
Wong, M. 14, 20, 21, 30, 31, 32, 44
Wood, D. H. 34, 52, 68, 84, 86, 87
Worgul, B. V. 50, 53, 54, 55, 56, 57, 58, 59, 60, 61, 63, 64, 65, 68, 69, 71
- Xu, Y. J. 4
- Yamamoto, O. 47
Yang, T. C. 39, 40, 41, 42, 44, 45, 47
Yochmowitz, M. G. 52, 68, 84, 87
Yoshida, T. 47
- Zhu, G. 3
Ziserman, H. I. 92

Report Documentation Page

1. Report No. NASA TM-4270		2. Government Accession No.		3. Recipient's Catalog No.	
4. Title and Subtitle Radiation Health Research, 1986-1990				5. Report Date April 1991	
				6. Performing Organization Code	
7. Author(s) Radiation Health Program, Life Sciences Division				8. Performing Organization Report No.	
				10. Work Unit No.	
9. Performing Organization Name and Address NASA OSSA Washington, DC				11. Contract or Grant No. NASW 4292	
				13. Type of Report and Period Covered Technical Memorandum	
12. Sponsoring Agency Name and Address National Aeronautics and Space Administration				14. Sponsoring Agency Code SBM	
15. Supplementary Notes					
16. Abstract This report consists of a collection of 225 abstracts of radiation research sponsored by NASA during the period 1986-1990. Each abstract has been categorized within one of four discipline areas: Physics, Biology, Risk Assessment and Microgravity. Topic areas within each discipline have been assigned as follows: Physics - Atomic Physics, Nuclear Science, Space Radiation, Radiation Transport and Shielding and Instrumentation; Biology - Molecular Biology, Cellular Radiation Biology, Tissue, Organs and Organisms, Radioprotectants and Plants; Risk Assessment - Radiation Health and Epidemiology, Space Flight Radiation Health Physics, Inter- and Intraspecies Extrapolation and Radiation Limits and Standards; and Microgravity. When applicable subareas have been assigned for selected topic areas. Keywords and author indices are provided.					
17. Key Words (Suggested by Author(s)) 1) Radiation Health 6) Radiation Biology 2) Space Radiation 7) Radiation Physics 3) Human Exploration 8) LifeSat 4) Research Programs 5) Risk Assessment				18. Distribution Statement Unclassified - Unlimited Subject Category 52	
19. Security Classif. (of this report) Unclassified		20. Security Classif. (of this page) Unclassified		21. No. of pages 120	
				22. Price A06	

